

**Multi-objective Performance Optimization & Thermodynamic Analysis of Advanced
Supercritical CO₂ Power Cycles for CSP using ANN & Genetic Algorithm**

Submitted By

Asif Iqbal Turja

180011113

Md. Mahmudul Hasan

180011211

Supervised By

Dr. Mohammad Monjurul Ehsan

**A Thesis submitted in fulfillment of the requirement for the degree of Bachelor of
Science in Mechanical Engineering**



Department of Mechanical and Production Engineering (MPE)

Islamic University of Technology (IUT)

May, 2023

Candidate's Declaration

This is to certify that the work presented in this thesis, titled, “**Multi-objective Performance Optimization & Thermodynamic Analysis of Advanced Supercritical CO₂ Power Cycles for CSP using ANN & Genetic Algorithm**”, is the outcome of the investigation and research carried out by me under the supervision of **Dr. Mohammad Monjurul Ehsan, Associate Professor.**

It is also declared that neither this thesis nor any part of it has been submitted elsewhere for the award of any degree or diploma.



Asif Iqbal Turja
Student No: 180011113



Md. Mahmudul Hasan
Student No: 180011211

RECOMMENDATION OF THE BOARD OF SUPERVISORS

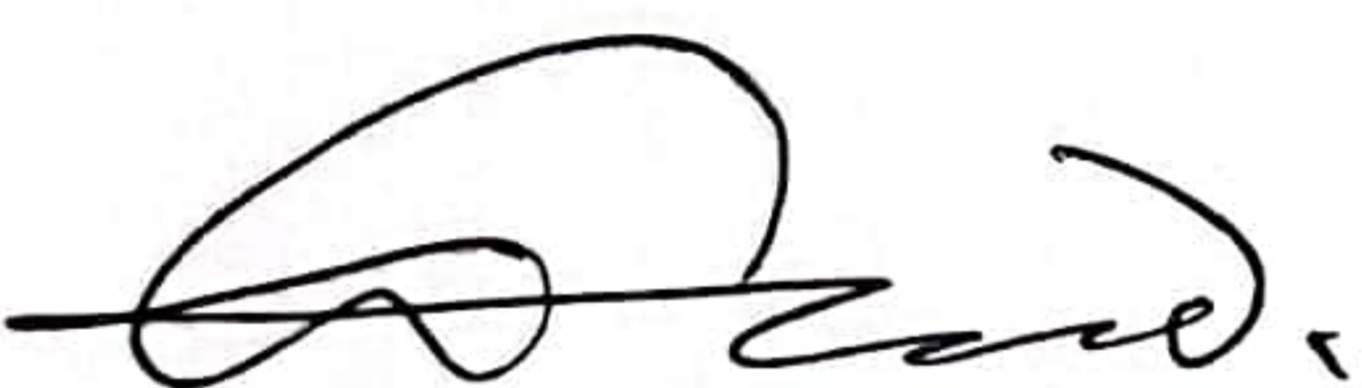
The thesis titled “Multi-objective Performance Optimization & Thermodynamic Analysis of Advanced Supercritical CO₂ Power Cycles for CSP using ANN & Genetic Algorithm” submitted by Asif Iqbal Turja, Student No: 180011113 & Md. Mahmudul Hasan, Student No: 180011211 has been accepted as satisfactory in fulfillment of the requirements for the degree of B.Sc. in Mechanical Engineering on 19th May, 2023.

BOARD OF EXAMINERS

1. 

Dr. Mohammad Monjurul Ehsan
Associate Professor
MPE Dept., IUT, Board Bazar, Gazipur-1704, Bangladesh.

(Supervisor)

2. 

Dr. Shamsuddin Ahmed
Professor
MPE Dept., IUT, Board Bazar, Gazipur-1704, Bangladesh.

(Examiner)

3. -----

Dr. Mohammad Ahsan Habib
Professor
MPE Dept., IUT, Board Bazar, Gazipur-1704, Bangladesh.

(Examiner)

Acknowledgment

All the gratitude and praise to the Almighty Allah to whom we surrender ourselves, for granting us the abilities to complete this work properly on time. Without His grace, guidance and protection this could have been more difficult.

We would like to convey our profound gratitude to Dr. Mohammad Monjurul Ehsan, Associate Professor, Department of Mechanical and Production Engineering, IUT for his constant encouragement, perseverance, patience and vast expertise throughout all stages of this work.

Abstract

In recompression, partial cooling, and main compression intercooling cycles, the main compressor inlet temperature (MCIT) and the turbine inlet temperature (TIT) have a substantial impact on a supercritical CO₂'s (sCO₂) thermal performance. These three cycles are evaluated thermodynamically from the perspectives of energy and exergy. A parametric study is conducted utilizing climate information for critical weather conditions to determine the influence of significant operational factors on the power plant's overall performance. Few studies on machine learning-based Brayton cycle performance prediction have been carried out in recent years, mostly due to a lack of reliable methodology and case studies. In this study, a detailed approach for machine learning application into the Brayton cycle study is offered in order to assess and improve the parameter and performance of the Brayton cycle. Firstly, a cycle dataset with three Brayton cycle configurations is created using thermodynamic modeling. Energy-exergy analysis allows to assess any possible effects on the environment that may arise from the power plant's exergy destruction. 54.48% energy efficiency is extracted from Recompression Cycle with 77.97% exergy efficiency is found. The datasets are then created using parametric analysis, and the simulated models are trained using machine learning methods (random forest, XGBoost, and LightGBM). To maximize sCO₂ cycle power output, the meridional surface is optimized. The random forest regressor had the highest R² (coefficient of determination) for recompression cycle among regression algorithms. Finally, the XGBoost regression, Random Forest, and Light Gradient Boosting prediction models for the Brayton cycle were built for machine learning to predict Net Work Output using a dataset containing 17250 values that can forecast error rates. In this study, ANN based Genetic Algorithm is used to optimize the output of thermodynamics models in the optimal condition with the variation of other parameters. TOPSIS decision-making tool is used for optimization. It should be emphasized that adding more input data would improve the prediction and optimization processes overall performance. In conclusion, The Brayton Cycle prediction and optimization method put forward in this paper is a promising technology that combines machine learning with energy use and would provide a new angle for research in this field. To conclude, the machine learning models can be used in power plant industries for better prediction and optimization as these algorithms are five times faster than traditional thermodynamic models.

Keywords: Supercritical CO₂ Brayton cycle; Concentrated solar power; Machine Learning; Exergy analysis; Artificial Neural Network; Optimization.

Table of Contents

Abstract.....	5
Chapter 1: Introduction	13
1.1 Objectives of the Study	13
1.2 Structure of the Thesis.....	13
Chapter 2: Literature Review	16
2.1 Superiority of sCO ₂ cycles	16
2.2 CSP plants integrated with sCO ₂ power cycles	18
2.3 Machine Learning Implementation	19
2.4 Multi-objective performance optimization.....	20
Chapter 3: Description of the model	22
3.1 Supercritical CO ₂ Brayton Cycle Configuration	22
3.1.1 Recompression cycle	23
3.1.2 Partial Cooling cycle	24
3.1.3 Main Compression Inter Cooling cycle.....	25
3.2 Designing CSP Loop at Optimum Condition.....	27
3.2.1 Sizing the Heliostat Field	27
3.2.2 Selection of Hot Salt.....	28
3.2.3 TES	28
Chapter 4: Computational Methodology	29
4.1 Thermodynamic Equations	29
4.2 Model Validation	31
4.3 Machine Learning Prediction Models	35
4.3.1 Random Forest Regressor:.....	35
4.3.2 XGBoost Regressor:	36

4.3.3 LightGBM:	37
4.4 Optimization Methods.....	38
4.4.1 Genetic Algorithm	38
4.4.2 Artificial Neural Network.....	42
4.4.3 TOPSIS	43
Chapter 5: Results & Discussions.....	45
5.1 Off-design Performance	45
5.1.1 Effect of MCIT	48
5.1.2 Effect of TIT	50
5.1.3 Effect of Pinch Temperature	53
5.1.4 Effect of Compressor Efficiency	53
5.1.5 Exergy Analysis	55
5.2 Seasonal TIT, MCIT observation	57
5.3 Machine Learning model error Evaluation	61
5.3.1 Genetic Algorithm Optimization Results	63
5.3.2 TOPSIS Decision Analysis Results	69
Chapter 6: Conclusion.....	70
6.1 Conclusion.....	70
6.2 Recommendation for future works.....	71
6.2.1 Design recommendation for future commercialization	71
6.2.2 Hyperparameter optimization & implementation of deep learning models	71
References	72

List of Tables

Table 1: Nomenclatures & Symbols	10
Table 2: Description of the S-CO ₂ Brayton cycles.....	22
Table 3: Components-wise exergy destruction equation of a main compression intercooling cycle.	30
Table 4: Initial parameters for simulation and analysis of system performance.....	33
Table 5: CSP loop Design Parameters.....	33
Table 6: Design variables (Recompression) utilized for the Current Study.....	41
Table 7: Design variables (Partial Cooling) utilized for the Current Study.	41
Table 8: Design variables (Main Compression Intercooling) utilized for the Current Study.	41
Table 9: Recompression S-CO ₂ Cycle pressure, temperature, enthalpy & entropy for each state point.	45
Table 10: Partial cooling S-CO ₂ Cycle pressure, temperature, enthalpy & entropy for each state point.	46
Table 11: Main Compression Intercooling S-CO ₂ Cycle pressure, temperature, enthalpy & entropy for every state point.	47
Table 12: Machine learning model prediction error comparison.	62
Table 13: Optimized conditions obtained from TOPSIS for best performance.	69

List of Figures

Figure 1: Supercritical CO ₂ power cycles in the literature.....	17
Figure 2: Cycle layout of Recompression sCO ₂ cycle equipped with TES.	23
Figure 3: T-s diagram of Recompression sCO ₂ cycle equipped with TES.....	24
Figure 4: Cycle layout of Partial Cooling sCO ₂ cycle equipped with TES.....	24
Figure 5: T-s diagram of Partial Cooling sCO ₂ cycle equipped with TES.....	25
Figure 6: Cycle layout Main Compression Inter Cooling sCO ₂ cycle equipped with TES.	26
Figure 7: T-s diagram of Main Compression Inter Cooling sCO ₂ cycle equipped with TES.	26
Figure 8: Cycle model validation for MCIT variation.....	31
Figure 9: Cycle model validation for TIT variation.....	32
Figure 10: Flow chart demonstrating cycle modelling, data extraction & performance optimization. ...	34
Figure 11: Decision tree diagram.....	36
Figure 12: XGBoost algorithm prediction tree.	37
Figure 13: LightGBM prediction tree diagram.....	38
Figure 14: Genetic algorithm network implemented with neural network.....	39
Figure 15: Neural network in MATLAB.	42
Figure 16: Exergy destruction & exergy efficiency comparison for recompression, partial cooling & intercooling cycle with the variation of the TIT at different compressor inlet temperature of 35°C and 40°C.	48
Figure 17: Exergy destruction & exergy efficiency comparison for recompression, partial cooling & intercooling cycle with the variation of the TIT at different compressor inlet temperature of 45°C and 50°C.	49
Figure 19: Cycle thermal efficiency & specific work comparison for recompression, partial cooling & intercooling cycle with the variation of the MCIT at different turbine inlet temperature of 350°C, 450°C, 550°C and 650°C.	52
Figure 20: Comparison of split ratio & cycle thermal efficiency with variation of recuperator pinch temperature.	53
Figure 21: Recompression SCO ₂ cycle specific work, split ratio, cycle efficiency & mass flowrate with the variation of compressor efficiency.....	53
Figure 22: Partial coolingSCO ₂ cycle specific work, split ratio, cycle efficiency & mass flowrate with the variation of compressor efficiency.....	54

Figure 23: Main compression inter cooling SCO ₂ cycle specific work, split ratio, cycle efficiency & mass flowrate with the variation of compressor efficiency	54
Figure 24: Exergy destruction in different components in Recompression S-CO ₂ cycle.	56
Figure 25: Exergy destruction in different components in partial cooling S-CO ₂ cycle.....	56
Figure 26: Exergy destruction in different components in main compression intercooling S-CO ₂ cycle.	57
Figure 27: Recompression SCO ₂ cycle hourly CSP plant performance for supplemented with TES at various seasonal climates.....	58
Figure 28: Partial cooling SCO ₂ cycle hourly CSP plant performance for supplemented with TES at various seasonal climates.....	59
Figure 29: Main compression inter cooling SCO ₂ cycle hourly CSP plant performance for supplemented with TES at various seasonal climates.....	60
Figure 30: 3D plot for REC, PAR, INT SCO ₂ BC parameters.	61
Figure 31: Heat map indicating correlation between cycle parameters.....	62
Figure 32: Multi-objective Pareto front for REC SCO ₂ BC.	63
Figure 33: GA performance (Epoch 1000) curve for REC SCO ₂ BC.....	63
Figure 34: Training state for REC SCO ₂ BC.	64
Figure 35: Error histogram for REC SCO ₂ BC.....	64
Figure 36: Multi-objective Pareto front for PAR SCO ₂ BC.....	65
Figure 37: GA performance (Epoch 1000) curve for PAR SCO ₂ BC.	65
Figure 38: Training state for PAR SCO ₂ BC.....	66
Figure 39: Error histogram for PAR SCO ₂ BC.	66
Figure 40: Multi-objective Pareto front for INT SCO ₂ BC.....	67
Figure 41: GA performance (Epoch 1000) curve for INT SCO ₂ BC.....	67
Figure 42: Training state for INT SCO ₂ BC.....	68
Figure 43: Error histogram for INT SCO ₂ BC.	68

Table 1: Nomenclatures & Symbols

Abbreviation	Meaning
H	Heater
RH	Re-Heater
HTR	High Temperature Recuperator
LTR	Low Temperature Recuperator
CSP	Concentrated Solar Power
REC	Recompression SCO ₂ cycle
PAR	Partial cooling SCO ₂ cycle
INT	Main compression Intercooling SCO ₂ cycle
PC	Pre-Compressor
RC	Re-Compressor
PCL	Pre-Cooler
ICL	Intercooler
MC	Main Compressor
SCO ₂ BC	Supercritical Carbon Di-oxide Brayton Cycle
ANN	Artificial Neural Network
GA	Genetic Algorithm
TES	Thermal Energy Storage
TOPSIS	Technique for Order Preference by Similarity to Ideal Solution

Symbol	Meaning
E	Exergy (kJ)
ϵ_{HTR}	Effectiveness of the high temperature recuperator
ϵ_{LTR}	Effectiveness of the low temperature recuperator
\dot{E}	Rate of exergy (kW)
h	Specific enthalpy (kJ/kg)
s	Specific entropy [kJ/(kg-K)]
e	Specific Exergy (kJ/kg)
\dot{m}	mass flow rate (kg/s)
P	Pressure (MPa)
\dot{Q}	Rate of Heat (kW)
T ₀	Reference temperature (K)
S-CO ₂	Supercritical Carbon Dioxide
T	Temperature (°C)
\dot{W}	Rate of Work (kW)
x	Split Ratio
η_{cyc}	Cycle efficiency
η_{exergy}	Second law efficiency
<u>Subscripts</u>	
in	Inlet
out	Outlet
CO ₂	Carbon Di-oxide
hel	Heliostat
cos	Cosine
s&h	Shading & blocking
ref	Reflectivity
rec	Receiver

Chapter 1: Introduction

1.1 Objectives of the Study

- To study the cycle performance with variation of different working parameters.
- To determine the optimal pressure & compressor inlet temperature for maximum thermal efficiency.
- To analyze exergy destruction of each component, exergy efficiency & overall performance of the cycle.
- To train, test & predict work output & efficiency of the cycle using machine learning regression algorithms (Random Forest, XGBoost, LightGBM).
- To determine optimized condition for maximum net work output using ANN & GA.

1.2 Structure of the Thesis

Research Background of S-CO₂ Brayton Cycle

Energy conservation and pollution reduction have grown in significance in recent years. Several contentious discussions about improving combined-cycle powerplants and lowering their environmental consequences have emerged as the first half of the 21st century progresses, most of which were previously beyond the ability of humans. Many researchers have proposed towards a number of specific designs and performance enhancements to simultaneously minimize the disastrous consequences of fuel consumption and improve plant efficiency [1]. In recent years, concentrated solar thermal power (CSP) plants have received a lot of support. The supply of conventional fundamental energy sources like coal, oil, and natural gas is constrained, and it is expected that they won't last for very long. Environmental problems related to conventional energy sources are in higher demand. Future energy consumption is anticipated to be dominated by renewable energy sources as a result of increased energy demand, which will reduce the need for fossil fuels and ease environmental concerns. Additionally, humans need several types of energy for their everyday lives as well as for industrial production, including electricity, heat, and cooling[2]. The CSP integrated power cycle has been proposed in recent literature as a solution for this problem. Concentrating solar power (CSP) facilities now uses oil, molten salt, or steam as heat transfer fluids (HTF) to transmit energy from the solar receiver to the power block. Supercritical CO₂ (s-CO₂) is being studied for use in CSP applications as both the working fluid and the HTF. It operates more readily at greater temperatures than steam and performs more well at lower temperatures. Thermal power facilities with closed loop Brayton cycles have been recommended as the potential locations for sCO₂ applications. These power cycles are projected to be the next generation of power cycles due to their lower cost,

increased thermal efficiency, and simpler plant design. The cooling of CO₂ close to the critical temperature and pressure is one of the major difficulties. The effective and seamless functioning of a thermal power plant depends on a dependable and well-designed cooling system. The S-CO₂ system operates at pressures and temperatures that are close to carbon dioxide's critical point. When CO₂ is cooled below the "pseudo-critical" line, its density and specific heat increase rapidly. The results of this include low compressor work and high heat transfer coefficients in the pre-cooler and recuperator. When the turbine and compressor input temperatures are the same as with an ideal gas, it provides higher efficiency than is feasible in ideal gas[3]. At temperatures appropriate for CSP applications, operating in a closed-loop recompression, supercritical carbon dioxide (S-CO₂) In comparison to supercritical or superheated steam, the Brayton cycle may have cycle efficiency that is comparable or even superior. S- CO₂ application to trough fields is complicated considering the high pressure needed, and exploratory study implies the fluid would be more viable for use in power towers.[4]. Five supercritical carbon dioxide cycle, the fundamental Brayton cycle, the regenerative Brayton cycle, the recompression Brayton cycle, the pre compression Brayton cycle, and the split expansion Brayton cycle are all examples of Brayton cycles, where the recompression Brayton cycle had the best thermal efficiency were thermodynamically compared to a solar power tower. Employing this cycle, the integrated system's maximum thermal efficiency was 40%. The cycle's maximum thermal efficiency stood at 52%.[5]. A study looked into how different parameters influenced the pre-cooler's design for utilization in the sCO₂ cycle. It was presented an innovative research study on the usage of S-CO₂ in power cycles for the production of electricity in the late 1960s. The simplicity and compactness of the systems is effective for many applications, even if the efficiency of a low-temperature cycle is not any higher than that of an identical steam cycle. In terms of efficiency and simplicity in high-temperature cycles, CO₂ exceeds a steam cycle.[6]

The majority of research in recent decades has been based on traditional methods of the specific experiment and thermodynamic modeling, whose workload and cost are relatively significant in solving large-scale problems, despite the high accuracy of the research results, as with the supercritical CO₂ Brayton Cycle works mentioned above. We search for a cost-effective and efficient approach that could rapidly resolve the calculation issue for the various performance indices of the CSP integrated supercritical CO₂ Brayton system while ensuring the accuracy of the results. The accuracy and working speed of this procedure require being guaranteed, and a suitable trade-off is needed between each of them. Recently, the use of AI has developed and grown, and this has led to a fresh approach to the issue at concern. As a result, this research offered an approach based on machine learning to accomplish performance prediction,

parameter analysis, and optimization [1]. Using a multi-layered approach, a precooler design and analysis code (PDAC), an artificial neural network (ANN), and a 3D Reynolds Averaged Navier-Stokes (RANS) model were designed. To accurately forecast the transcritical ORC's thermal efficiency and cycle high pressure for the R1234ze(E) working fluid, Zhi et al. [7] developed an artificial neural network model in which it was observed that channel flow rate and optimum exit temperature had a significant effect on pressure losses.

A pinch point that develops inside the heat exchanger when the exit temperature is below the pseudocritical temperature results in a significant increase in size and pressure losses [8]. For the design, planning, and operation of power systems, load forecasting is a vital aspect. In this study a hybrid forecasting model based on limit gradient lifting (XGBoost) and gating recurrent neural network (GRU) is developed.[9] The results show that the combined model can effectively incorporate the benefits of the two models and is much more accurate than either the single model or the commonly used forecasting methods.[10]

The efficiency of coal-fired power plants is influenced by many factors, including the main steam/reheat steam pressures and temperatures, turbine extraction pressures, and surplus air ratio for a certain fuel. To estimate the energy input from fuel (coal), the Artificial Neural Network (ANN) is trained using data from the flow-sheet application's simulation of a power plant.[11] This study combines ANN and GA-based (neuro genetic) techniques to optimize a high ash coal-fired supercritical power plant for the climate of India. The created model may also be used for optimization when a quick response is required.[12].

Chen et al [13] develops a predictive model that predicts the combined cycle power plant's hourly full load electrical output by investigating and examining various machine learning regression methodologies. The dataset's input variables, which are four factors, have an impact on how well a power plant can handle its base load. The greatest performance of the highest subset, which includes the whole set of input variables, has been seen using the most efficient technique, the Bagging algorithm with REPTree[14].

Chapter 2: Literature Review

2.1 Superiority of sCO₂ cycles

The advantages of supercritical CO₂ power cycles over Rankine cycles were documented by Persichilli et al.[15], who emphasized their compactness, reduced cost, and greater cycle efficiency. Different sCO₂ power cycles were evaluated by Besarati and Goswami [16] who found that partial cooling and intercooling arrangement offered the best performance. The optimization of a straightforward and recompression sCO₂ cycle was done by Dyreby et al.[17]. In order to increase the cycle efficiency, they investigated the association between recuperator size and lowest cycle temperature. Testing of the trans-critical CO₂ cycle at the Sandia National Laboratory by Wright et al. [18] revealed that it performed better than the Rankine cycle. By installing numerous reheat stages in between the turbines, the efficiency was raised by a further 4-5%. To make use of the waste heat[19] investigated the thermo-economic feasibility of four distinct sCO₂ bottoming cycle topologies cascaded with steam Rankine cycles. The combined supercritical and trans-critical CO₂ cycle investigation was also carried out by [20] to observe the performance increase of 17% compared to a straightforward regeneration cycle. Based on recuperator efficiency and pinch point temperature control in the recuperator[21] improved the sCO₂ recompression cycle performance. Additionally, the split ratio and pressure ratio were improved. Brayton cycles operate at temperatures relevant for applications of concentrating solar power (CSP) based on various cycles. They are lighter and smaller in volume, have less thermal mass, and simpler power blocks. The installation, maintenance, and operating costs of the s-CO₂ process are further decreased by the smaller size and simpler gear. In a high-efficiency operation, they started with Dostal's recompression model and investigated its partial cooling cycle arrangement.

Mohammad et al. [22] studied the Solar system integrated with Brayton cycle and Bottoming Rankine cycle in which solar collector operates as a central receiver, reflecting sunlight to ensure it enters the flow of fluid and stores energy depending on how much heat required to commence the cycle. The two desired functions of this cycle's optimization aim to decrease the cost of producing power and enhance energy effectiveness. The ORC cycle, MED desalination unit, and supercritical carbon dioxide solar Brayton cycle are integrated, with the multi-effects desalination system working on the ORC cycle's waste heat. This hybrid arrangement is used for both the production of freshwater and power.

They studied recompression with main-compression intercooling rather than Dostal's precompression setup since it lacked the requisite performance gain. To evaluate the possibility for additional efficiency gains, they compared examples with and without reheating in all cycle configurations. In this paper, Cycle

thermodynamic calculations disregarded pressure losses and assumed constant heat exchanger effectiveness. Recovered Brayton cycles are extremely sensitive to loop pressure losses and heat exchanger performance. Consequently, this paper can include transient and off-design activities, and integrating more realistic heat exchanger components.[19]

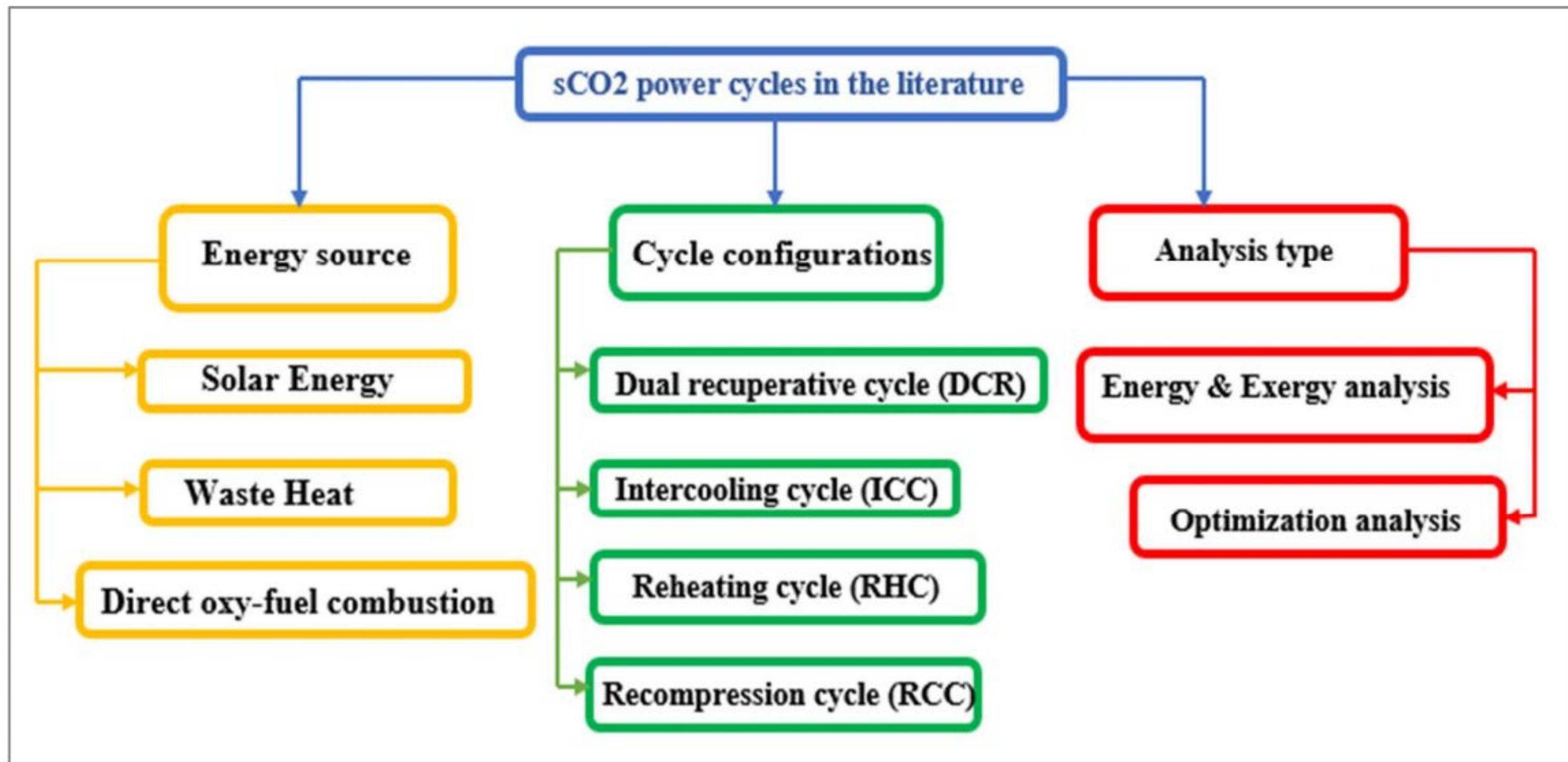


Figure 1: Supercritical CO₂ power cycles in the literature.

The organic Rankine cycle (ORC) may recover and utilize low-grade thermal energy. Recent machine learning ORC performance prediction research are few. This research showed how to utilize machine learning to anticipate and optimize ORC performance. This work uses gradient boosting. Due to its thermophysical qualities, CO₂ is employed in nuclear reactors, power plants, refrigeration, and air conditioning systems. These correlations and their applications can provide valuable insight into thermal design and heat exchanger optimization, notably in thermal power plants. Supercritical CO₂ pressure drop, convective heat transfer, buoyancy influence, and wall temperature distribution are explained. Application, experimental, and numerical investigations for a unique heat transfer correlation for sCO₂ may be applied for a wide range of operational parameters, including micro- to macro-tube size, mass flow, heat flux, temperature, and pressure. P. Li, Z. Qiao et al. [23] examined using a combined supercritical CO₂ Brayton and organic Rankine cycle (sCO₂-ORC) to harness solar energy. The thermodynamic performance is estimated using a solution approach. When employing CO₂-Enhanced Geothermal System (EGS), the sCO₂-ORC combined cycle performs thermodynamically at the highest level. R218, RC318 and R245ca are the best working fluids for supplementary heat sources.

2.2 CSP plants integrated with sCO₂ power cycles

The sCO₂ was heated up directly and utilized as a working fluid and a heat transfer medium in four different power cycle architectures connected to a central receiver to evaluate the impact of turbine input temperature.[24] A thermal energy storage system using molten salt technology was used to thoroughly investigate the system performance of several solar-assisted sCO₂ power cycles.[25] Multiple solar-assisted sCO₂ closed-loop Brayton cycle configurations with recuperation and recompression were used extensive exergetic analysis.[26] The highest thermal efficiency of 55.2% at 850 °C and the best performance were found in the recompression cycle, according to their findings. For central solar receiver systems, the sCO₂ recompression cycle they proposed might be a strong contender[21].

Ma et al.[27] described the dynamic models that were used to report on how ambient air temperature and solar energy input influenced the operation of directly heated sCO₂ Brayton cycles in the winter and summer. In order to utilize solar electricity throughout various seasonal fluctuations, Ehsan et al. [28] mentioned the study of the recompression cycle's fluctuations. Based on the overall plant efficiency, the impact of the mass flow rate, operating pressure, effective recuperator area, and the number of compression and expansion stages were examined [29] .

T. Conboy et el. [30] demonstrated a bypass mechanism has been created to enable preheating of the hot-leg prior to full utilization of the turbines. In the test loop, this system avoids reverse flow factors, but when temperatures rise, it must be brought off. Experiment controllers use control concerns and techniques to transition the demonstration loop from cold start-up circumstances to steady-state power generation. When closing down the turbines, it is important to keep regard to the speed balance of the compressors in order to prevent overflow situations. Speeds must be adjusted in order to optimize power output for a given input temperature. Ruiz-Casanova et al. [31] have investigated that this study analyzes the thermodynamic effectiveness of four independent supercritical carbon dioxide Brayton cycles with the aim of producing electricity utilizing a low-grade geothermal resource. Studies demonstrate that, in compared to cycles without intercooling, intercooled cycles can reduce specific compression work under identical conditions of operation. Based to the parametric study, Productivity is not immediately affected by operating pressures or the cycle's lowest temperature. The intercooled recuperated Brayton cycle alternative has the best performance. Chen R et al. [32] studied both off-design and on-design models to analyze the operational efficiency of the power plant for six 10 MW S-CO₂ Brayton cycles. A genetic algorithm was used to identify the optimal layout for each cycle while adhering to the same boundary

design constraints. better complexity cycles showed higher performance degradation as ambient temperature increased but they may also demonstrate increased peak productivity and focused work at the design-point. The intercooling system operated with maximum cycle efficiency within the design specifications. Liu T Y, et al [33] have investigated the effects of cycle structure and the addition of optimization variables on the comparison, along with various efficiency and cost tradeoff criteria. In addition, four arrangements with various compromise decisions are suggested. The outcomes of the design point and cycle efficiency are influenced by multiple optimized factors. When moderate cycle beginning cost predominates ($W_{th} > 0.701$), simple recuperative and reheating cycles are also suggested. Chen R et al. [34] have investigated the importance of the optical and thermal-to-electricity subsystems' design elements and annualized performances is discussed in relation to integrated CSP facilities' overall optimization. For a STP system with a solar field, a SCO₂ Brayton cycle, a UBFB particle receiver, and particle storage, it constructed a component-level integral model. Developments in optimal IR and system efficiency can be accomplished by enhancements in heliostat beam efficiency and power block effectiveness.

2.3 Machine Learning Implementation

Khadse et al [35] studies on the thermodynamic parameters of recuperated (RC) and recuperated recompression (RRC) S-CO₂ Brayton cycle configurations for exhaust heat recovery from a next-generation heavy-duty simple cycle gas turbine. The major objective is to extract as much power as possible from the exhaust stream, and the optimal turbine intake temperature will determine the amount of CO₂ that must be flowed and the boundary conditions for the main heat exchanger. This research suggests a machine learning-based approach to performance prediction, parameter analysis, and optimization. The strategy was inspired by machine learning, which was used to forecast the chemical characteristics of MOF materials.[36] A back propagation neural network (BPNN) is used by the ORC system for recovering waste heat from diesel engines to anticipate the output power, evaporator outlet exhaust temperature, and heat exchanger efficiency. [37]This method is based on Meng et al.'s idea of using machine learning to forecast the chemical properties of MOF materials and their use of Back Propagation Neural Network (BPNN) to predict the performance of the heat exchanger.[38]

Siddique et al.[39] studies on determining which of four machine learning (ML) algorithms—linear regression (LR), gradient-boosted regression tree (GBRT), K nearest neighbor (KNN), and artificial neural

networks (ANN)—makes the best accurate predictions concerning CCGT power. The prediction is based on four CCGT-related variables: ambient inlet air temperature, atmospheric pressure, relative humidity, and vacuum (exhaust pressure of the gas turbine). Results are predicted using the machine learning and data mining software suite Rapid Miner. It displays the recommended architecture for CCGT power prediction using ML algorithms.[40]

Tufekci et al.[41] studies regression approaches are designed as learning algorithms to predict the full load electrical power output of a combined gas and steam turbines. The dataset is seen as a pair (X_i, Y_i) , which is referred to as an instance. a regression method that develops a mapping function using machine learning.

2.4 Multi-objective performance optimization

This work's operational parameter ranges have been used to neuro-genetic optimization. The ideal characteristics of the researched power plant configuration are determined in two phases using a neuro-genetic method.[42] Assuming standard ranges, the first stage involves establishing the optimized values of operating parameters like excess air ratio, IP turbine (reheat steam) pressure/temperature, and LP turbine pressure, while the second stage involves establishing the optimized extraction pressures of turbine bleed streams to feedwater heaters (FWHs).

In this study the steam turbine power plant that was optimized and thermo-economically modeled is explored. Data from currently operational power plants are utilized for modeling, results verification, and optimization. The quick and elitist Non-dominated Sorting Genetic Algorithm (NSGA-II) is used to apply 15 design variables to concurrently enhance thermal efficiency and reduce overall cost rate. When compared to the actual data of the operating powerplant, the optimization findings demonstrate a simultaneous gain in efficiency of 3.76% and drop-in overall cost rate of 3.84%. The Artificial Neural Network (ANN) is used to demonstrate a correlation between two goals and fifteen choice factors with sufficient accuracy[43]. A unique triple cascade waste heat recovery system with a supercritical CO₂ power cycle and a transcritical CO₂ regeneration cycle is described for high temperature exhaust waste heat produced while a gas turbine is running in J. Du et al[44].

The heat exchanger contributes to a significant amount of energy loss in the integrated system's thermal performance, and the turbine, compressor, and other work-producing components have significant capital expenses. The target functions for the system's optimization with a variety of goals include the net power production, energy efficiency, and cost per unit of energy. The multi-objective system optimization based

on variables sensitivity analysis employs the NSGA-II algorithm and TOPSIS decision. An artificial neural network with many layers was utilized to model the Afyon Geothermal Power Plant. The 100% data set that was obtained from the real Binary Geothermal Power Plant was divided into 80% training data and 20% test data. The system of the geothermal power plant was numerically modeled using three inputs and five outputs. The results are supplied together with the outputs from the Artificial Neural Network-based Binary Geothermal Power Plant system. The plant's mass flow rates and geothermal water temperature are 110 C and 150 kg/s, respectively, while its energy and exergy efficiencies are 10.4% and 29.7%.

The optimal simple payback period and exergy cost for the plant's electricity are predicted to be 2.87 years and 0.0176 USD per kWh, respectively[45]. Q. Jin et al.[46] developed a model using time-dependent thermodynamics and a neural network model using data samples. Cycle thermal efficiency, net power production, sustainability function, and exergy efficiency are the goals of multi-objective optimization. The results of the decision-making process employing the Shannon Entropy methodology have a lower deviation index, and the outcomes of the TOPSIS and LINMAP techniques are likewise consistent with one another.

Chapter 3: Description of the model

3.1 Supercritical CO2 Brayton Cycle Configuration

All heat exchangers and devices (compressors and turbines) were mass, energy, and exergy balanced for the thermodynamic study of the supercritical CO2 Brayton cycle designs. To determine if a temperature pinch point problem exists, [47] discretized the heat exchangers. An effectiveness factor for the whole hot stream was taken into account for setups with the LTR, and the HTR was simulated by assuming a heat exchanger effectiveness [16]. Split ratio is another crucial factor in S-CO2 Brayton cycles with LTR. (SR), which is the proportion of the total mass flow rate of the S-CO2 Brayton cycle to the mass flow rate of the cold stream entering the LTR. An energy balance on the LTR determines the SR, which is used to compute thermal performance and compression power. Table 2 demonstrates the key features of each setup. There is a thorough explanation of each cycle by Padilla et al. [48]

Table 2: Description of the S-CO2 Brayton cycles.

Cycle	Compressor intercooling	Recuperators	Recompressor	Description
RC	No	HTR & LTR	Yes	Brayton cycle modified. Splitting the LTR's hot steam reduces the cold stream's heat capacity. An additional compressor is used.
PC	Yes	HTR & LTR	Yes	Brayton cycle modified. Splitting the stream exiting the main compressor reduces the cold stream's heat capacity. To minimize compressor input power, an intercooling phase was added to the split fraction sent to the LTR. Recompressor is utilized in this configuration.
MC	Yes	HTR & LTR	Yes	A modified RC cycle. After the MC is introduced, an intercooling step is added to lower the power input to the compressors.

3.1.1 Recompression cycle

The Simple Brayton cycle has a pinch point issue, which reduces cycle efficiency, since the hot and cold fluid streams have different heat capacities. To solve this problem, the recompression cycle also includes the low temperature recuperator and the recompression compressor. The recompression compressors receive a fraction of the working fluid's total mass flow rate (sCO₂)[49].

The mass flow rate through the high-pressure stream compared to the low-pressure stream is decreased by the recompression cycle. This is accomplished by separating the low-pressure stream into two distinct streams after it leaves the low-temperature recuperator, which are subsequently compressed in the precooler and main compressor[50].

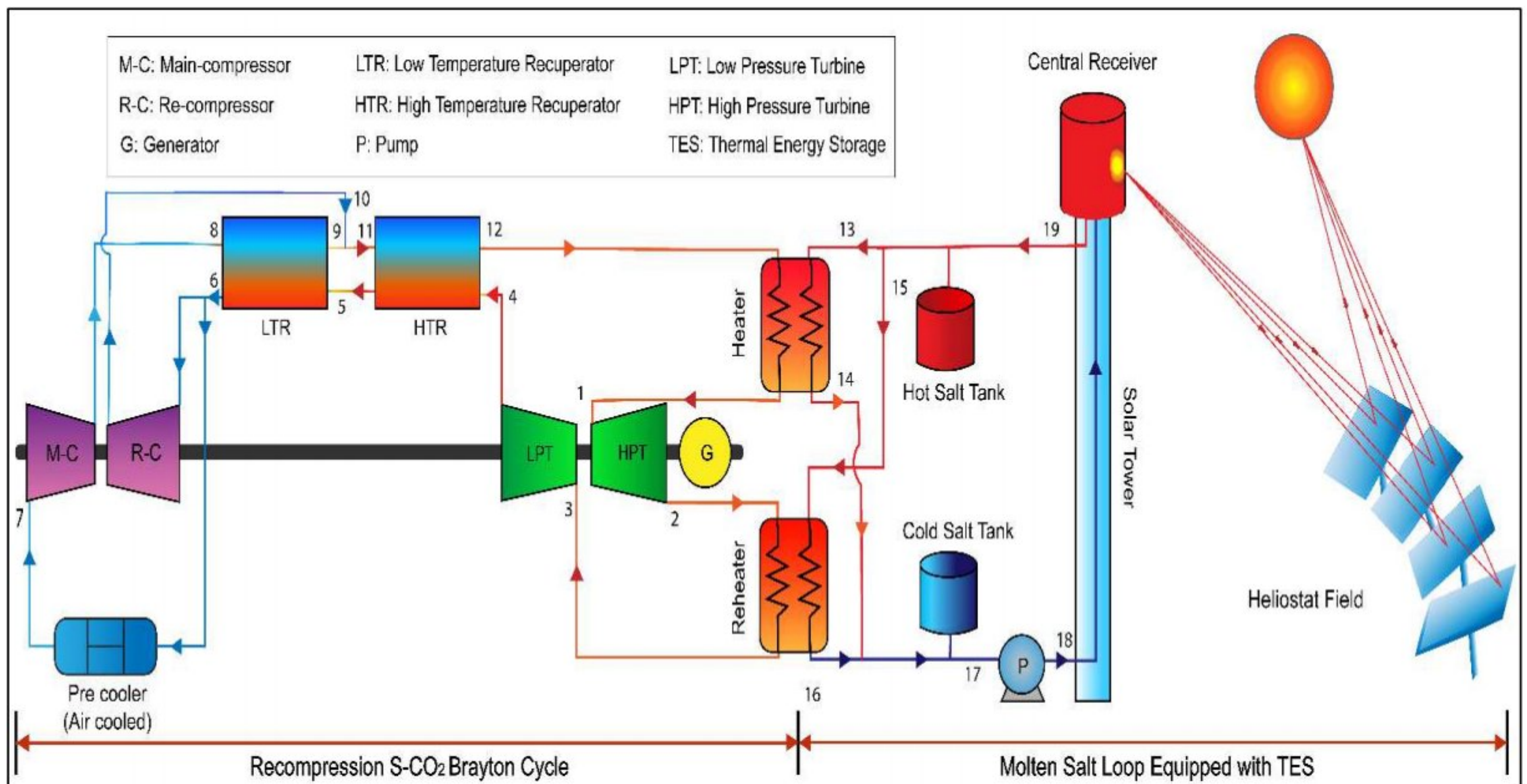


Figure 2: Cycle layout of Recompression sCO₂ cycle equipped with TES.

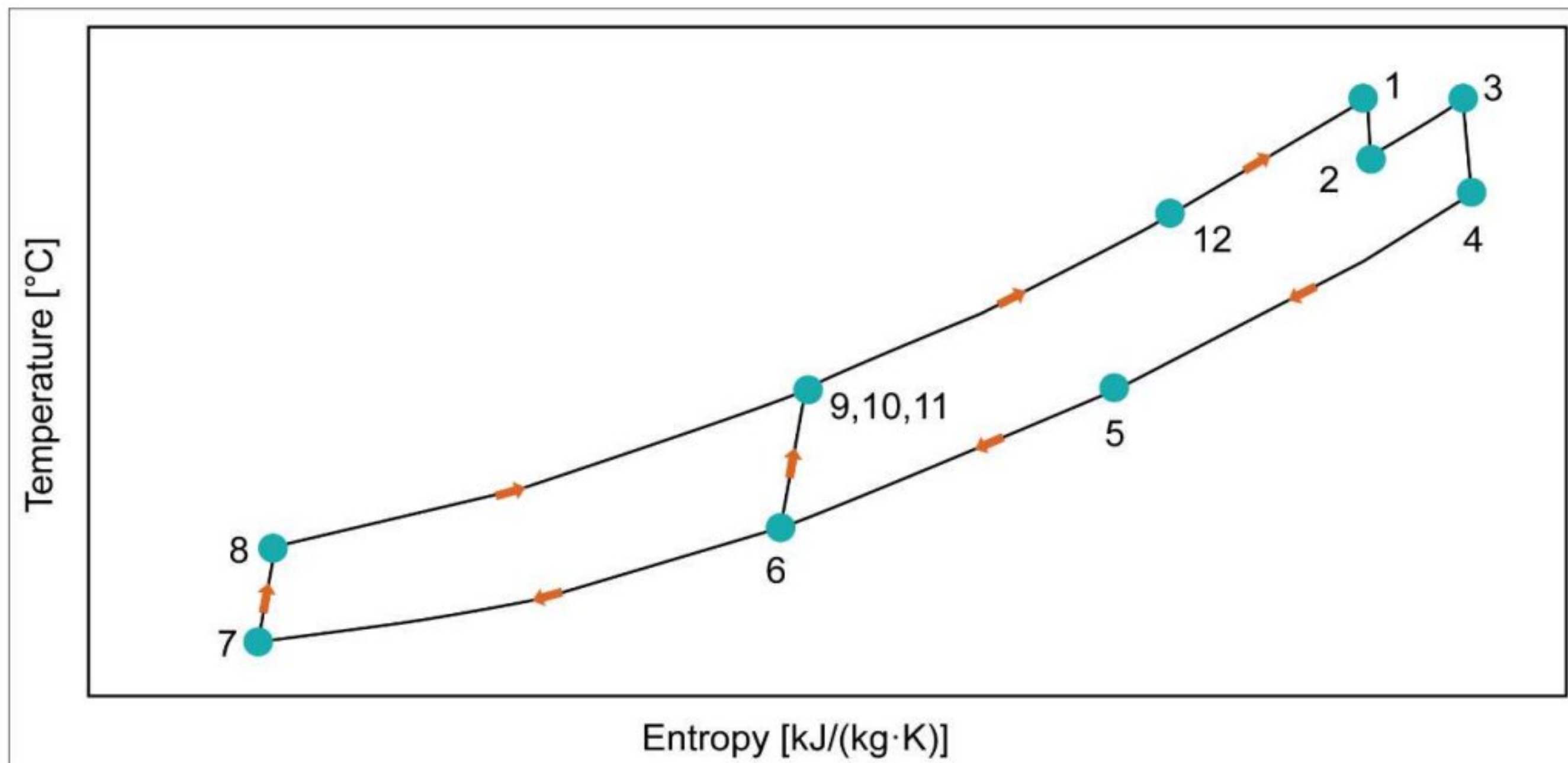


Figure 3: T-s diagram of Recompression sCO₂ cycle equipped with TES.

3.1.2 Partial Cooling cycle

The sCO₂ Simple Brayton cycle's cycle efficiency may also be increased by partial cooling. The partial cooling cycle is analogous to the intercooling cycle in terms of the parts of the turbomachinery and the number of heat exchangers. A low-temperature recuperator's working fluid stream flows mostly in the pre-cooler's direction during partial cooling.[51]

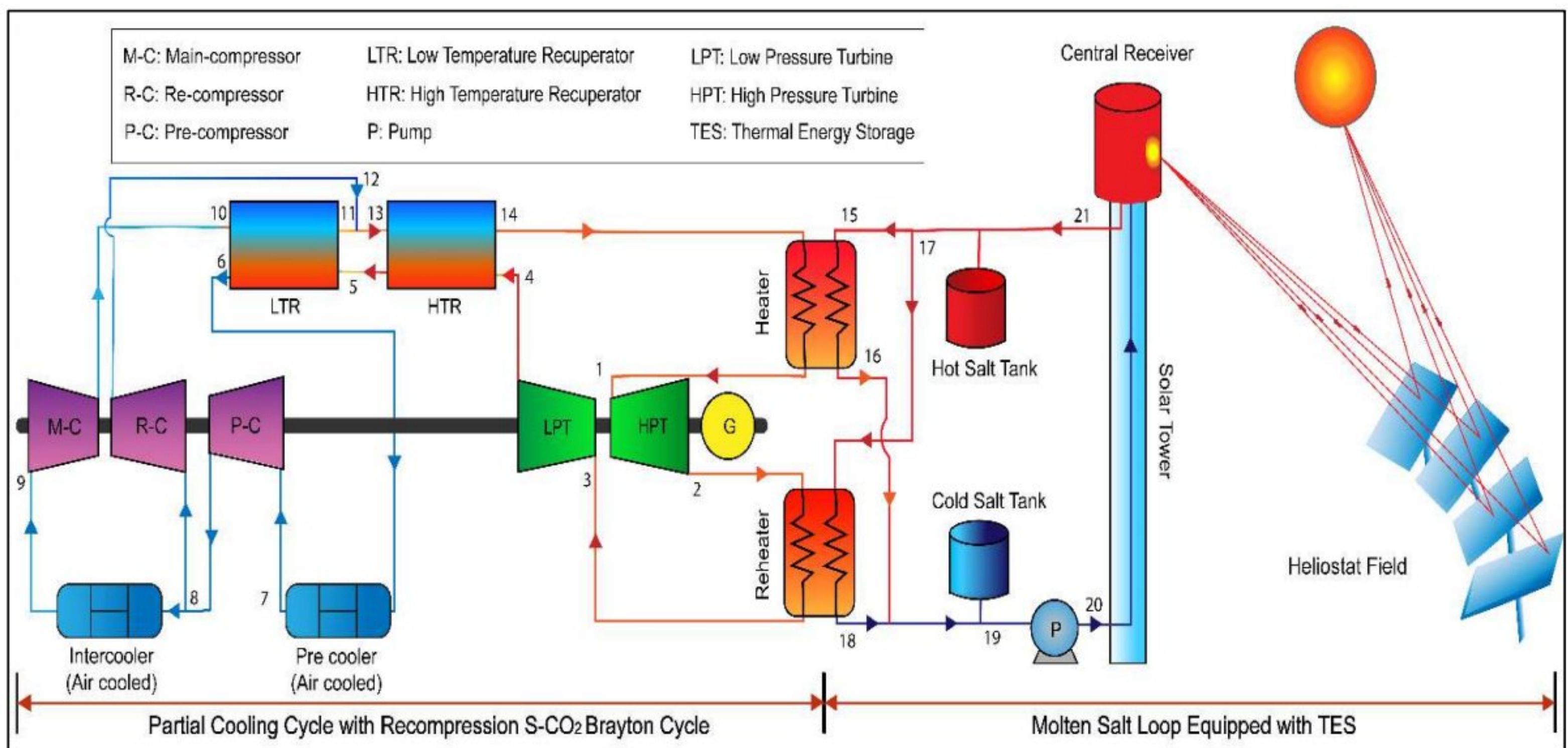


Figure 4: Cycle layout of Partial Cooling sCO₂ cycle equipped with TES.

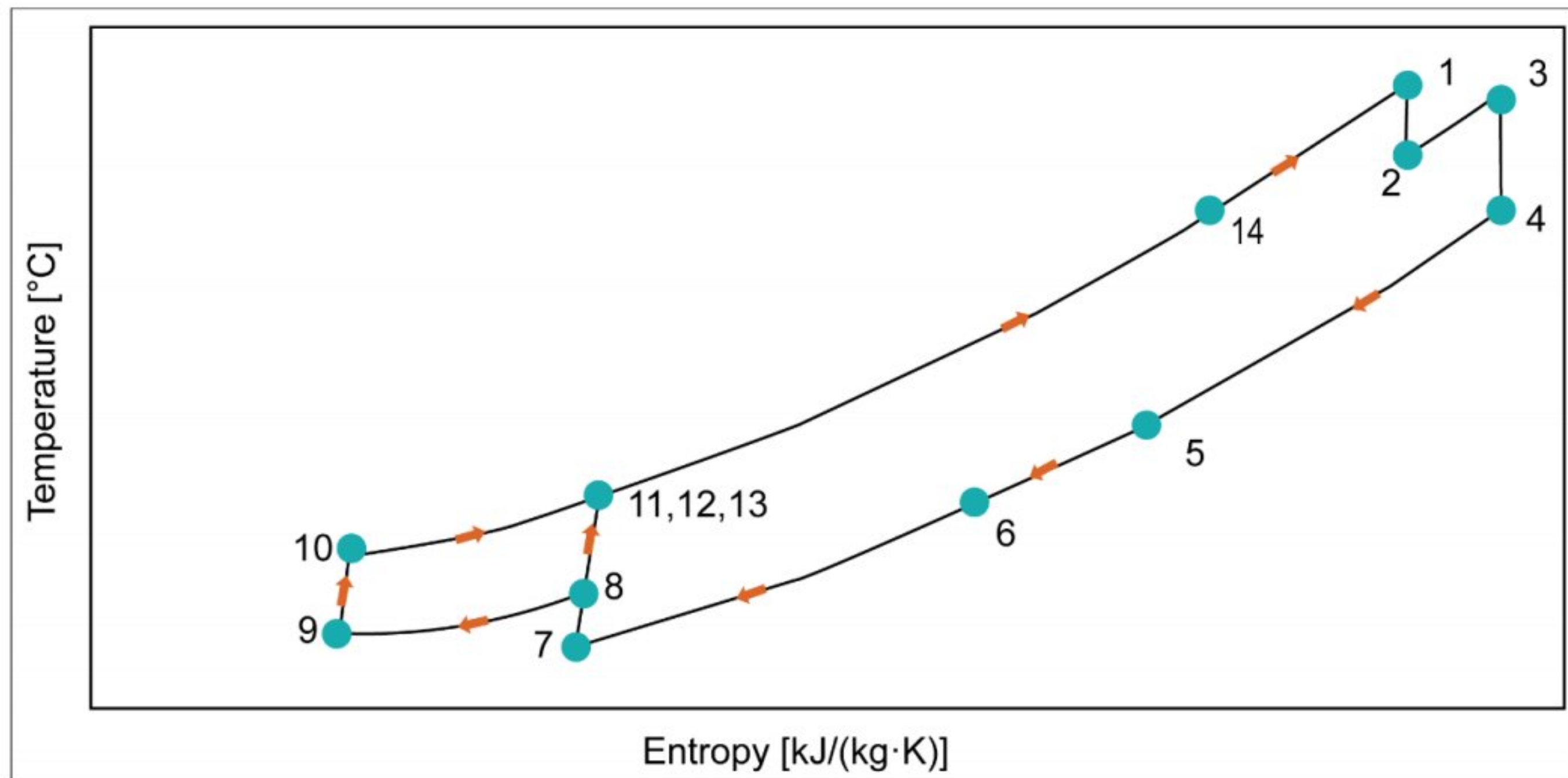


Figure 5: T-s diagram of Partial Cooling sCO₂ cycle equipped with TES.

One possible intercooling recompression configuration divides the stream after the pre-compressor. Before it enters the pre-compressor, the turbine exhaust flow is cooled by a pre-cooler. One can see split flow coming out of the pre-compressor.[52] One route serves the re-compressor, while the other serves the primary compressor, intercooler, and re-compressor. Because the pre-compressor's inlet pressure is at an intermediate pressure after it, the re-compressor is used for a portion of the turbine pressure ratio.[53]

3.1.3 Main Compression Inter Cooling cycle

In Main compression Intercooling Cycle one way to conceptualize it is as two distinct intercooling stages that are separated from the primary compressor. The main compressor receives the working fluid under significant pressure and temperature conditions.[54] Before entering the main compressor, the portion of the stream leaving the pre-cooler passes through an intercooling stage and a compressor that is operating at a significantly lower pressure. The recompression cycle's heat recovery procedure is the same as what was previously described for that cycle.[55]

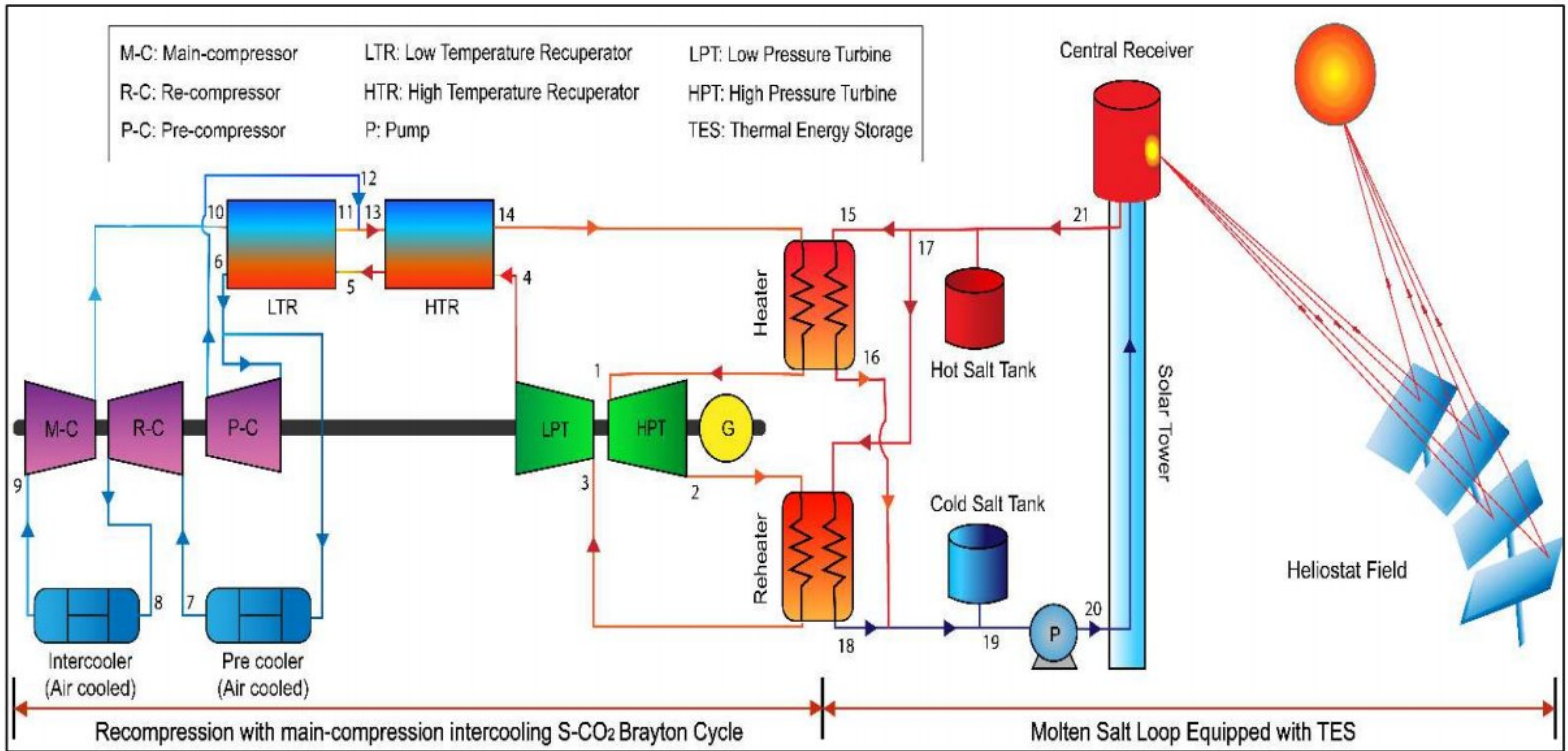


Figure 6: Cycle layout Main Compression Inter Cooling sCO₂ cycle equipped with TES.

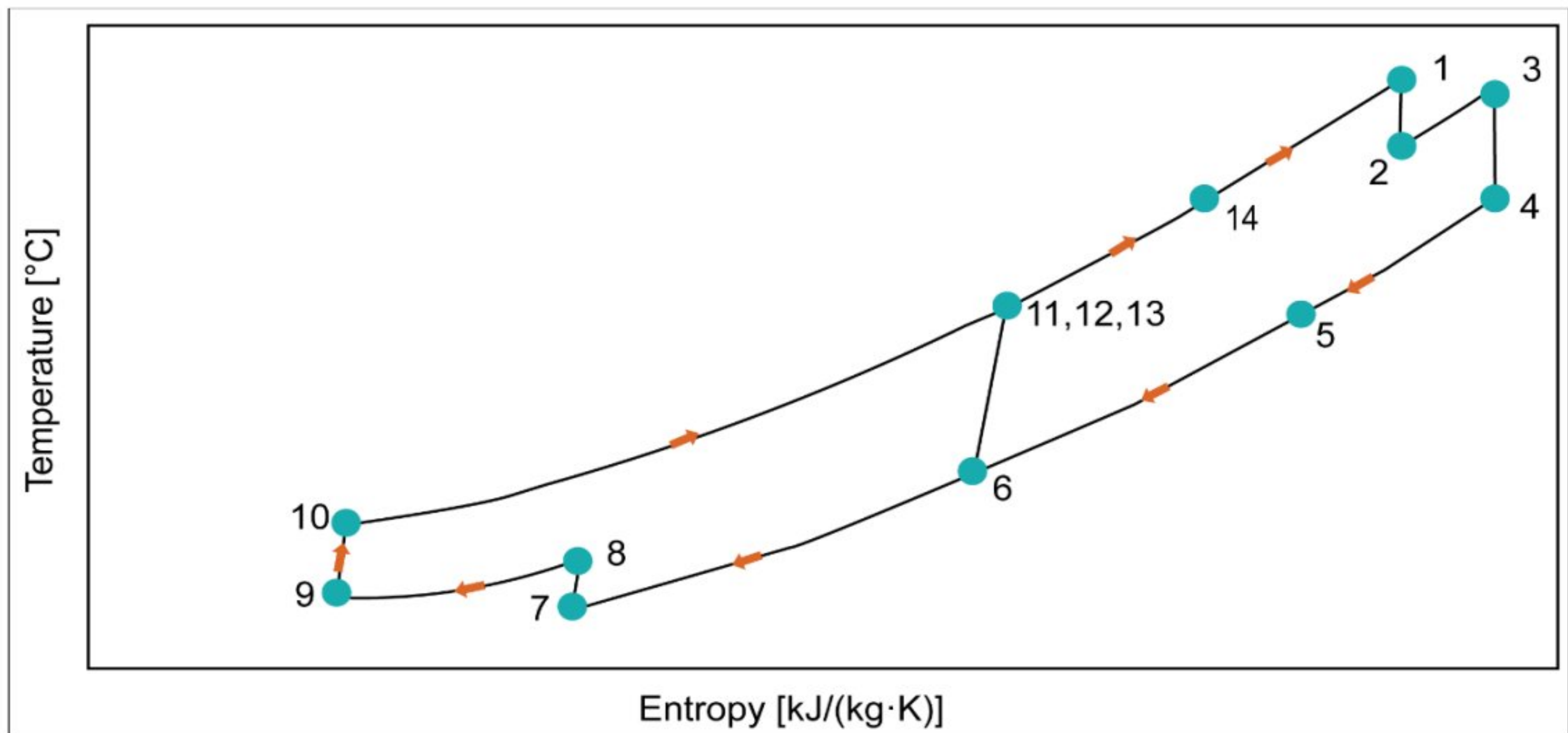


Figure 7: T-s diagram of Main Compression Inter Cooling sCO₂ cycle equipped with TES.

The exit pressure of the turbine is the same as the input pressure of the re-compressor. What unites them is the idea that both the intercooling cycle and the recompression cycle involve multistage compression with intercooling.[56]

3.2 Designing CSP Loop at Optimum Condition

3.2.1 Sizing the Heliostat Field

Shahin M. et al [57] proposes a concept that incorporates a traditional Rankine cycle for the generation of electrical and thermal energy with a sun extracting system comprising sensors that heat a heat transfer fluid. The suggested framework is subjected to a thermodynamic study to assess and enhance its effectiveness. To find out the impact of various features and operating characteristics on the total efficiency and power output, a parametric analysis is conducted. To choose the best alternative to pair with the suggested model, a comparison of the parabolic trough and the heliostat field is offered. The results demonstrate that the heliostat field outperforms the parabolic trough in terms of performance.

The heliostat field and the receiver formed the solar subsystem. The heliostat field is formed up of several heliostats, each having an aperture area of A_{hel} , which focuses and reflects solar radiation into the receiver. The sun's direct normal irradiance (DNI) and the heliostat field efficiency determine how much solar thermal energy enters the receiver.[58]

To be able to improve accuracy and reduce capital costs, it is crucial to size a solar tower power plant with thermal energy storage properly. To determine the thermo-economic efficiency of the system under various solar resources, key design variables including model direct normal irradiance, solar wide-ranging, and thermal storage hours have been investigated. Since it accounts for 40% of energy losses and 50% of the power plant's overall costs, the heliostat field's ideal design is particularly essential [59].

$$\eta = \eta_{cos} \times \eta_{att} \times \eta_{int} \times \eta_{s\&b} \times \eta_{ref}$$

The effectiveness of the cosine effect, atmospheric attenuation, interception, shading and blocking, and the heliostats' reflectivity are all represented by the equations η_{cos} , η_{att} , η_{int} , $\eta_{s\&b}$ and η_{ref} . The astigmatic effect, tracking error, mirror slope error, and sun-shape error all affect how well objects are intercepted. The placement of the heliostats, the orientation of the sun, and the relative positions of surrounding heliostats all affect $\eta_{s\&b}$, making it the parameter that requires the most calculation.

The heat flux that enters the aperture region of the solar receiver circulated to the molten salt solution. Some optics, convective, and irradiation losses happen along the path from the aperture to the molten salt.[60]

3.2.2 Selection of Hot Salt

Solar salt, a composition of $\text{NaNO}_3/\text{KNO}_3$ wt.% of (60/40) having heat capacity of $1.55 \text{ kJ kg}^{-1} \text{ K}^{-1}$ is considered as TES material in CSP because of having melting point 240°C & considerate cost 0.5-1 (\$/kg) [61].

3.2.3 TES

Systems for thermal energy storage (TES) have grown in significance as a result of their ability to improve energy efficiency and incorporate renewable energy sources. However, research is being done on how storage material characteristics affect system performance. Concentrating solar power, or CSP, makes it possible to integrate simple, efficient, and cost-effective thermal energy storage (TES) by turning solar energy into heat as an extra step before creating electricity. The system designs that have been used up till now for reasonably priced CSP TES systems are the two-tank TES and steam accumulator.

Stekli et al [62] described the energy extracted from the system must also be at the highest temperature feasible for contact with the thermodynamic power cycle, whose performance is controlled by Carnot efficiency. A CSP TES system's capacity to do work is reduced and less thermal energy can be turned into electricity, which lowers exergetic efficiency, if the discharge temperature is lower than the temperature at which the system was charged.

Although PCM-based TES systems suffer from poor thermal conductivity, they offer great latent heat storage capabilities. While they may need to operate at greater temperatures, molten salts offer better heat transfer capacities. High energy density and long storage times are features of thermochemical storage materials; however, system complexity and reaction kinetics provide difficulties. Latent heat storage (LHS) systems use temperature-invariant phase changes to store heat. Organic and inorganic substances, as well as their eutectics and combinations, are classified as phase change materials (PCMs). Due to their extreme melting points and elevated energy densities, PCMs including carbonates, fluorides, and chlorides are a few examples that are suited for CSP storage. Although several LHS storage arrangements have been studied, the shell and tube PCM structure is the most practical and popular one[63].

Steam accumulators store heat through sensible heat storage, which takes the form of pressured, saturated water. The cycle's excess steam is pumped into a pressurized vessel filled with liquid water to start the process of charging. When the saturated liquid fills 90% of the tank, the system has been fully charged. The most often used horizontal accumulators have a wide water surface area and an elevated water level.[64]

Chapter 4: Computational Methodology

4.1 Thermodynamic Equations

The design models of recompression, partial cooling & main compression inter cooling cycle configurations are modified here from prior work in order to examine the performance under off-design conditions. The components of the heat exchanger and turbomachinery's off-design models are then merged with these models and evaluated using real measured climate conditions and variations in power demand, together with data from the literature that is already available. The developed models are based on the following assumptions.

- Except for the solar field components, there are very little heat losses from the cycle components to the ambient air.
- A 360° external cylinder receiver is used to collect more of the light that is reflected from the edge of the solar field.
- All heat recuperators and pipelines ignore pressure drop and friction losses.
- The system's kinetic and potential energy hardly change over time.
- For the two primary compression stages, it is assumed that the input temperatures are same.

The total system is broken down into the solar sub-system and the power cycle for thermodynamic study. Each component of the system has its own thermodynamic model, and the simulation model is programmed in Python programming environment using CoolProp library. The energy and exergy balance equations are written as follows for a control volume following a steady state process:

$$\text{Compressor isentropic efficiency, } n_C = \frac{h_{8,s} - h_7}{h_8 - h_7}$$

$$\text{Turbine isentropic efficiency, } n_T = \frac{h_1 - h_2}{h_1 - h_{2,s}}$$

$$\text{Work input to the compressor, } \dot{W}_C = \dot{m}_{CO_2} (h_8 - h_7)$$

$$\text{Work output from the turbine, } \dot{W}_T = \dot{m}_{CO_2} (h_4 - h_5)$$

$$\text{Heat input by the heater, } Q_H = \dot{m}_{CO_2} (h_1 - h_{12})$$

$$\text{Net work output, } \dot{W}_{net} = \dot{W}_T - \dot{W}_P$$

$$\text{Recuperator effectiveness, } \varepsilon_R = \frac{\dot{m}_{CO_2}(h_4 - h_5)}{Q_{max}}$$

$$\text{Ratio of pressure ratios, } RPR = \frac{\frac{P_{high}}{P_{intermediate}} - 1}{\frac{P_{high}}{P_{low}} - 1}$$

$$\text{Split ratio, } SR = \frac{\dot{m}_9}{\dot{m}_9 + \dot{m}_{10}}$$

$$\text{Thermal efficiency of the cycle, } n_{cyc} = \frac{W_{net}}{Q_H}$$

$$\text{Second law efficiency of the cycle, } n_{exergy} = \left(1 - \frac{X_{dest}}{X_{in}}\right)$$

$$\text{Receiver heat input, } \dot{Q}_{rec,in} = \eta_{cos} \cdot \dot{Q}_{sun} = \eta_{field} \cdot (DNI) \cdot A_{hel} \cdot N_{hel}$$

$$\text{Receiver efficiency, } \eta_{rec} = \frac{\dot{Q}_{rec,net}}{\dot{Q}_{rec,in}}$$

Table 3: Components-wise exergy destruction equation of a main compression intercooling cycle.

Component	Equation
Heater	$X_H = \dot{m}_{CO_2}[(h_{14} - h_1) - T_0 (s_{14} - s_1)] + \dot{m}_{CO_2} \left[1 - \left(\frac{T_0}{T_H}\right)\right] \dot{Q}_H$
Reheater	$X_{RH} = \dot{m}_{CO_2}[(h_2 - h_3) - T_0 (s_2 - s_3)] + \dot{m}_{CO_2} \left[1 - \left(\frac{T_0}{T_{RH}}\right)\right] \dot{Q}_{RH}$
HTR	$X_{HTR} = \dot{m}_{CO_2}[(h_4 - h_5) - T_0 (s_4 - s_5)] + \dot{m}_{CO_2}[(h_{12} - h_{14}) - T_0 (s_{12} - s_{14})]$
LTR	$X_{LTR} = \dot{m}_{CO_2}[(h_5 - h_6) - T_0 (s_5 - s_6)] + \dot{m}_{CO_2}(1 - SR)[(h_{10} - h_{12}) - T_0 (s_{10} - s_{12})]$
Main compressor	$X_{MC} = SR \cdot \dot{m}_{CO_2}[(h_9 - h_{10}) - T_0 (s_9 - s_{10})] + W_{MC}$
Re-compressor	$X_{RC} = (1 - SR) \cdot \dot{m}_{CO_2}[(h_6 - h_{12}) - T_0 (s_6 - s_{12})] + W_{RC}$
Pre-compressor	$X_{PC} = \dot{m}_{CO_2}[(h_7 - h_8) - T_0 (s_7 - s_8)] + W_{PC}$
HPT	$X_{HPT} = \dot{m}_{CO_2}[(h_1 - h_2) - T_0 (s_1 - s_2)] - W_{HPT}$
LPT	$X_{LPT} = \dot{m}_{CO_2}[(h_3 - h_4) - T_0 (s_3 - s_4)] - W_{LPT}$
Pre-cooler	$X_{PCL} = SR \cdot \dot{m}_{CO_2}[(h_6 - h_7) - T_0 (s_6 - s_7)]$

Intercooler	$X_{ICL} = SR \cdot \dot{m}_{CO_2} [(h_8 - h_9) - T_0 (s_8 - s_9)]$
Exergy input	$X_{in} = \dot{m}_{CO_2} [1 - \left(\frac{T_0}{T_1}\right)] \dot{Q}_H + \dot{m}_{CO_2} [1 - \left(\frac{T_0}{T_3}\right)] \dot{Q}_{RH}$
Total Exergy destruction	$X_{dest} = X_H + X_{RH} + X_{HTR} + X_{LTR} + X_{MC} + X_{RC} + X_{PC} + X_{HPT} + X_{LPT} + X_{PCL} + X_{ICL}$

4.2 Model Validation

Independent validation was performed on the mathematical models for the REC, PAR and INT SCO₂BC. The previous literature and Reference respectively, were used to validate the models under the identical operating conditions as the relevant literature. Figure 14 & Figure 15 provided the REC, PAR and INT's computed thermal efficiency with variation of MCIT & TIT respectively. At the same operating conditions, calculated thermal efficiencies for all three cycles were found to be quite similar to the literature. Results are compared with previous studies to validate the model.

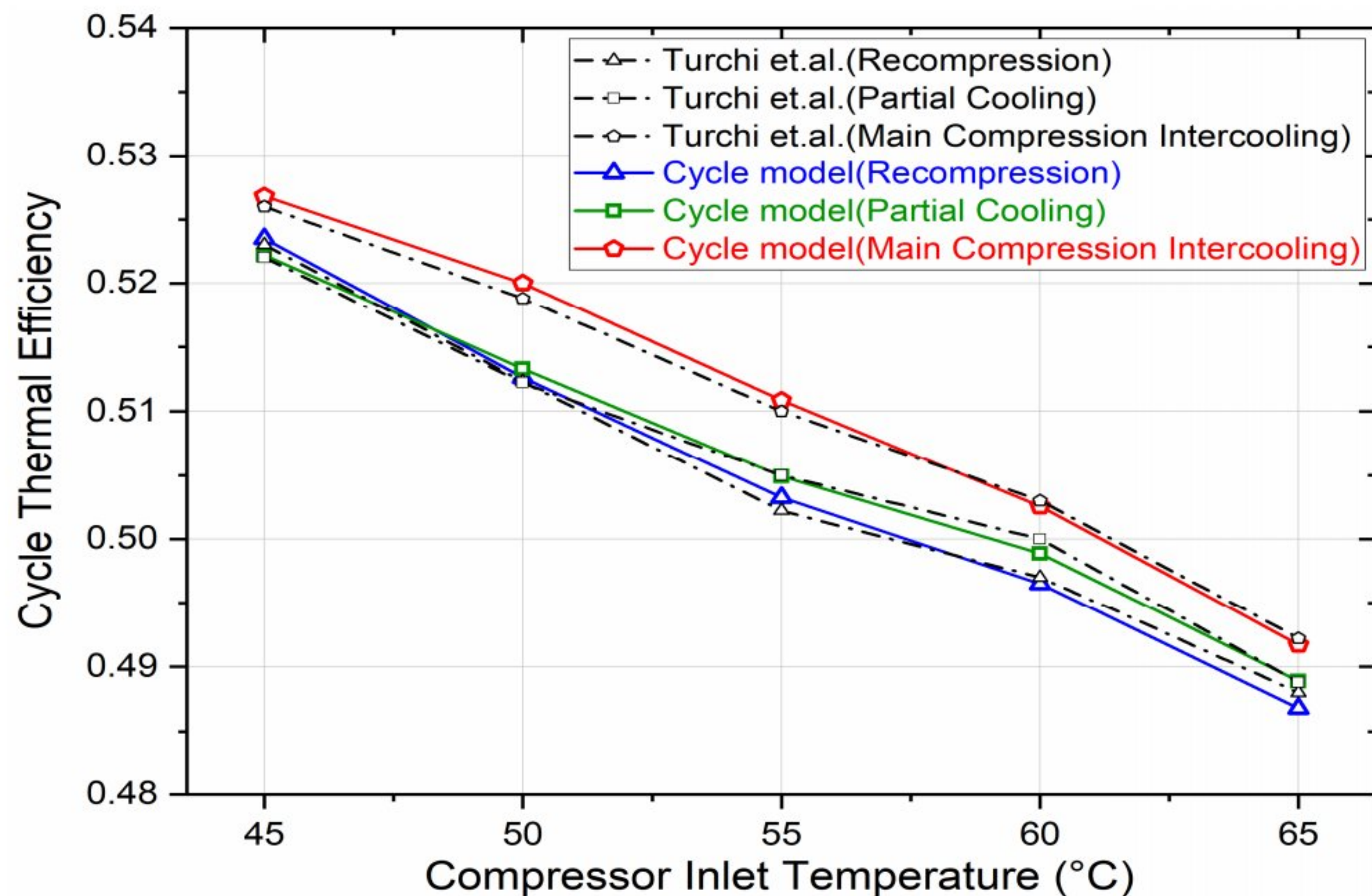


Figure 8: Cycle model validation for MCIT variation.

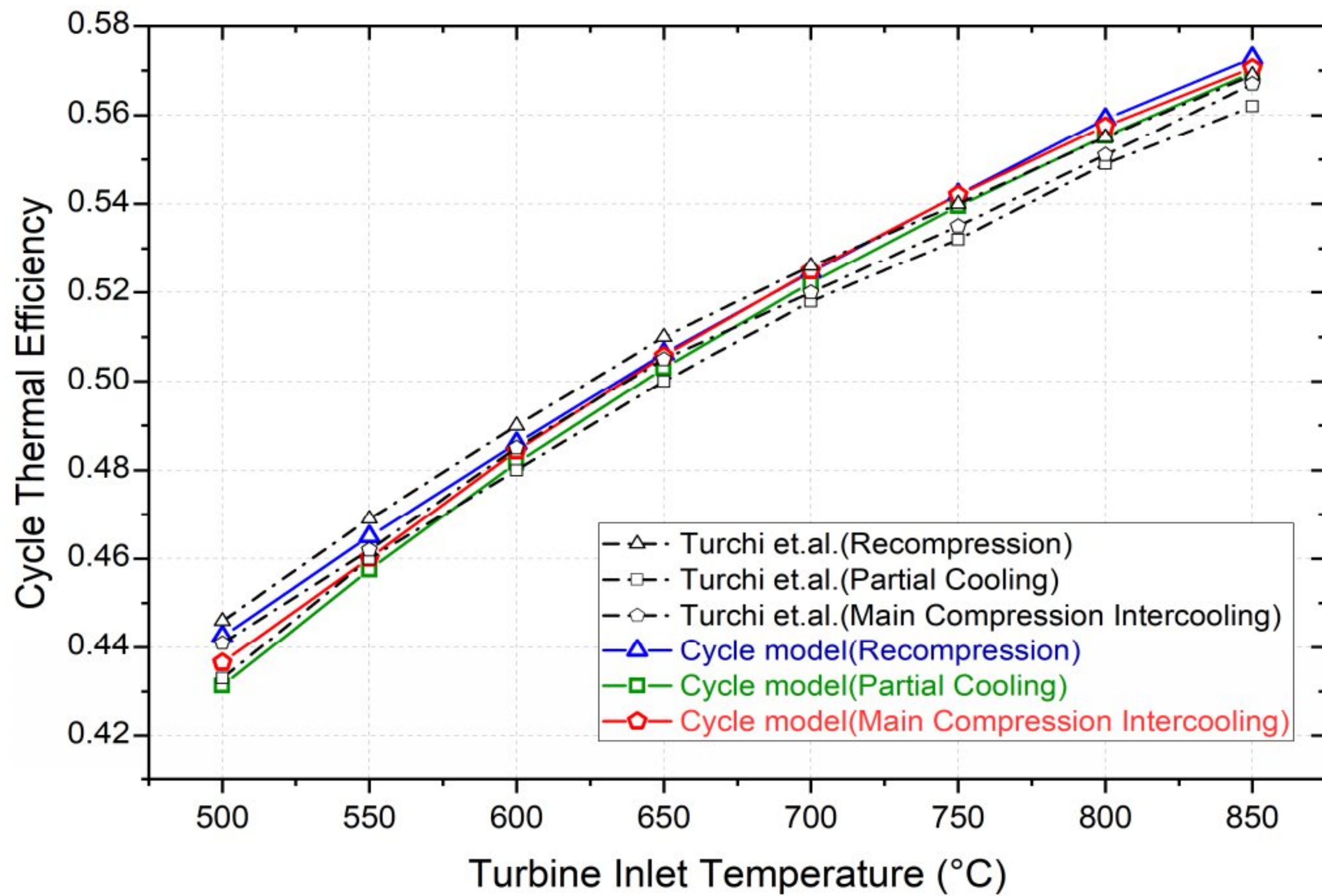


Figure 9: Cycle model validation for TIT variation.

The model has good agreement when compared to the literature. Due to variations in the recuperator representation, there is a little departure from the literature. Unlike the current study, where the temperature difference constraint in the LTR is fixed, the literature models recuperators by determining the heat exchanger effectiveness.

The intermediate pressure's setting is responsible for the additional variation. For each condition set in the current investigation, the intermediate pressure is optimized. The method used to determine the intermediate pressure in previous studies is not specified. This tested model offers a method for simulating a concentrated solar power system with sCO₂ power cycles.

Cycle Design Parameters

Table 4: Initial parameters for simulation and analysis of system performance

Maximum pressure	25 MPa
Turbine inlet temperature	600 °C
Minimum pressure	8 MPa
Main compressor inlet temperature	34 °C
Pinch temperature	7 °C
Mass flow rate of the S-CO ₂ cycle	1 kg/s
Effectiveness of HTR	0.97
Effectiveness of LTR	0.88
Compressor isentropic efficiency	0.89
Turbine isentropic efficiency	0.90

Table 5: CSP loop Design Parameters

Parameters	Symbol	Value	References
Direct normal irradiance	DNI(W/m ²)	600	[58], [65]
Cosine effect efficiency	η_{cos}	0.8267	[58], [59]
Shading and blocking efficiency	$\eta_{s\&b}$	0.9698	[58], [59]
Interception efficiency	η_{int}	0.971	[58], [59]
Atmospheric attenuation efficiency	η_{att}	0.9383	[58], [59]
Reflectivity efficiency of heliostat	η_{ref}	0.88	[58], [59]
Number of heliostats	N_{hel}	624	[58], [59]
Reflective area of each heliostat	$A_{hel}(m^2)$	9.45 x 12.84	[58], [59]
Receiver aperture area	$A_{rec}(m^2)$	68.1	[58], [59]

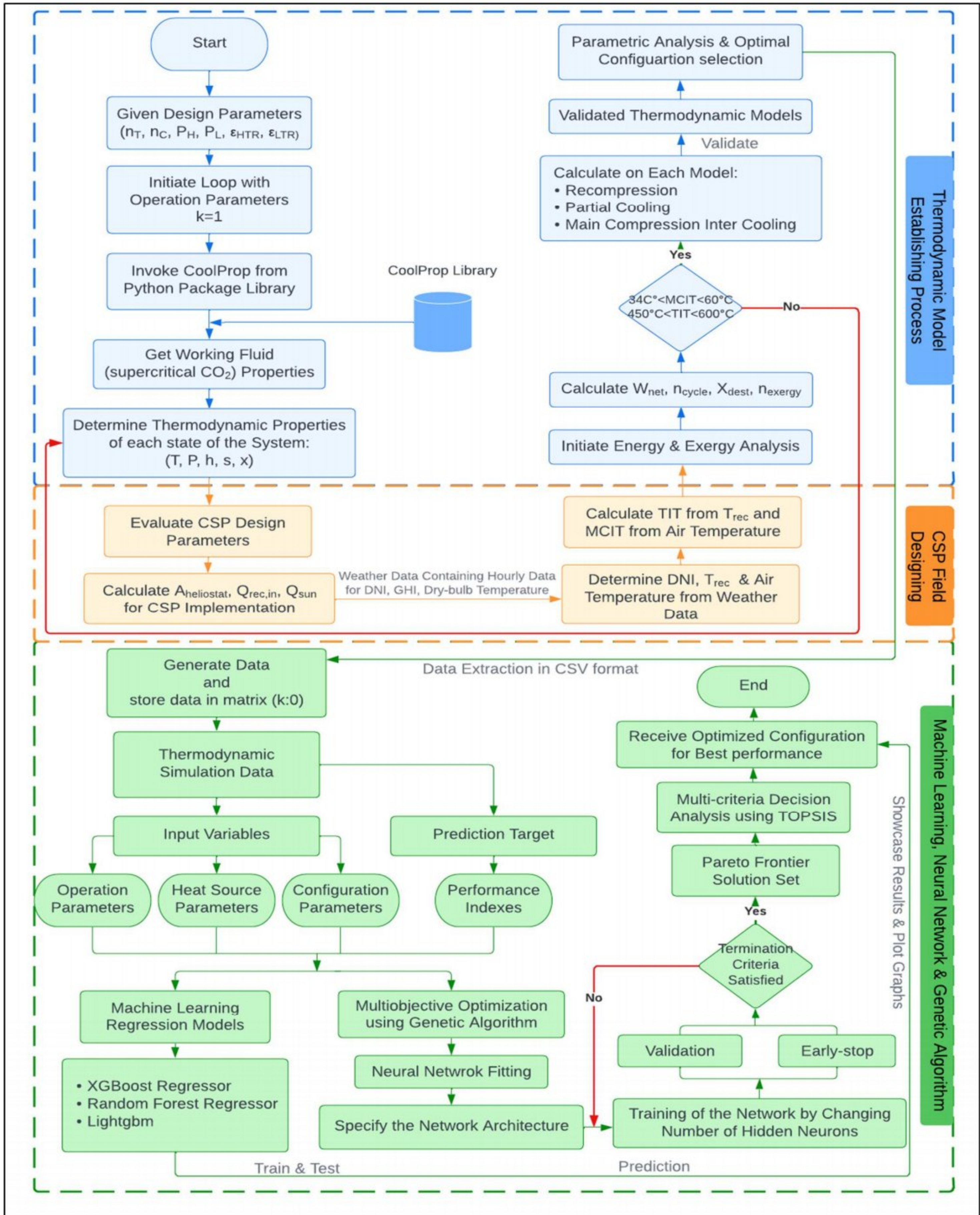


Figure 10: Flow chart demonstrating cycle modelling, data extraction & performance optimization.

Fig 10 shows the advanced SCO2BC with CSP system design methodology of this research. The procedure is established by a standard thermodynamic model (shown in blue). Input of the operation parameters into these verified thermodynamic models for calculation is the first step in the conventional system design process. And each model should go through this calculating process again. CSP loop is integrated (shown in orange) with the main cycle to visualize changes in TIT with DNI variation. Better performance indicators are obtained through analysis and optimization of the output findings. After evaluating the performance indicators of several setups, the best configuration may finally be manually chosen. The same procedure for creating thermodynamic models is part of a machine-learning (show in green) approach to goal-oriented design. Following the generation of numerous sets of simulation data, a machine-learning regression model is trained using this data to predict performance indicators of systems, such as the net output power, exergy destruction and cycle thermal efficiency. In this study, a collection of Pareto frontier solutions is generated by combining the regression model with genetic algorithms. Then, using this set of Pareto optimization results, TOPSIS is utilized to determine which configuration is best for the given parameters.

4.3 Machine Learning Prediction Models

4.3.1 Random Forest Regressor:

The supervised learning approach used in machine learning includes the Random Forest algorithm. A model for accurate prediction of incoming input data is initially constructed in a supervised learning model by taking into account the goal value and a known dataset. It is based on the idea of ensemble learning and can be used to solve classification and regression issues in machine learning. Random Forest significantly use several distinct decision trees as opposed to depending on a single decision tree. With the aid of projections from each tree, the random forest predicts the outcome based on the votes of the majority of projections.

Decision Tree with Regression:

The decision tree is generated using the approach of least squares. After analyzing each of its potential values and identifying the separation point (sp), $x(n)$ is divided into $R1$ and $R2$, two distinct root nodes. Determining the values $c1$ and $c2$ for identifying the minimal value in the output y , respectively, to get the minimum value. This ap is hence the optimal separating point for $x(n)$ is

$$\min_{sp} [\min_{c1} \sum_{xi \in R1} (yi - c1)^2 + \min_{c1} \sum_{xi \in R2} (yi - c1)^2]$$

Based on each node, the output value is being. For instance, for R1, output value of the corresponding is found be:

$$C_{0} = \frac{1}{N_1} \sum_{x_i \in R_1} y_i$$

All output values are being averaged in order to predict the value with the highest degree of accuracy.

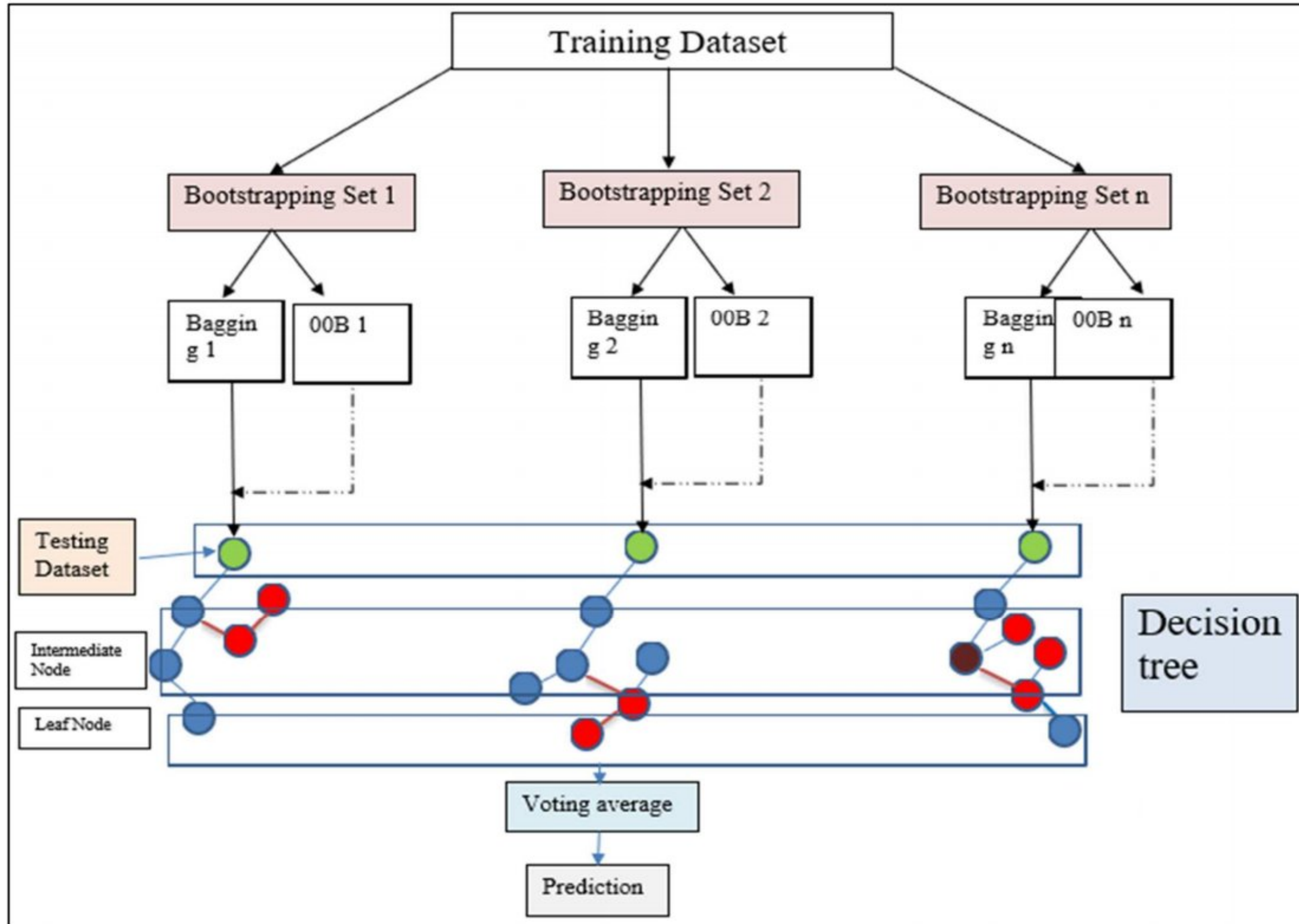


Figure 11: Decision tree diagram.

4.3.2 XGBoost Regressor:

A supervised learning approach called XGBoost integrates the estimates of several simpler variables to attempt to accurately predict a target variable (weaker one). In weaker models, regression trees act as the weak learners and each one converts an input data point to a leaf that outputs a continuous score. incorporating fresh trees that anticipate the residuals or errors of previous trees into the prior trees to obtain the final prediction. XGBoost minimizes a regularized (L1 and L2) objective function with a convex loss

function (based on the difference between the predicted and target outputs) and a penalty term for model complexity.

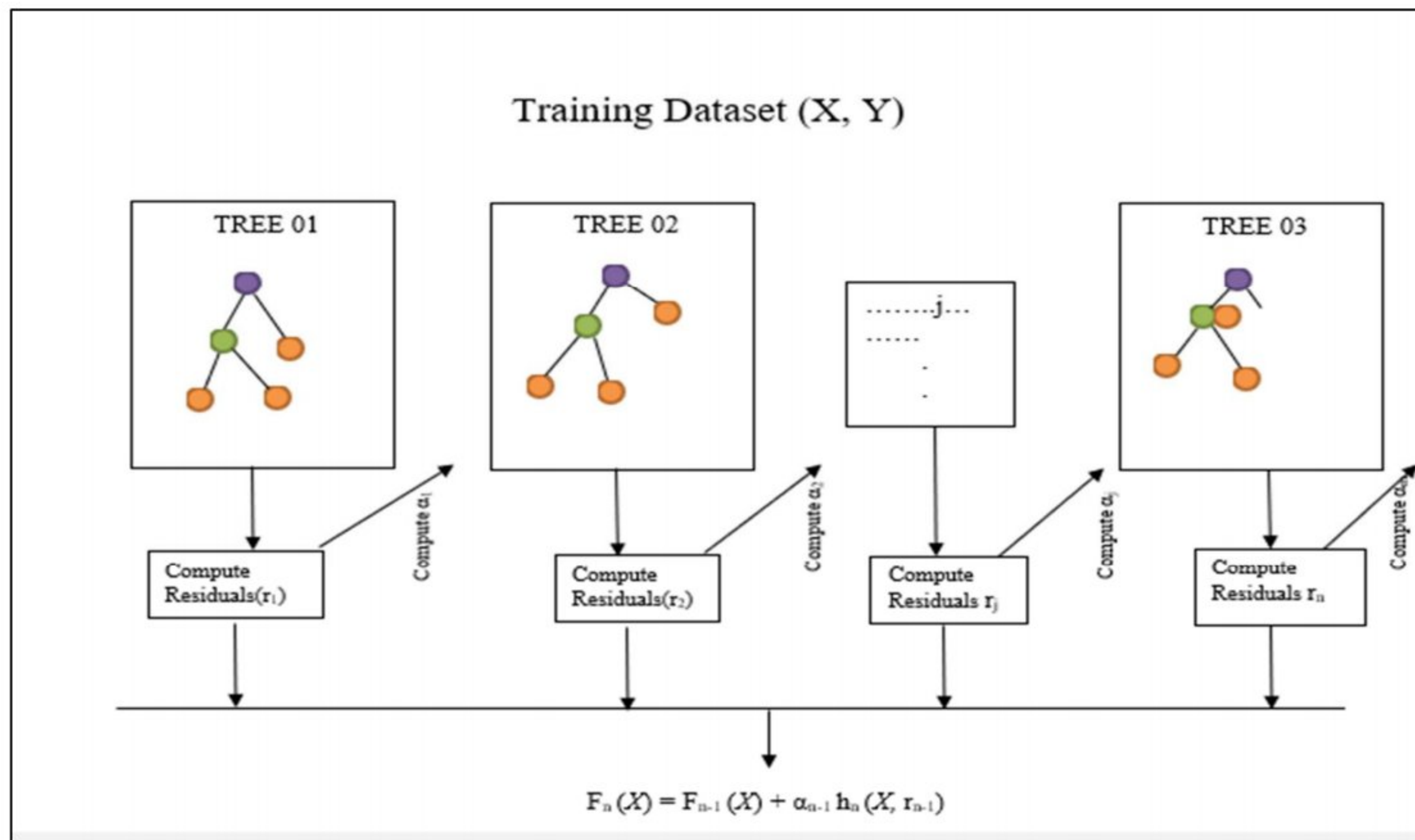


Figure 12: XGBoost algorithm prediction tree.

4.3.3 LightGBM:

LightGBM is a highly efficient gradient boosting framework specifically designed for regression tasks. It uses cutting-edge algorithms to improve training speed and accuracy while using decision trees as the foundational learners. Gradient-based one-side sampling (GOSS) is an approach that uses intelligent selection to choose examples with bigger gradients for more efficient model training. In order to create a more accurate and effective learning process, LightGBM additionally makes use of leaf-wise tree development, where nodes are divided based on the largest benefit. Additionally, it provides multiple regularization strategies, including L1 and L2 regularization, enabling improved generalization and avoiding overfitting.

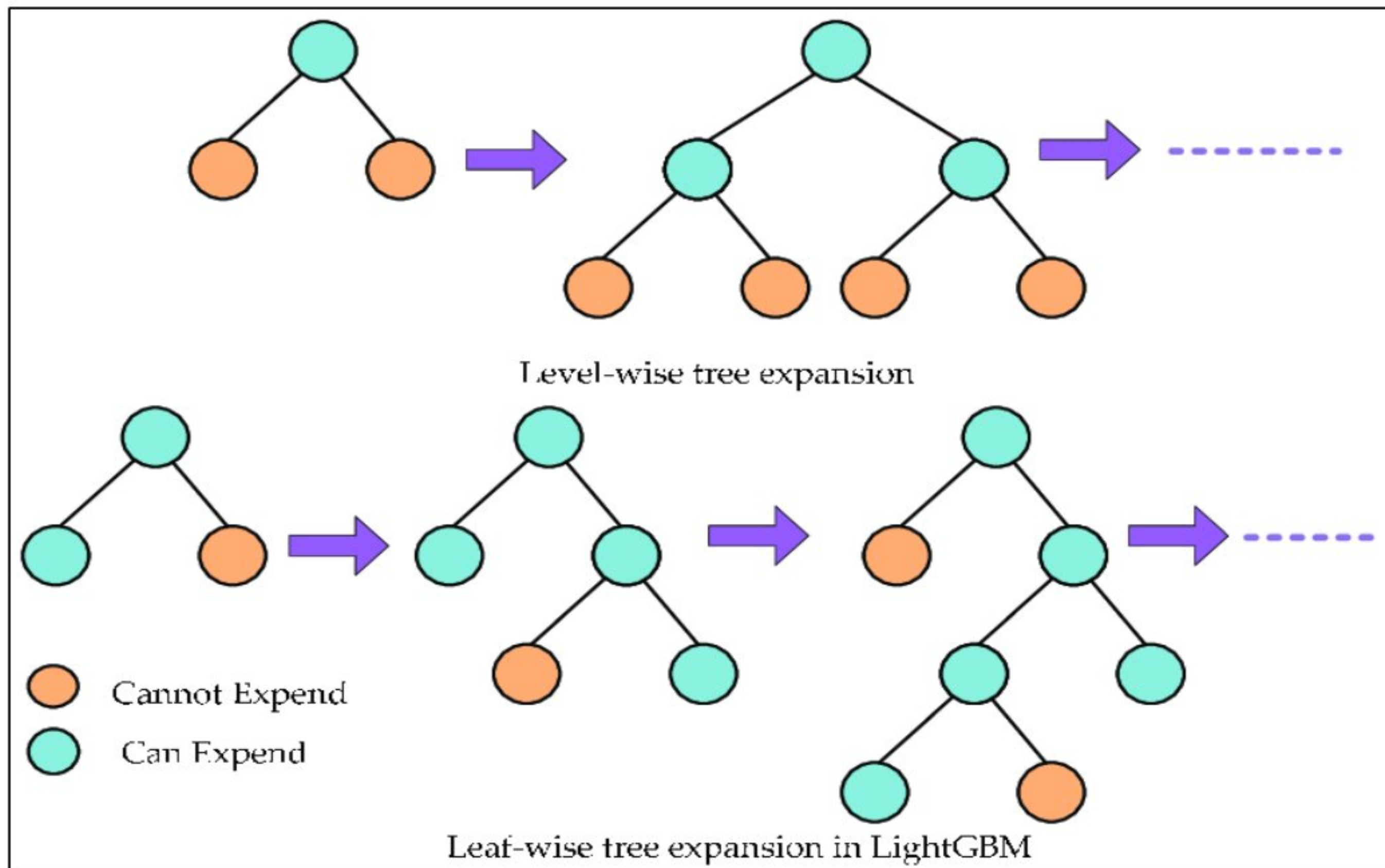


Figure 13: LightGBM prediction tree diagram.

The framework allows for flexibility in adjusting the learning rate, allowing for precise control of the convergence pace and model performance. Furthermore, LightGBM offers early stopping, enabling the training process to be stopped if the model performance on a validation set does not increase, saving time and computational resources. It can handle huge datasets and make use of multi-core CPUs or distributed computing systems for faster processing thanks to its parallel and distributed training capabilities. With great performance, scalability, and flexibility, LightGBM excels at producing precise regression models.

4.4 Optimization Methods

4.4.1 Genetic Algorithm

A genetic algorithm is an optimization and heuristic search method that draws inspiration from biology and the process of natural selection. It is frequently used to address optimization issues where more conventional techniques may be inefficient or unproductive. The process starts with a population of potential answers that are frequently represented as a collection of strings or binary sequences known as chromosomes. Every chromosome symbolizes a possible answer to the current issue. Randomly or in accordance with a predetermined strategy, the population is initialized. The algorithm then goes through a number of generations—a series of iterations. The algorithm uses a fitness function unique to the

problem domain to assess each population member's fitness or quality in each generation. A solution's level of problem-solving effectiveness is quantified by the fitness function, which normally gives better solutions a higher fitness score.

The selection procedure, which comes after, involves choosing people from the current population to be the parents of the following generation. Individuals with better fitness scores are often more likely to be picked because selection is typically based on fitness scores. As better suited solutions are more likely to result in offspring with desired traits, the objective is to prefer them. Following the selection of the parents, new people for the following generation are produced by genetic processes including crossover and mutation. Crossover is the process of fusing the genetic material from two parent chromosomes to produce child chromosomes. To encourage diversity and keep the algorithm from being locked in local optima, mutation introduces minute random modifications to the chromosomes.

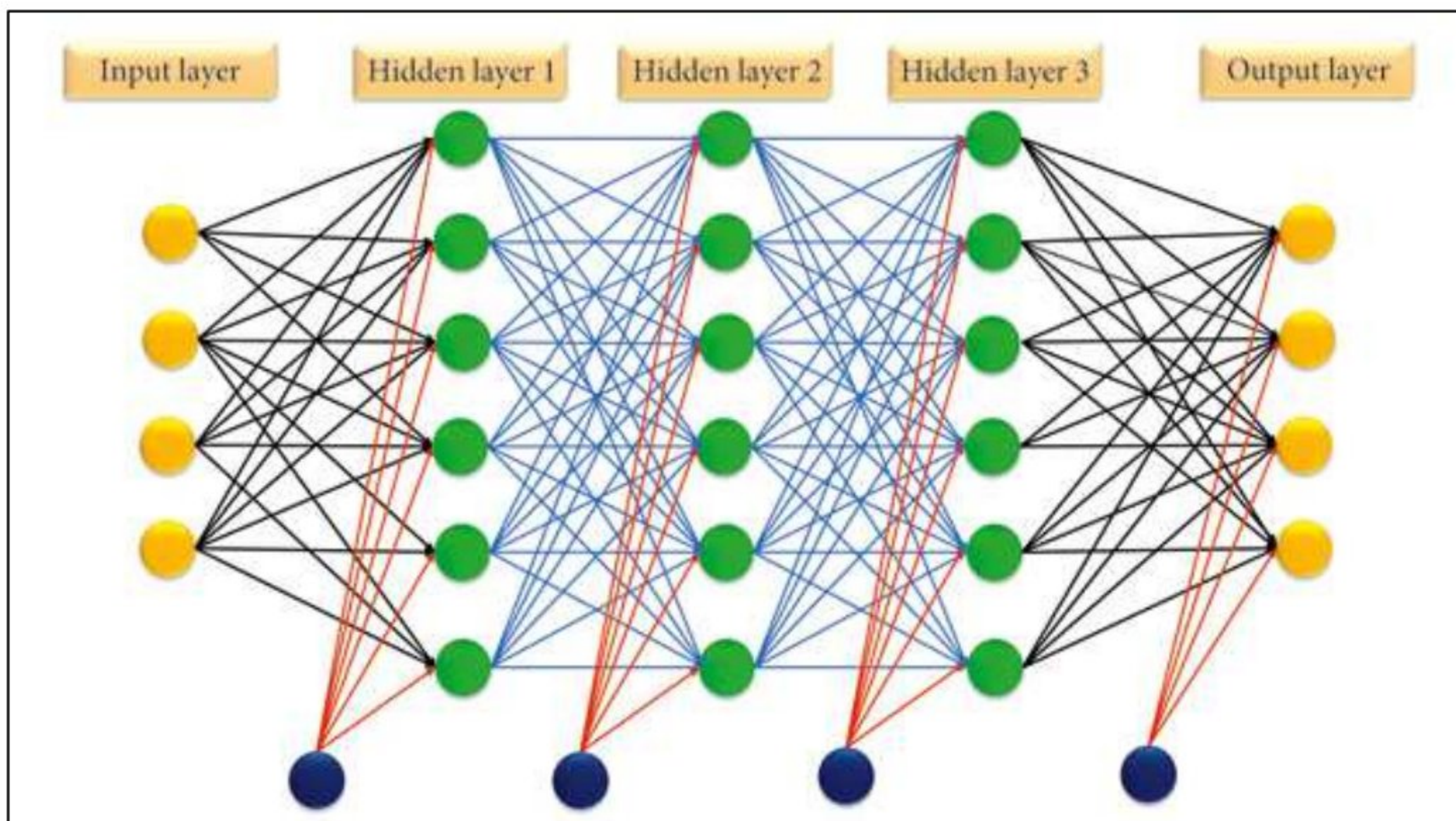


Figure 14: Genetic algorithm network implemented with neural network.

The population can change throughout time thanks to the recurrent cycles of evaluation, selection, crossover, and mutation. The objective is for the algorithm to converge to an optimal or nearly optimal answer to the problem. The algorithm's termination condition may depend on a number of variables, including attaining a predetermined number of generations, arriving at a workable solution, or failing to notice appreciable progress after multiple iterations. As adaptive algorithms for resolving real-world

issues and as computer representations of biological evolutionary processes, genetic algorithms have been applied in the fields of science and engineering.[66] In order to get the most accurate response genetic algorithms (GA) models the selection process and genetic mechanisms in Darwin's biological evolution hypothesis. There are two significant ways in which the genetic algorithm differs from a traditional derivative-based (gradient-based) optimization method. At each iteration, the GA produces a population of points. The population's best point gets closer to the optimal outcome.[67]. Multiple objective functions are able to concurrently minimized or maximized by using multi-objective optimization. It may be stated to be[44]

$$\min F(X) = [f_1(X), f_2(X), f_3(X) \cdots f_m(X)]^T$$

Subjected to

$$\begin{aligned} g_j(X) &\leq 0, j = 1, 2, \dots, m \\ h_i(X) &= 0, i = 1, 2, \dots, n \\ x_{k,min} &\leq x_k \leq x_{k,max} \end{aligned}$$

In this current study, six parameters were accounted for the optimization procedure, i.e., DNI, MCIT, TIT, Pinch Point, RPR, SR. The most adopted optimization algorithm method is constraint satisfaction based Genetic Algorithm working on resolving problems with global maximizing and minimization [68]–[74].

Generally, multiple random combined sets of the design variables, referred to as populations, are used to implement multi-objective optimization using Genetic Algorithm. The optimal procedures identified could be used to determine the population size[75]. Each member of the population has been put to the test by the MOOGA using a fitness function table. The top 1–5% of the population frequently passes over to the next generation unmodified, while the remainder of the population develops via mutations and crossings. Until any stoppage conditions are satisfied, the procedure continues. The current optimization problem was handled in the MATLAB environment with a population of 50.[76]

Scaling and selection were done implementing the built-in functions' rank and stochastic uniform. The 5%, 80%, and 15% values for elite size, crossover, and mutation percentages were employed, correspondingly. The upward moving factor was increased to 0.2. The Lagrangian function was used as nonlinear constraint technique function[67]. The upper constraint of maximum DNI, MCIT, TIT, Pinch Temp, RPR, SR and the lower bounds of minimum temperatures & Split Ratio were both set to be somewhat higher than CO2 critical levels.

Table 6: Design variables (Recompression) utilized for the Current Study.

Design Variable	Lower Bounds	Upper bounds
Direct Normal Irradiance (DNI) [W/m ²]	271.875	553.125
Main Compressor Inlet Temperature (MCIT)[°C]	34	55
Turbine Inlet Temperature (TIT)[°C]	400	700
Pinch Point Temperature Difference (Pinch)[K]	5	20
Split Ratio (SR)[x]	0.6445	0.7968

Table 7: Design variables (Partial Cooling) utilized for the Current Study.

Design Variable	Lower Bounds	Upper bounds
Direct Normal Irradiance (DNI) [W/m ²]	271.875	553.125
Main Compressor Inlet Temperature (MCIT)[°C]	34	55
Turbine Inlet Temperature (TIT) [°C]	400	700
Pinch Point Temperature Difference (Pinch)[K]	5	20
Ratio of Pressure ratio (RPR)[Pr]	0.3	0.9
Split Ratio (SR)[x]	0.23	0.98

Table 8: Design variables (Main Compression Intercooling) utilized for the Current Study.

Design Variable	Lower Bounds	Upper bounds
Direct Normal Irradiance (DNI) [W/m ²]	271.875	553.125
Main Compressor Inlet Temperature (MCIT) [°C]	34	55
Turbine Inlet Temperature (TIT)[°C]	400	700
Pinch Point Temperature Difference (Pinch)[K]	5	20
Ratio of Pressure ratio (RPR)[Pr]	0.3	0.9
Split Ratio (SR)[x]	0.5566	0.8

Net work output, 1st law efficiency, 2nd law efficiency Exergy Destruction are taken into consideration as an objective function for current research since the primary objective of the optimization is to maximize power from the cycle.

4.4.2 Artificial Neural Network

Learning from experience is performed by artificial neural networks and the ability to generalize from given training data to unknown data is possessed by them. Additionally, the operation can be performed quickly and utilized for real-time operation. The calculation of an artificial neuron model involves the introduction of inputs, multiplication of weights, and application of the results to the transfer function. A multilayer structure is typically possessed by artificial neural networks, which consist of an input layer, one or more hidden layers, and an output layer. The same type of transfer function is used in each hidden layer.

A sigmoid transfer function is generally used in MATLAB's multilayer neural network. The backpropagation neural network is widely used. In backpropagation learning, weight and bias values are repeatedly calculated according to the development of multi-layer structure.

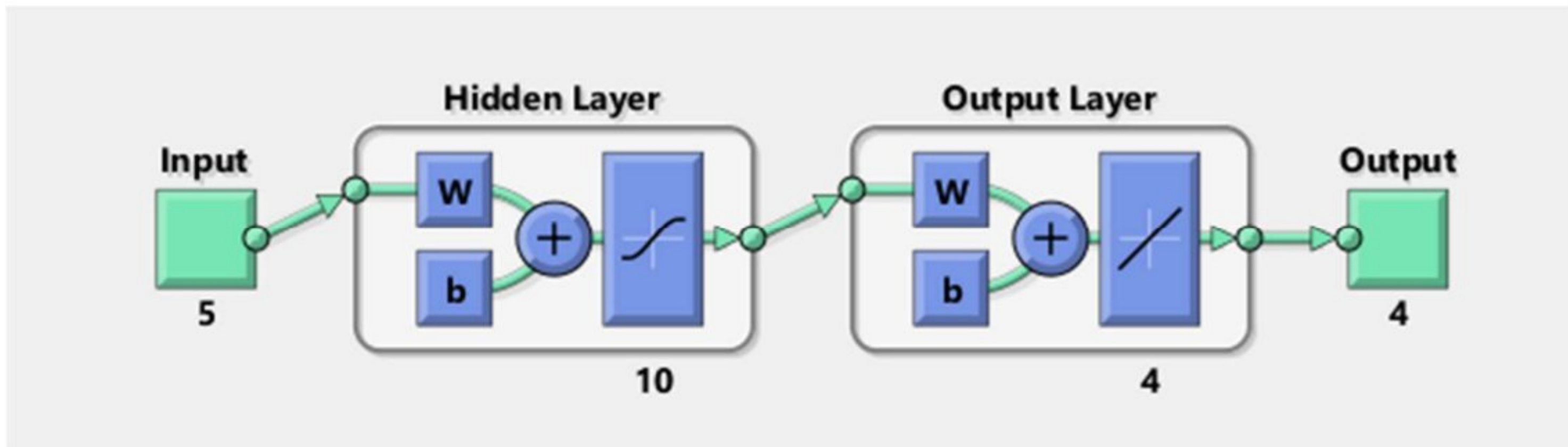


Figure 15: Neural network in MATLAB.

In this study, a MATLAB-embedded feedforward net neural network is utilized. All kinds of input-output mapping can be handled by Feedforward net, and the arguments hidden size and trainFcn are used. The column vector size and training function of the hidden layer are meant by each, with 10 and trainlm as the default values. The weights and biases are updated by the training function trainlm using Levenberg-Marquardt optimization. The fastest backpropagation algorithm in the toolbox is often Trainlm and it is required to use more memory than other algorithms. However, it is used first in supervised algorithms.

4.4.3 TOPSIS

The optimal option is chosen using multi-criteria decision making (MCDM). Assuming K decision-makers are evaluating m decisions based on n criteria. The evaluations and weights are first combined using arithmetic mean or another appropriate approach in the traditional TOPSIS method[77]. After that, the sum of the ratings and weights are put together to create the decision (D) and weight (W) matrix shown as follows[78]:

$$D = \begin{bmatrix} x_{11} & x_{12} & \cdots & x_{1n} \\ x_{21} & x_{22} & \cdots & x_{2n} \\ \vdots & \vdots & \cdots & \vdots \\ x_{m1} & x_{m2} & \cdots & x_{mn} \end{bmatrix}$$
$$W = [w_1 \quad w_2 \quad \cdots \quad w_n]$$

Subjected to

x_{ij} = aggregate rating of i^{th} alternative for j^{th} criterion

w_j = the weight for j^{th} criterion.

Vector or linear normalization is used to scale up diverse criteria to a similar level. Decision matrix (R) that has been normalized by[78]:

$$R = \begin{bmatrix} r_{11} & r_{12} & \cdots & r_{1n} \\ r_{21} & r_{22} & \cdots & r_{2n} \\ \vdots & \vdots & \cdots & \vdots \\ r_{m1} & r_{m2} & \cdots & r_{mn} \end{bmatrix}$$

Subjected to

r_{ij} = normalized rating of i^{th} alternative for j^{th} criterion

An available list of options is evaluated and the optimal alternative is selected using the Technique for Order of Preference by Similarity to Ideal Solution (TOPSIS), a multi-criteria decision-making technique.

The decision matrix, which depicts how options perform relative to each criterion, was created using this linear approach. Normalization methods are used to transform raw data into dimensionless values to guarantee fairness in assessing criteria.[79] To account for their relative weight in the decision-making process, several weighting techniques are examined.

$$i_{\text{opt}} \in \max \left\{ \frac{ED_i^+}{ED_i^+ + ED_i^-} \right\}$$

$$B_{ij} = F_{ij} / \sqrt{\sum_{i=1}^m F_{ij}^2}, G_{ij} = w_j^{\text{TOPSIS}} \cdot B_{ij}$$

$$ED_i^- = \sqrt{\sum_{j=1}^m (G_{ij} - G_j^{\text{negative}})^2}$$

In the equation[66], w_j^{TOPSIS} is the weight of the j -th optimization objective, G_j^{negative} is the value of the j -th target with an NIP (negative ideal point) after normalization, and Distance i is the Euclidean distance between the i -th feasible option and (NIP). For a simple computation, $w_j^{\text{TOPSIS}} = 1$ is utilized in this study.

The ideal (P^+) and negative-ideal (P^-) strategies are determined as Equations [80] respectively:

$$P^+ = \{v_1^+, \dots, v_n^+\} = \left\{ \left(\max_j v_{ij} \mid i \in R^+ \right), \left(\min_j v_{ij} \mid i \in R^- \right) \right\}$$

$$P^- = \{v_1^-, \dots, v_n^-\} = \left\{ \left(\min_j v_{ij} \mid i \in R^+ \right), \left(\max_j v_{ij} \mid i \in R^- \right) \right\}$$

Chapter 5: Results & Discussions

5.1 Off-design Performance

Parametric analysis evaluates the thermodynamic effects of supercritical CO₂ Brayton Cycle factors such as main compressor inlet temperature, pressure ratio, turbine inlet temperature, and pinch temperature differential of LTR and HTR. Table 3 & Table 4 show system performance simulation and analysis beginning parameters & CSP loop design parameters. Figures indicate vascular conditions during study. In the following explanation, DNI 600 w/m² is considered as design point, so the turbine inlet temperature change is equal to the heat source inlet.

Table 9: Recompression S-CO₂ Cycle pressure, temperature, enthalpy & entropy for each state point.

State (i)	T (°C)	P (MPa)	h (kJ/kg)	s (kJ/kg·K)
1	600	25	1094.689	2.767
2	546.108	16.5	1032.902	2.775
3	600	16.5	1099.484	2.854
4	509.777	8	996.47	2.869
5	200.327	8	640.034	2.291
6	82.934	8	495.911	1.939
7	34	8	320.691	1.391
8	75.834	25	350.18	1.401
9	192.324	25	572.98	1.957
10	192.327	25	572.98	1.957
11	192.327	25	572.98	1.957
12	468.0952	25	929.416	2.562

Table 10: Partial cooling S-CO₂ Cycle pressure, temperature, enthalpy & entropy for each state point.

State (i)	T (°C)	P (MPa)	h (kJ/kg)	s (kJ/kg·K)
1	600	25	1094.689	2.767
2	544.433	16.5	30.842	2.773
3	600	16.5	1099.484	2.854
4	506.897	8	993.036	2.864
5	103.09	8	523.998	2.016
6	60.936	8	459.916	1.834
7	35	8	352.291	1.494
8	48.558	10.498	358.523	1.496
9	35	10.498	286.459	1.268
10	56.523	25	307.531	1.275
11	92.35	25	387.409	1.505
12	92.35	25	387.409	1.505
13	92.35	25	387.409	1.505
14	409.56	25	856.447	2.459

Table 11: Main Compression Intercooling S-CO₂ Cycle pressure, temperature, enthalpy & entropy for every state point.

State (i)	T (°C)	P (MPa)	h (kJ/kg)	s (kJ/kg·K)
1	600	25	1094.689	2.767
2	544.433	16.5	1030.842	2.773
3	600	16.5	1099.484	2.854
4	506.897	8	993.0367	2.864
5	178.593	8	615.201	2.237
6	64.746	8	446.908	1.855
7	34	8	320.691	1.391
8	43.582	10.5	325.598	1.393
9	34	10.5	282.898	1.256
10	54.746	25	303.707	1.263
11	168.462	25	534.376	1.872
12	168.462	25	534.376	1.872
13	168.462	25	534.376	1.872
14	454.293	25	912.211	2.538

5.1.1 Effect of MCIT

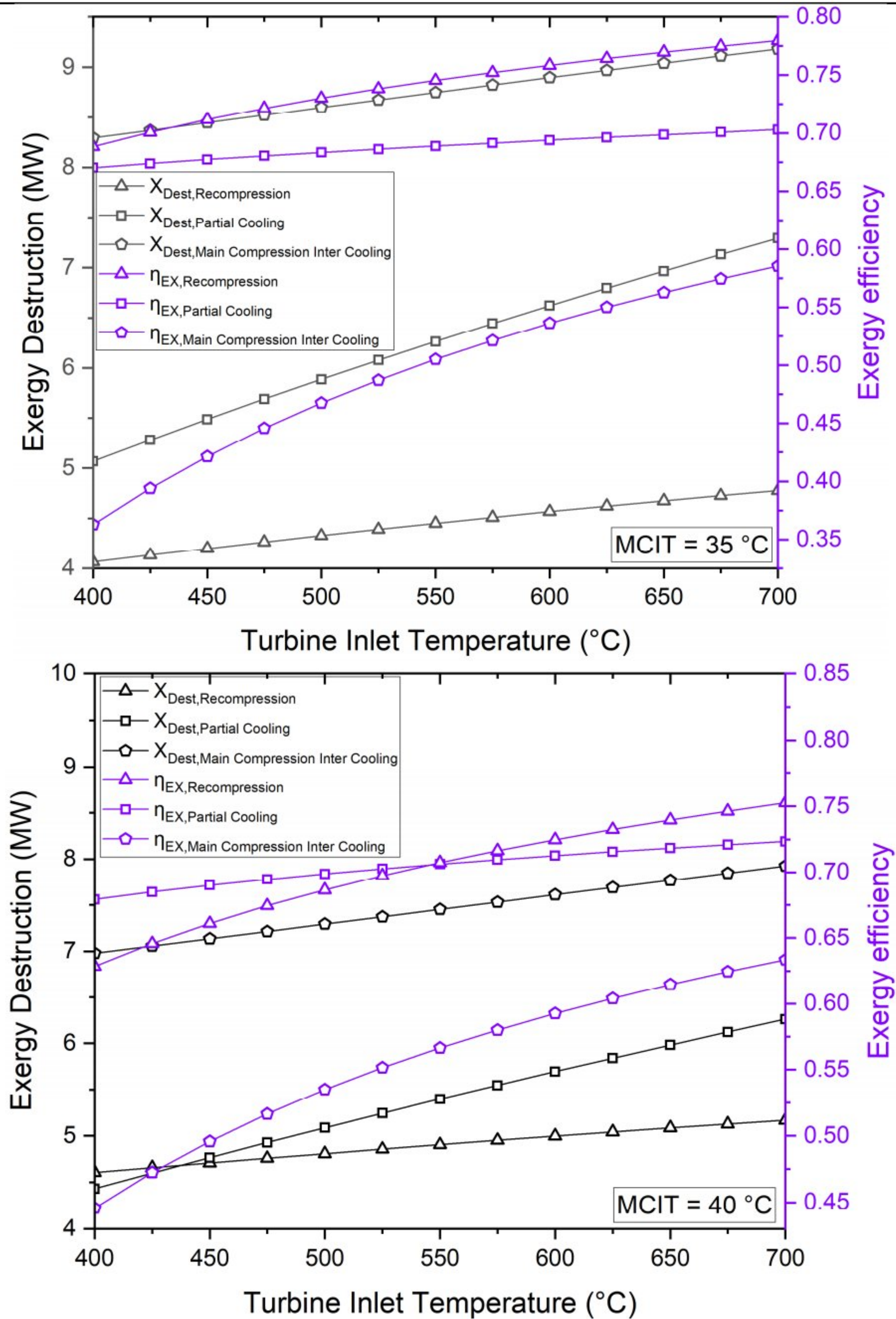


Figure 16: Exergy destruction & exergy efficiency comparison for recompression, partial cooling & intercooling cycle with the variation of the TIT at different compressor inlet temperature of 35°C and 40°C.

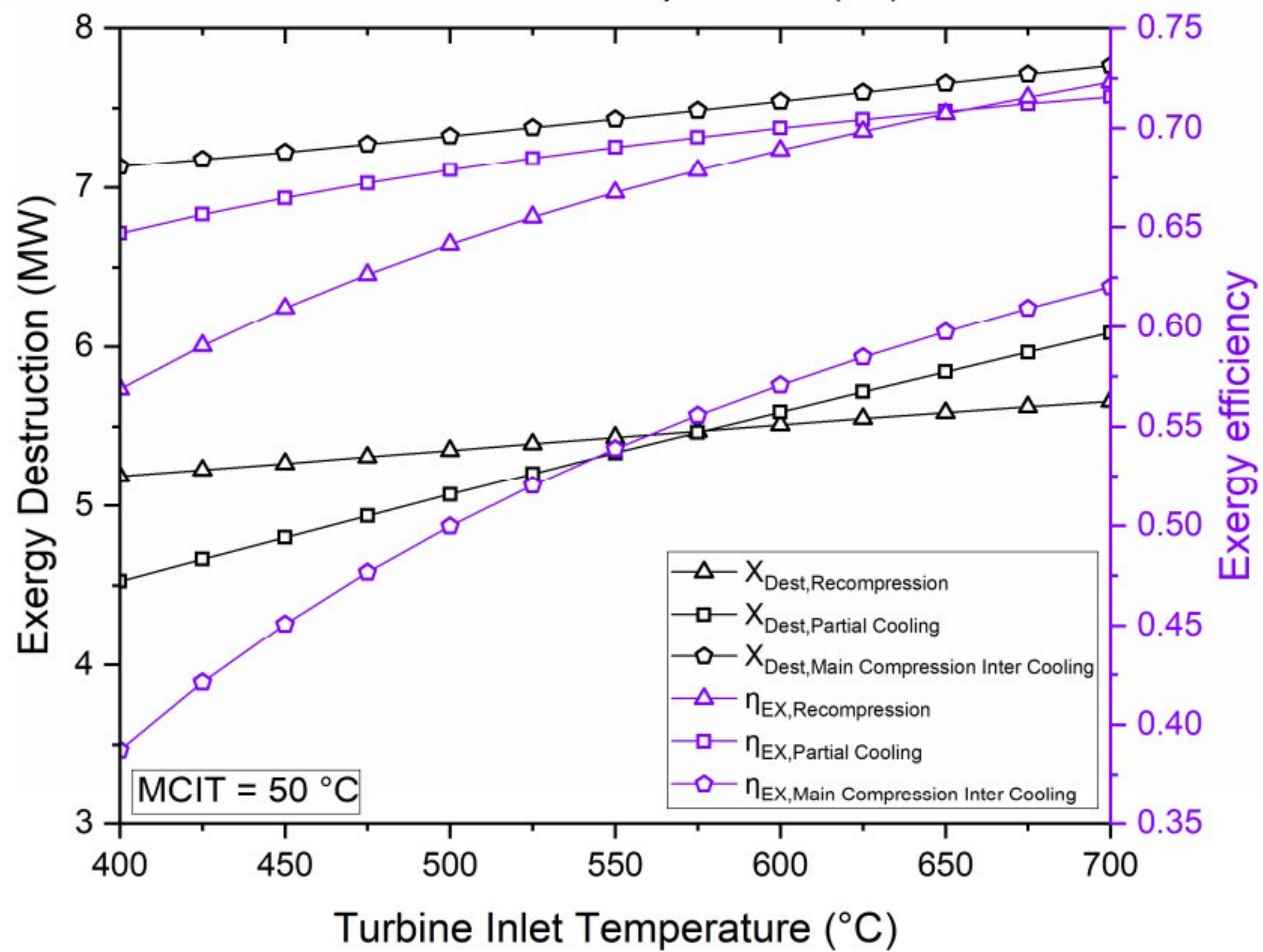
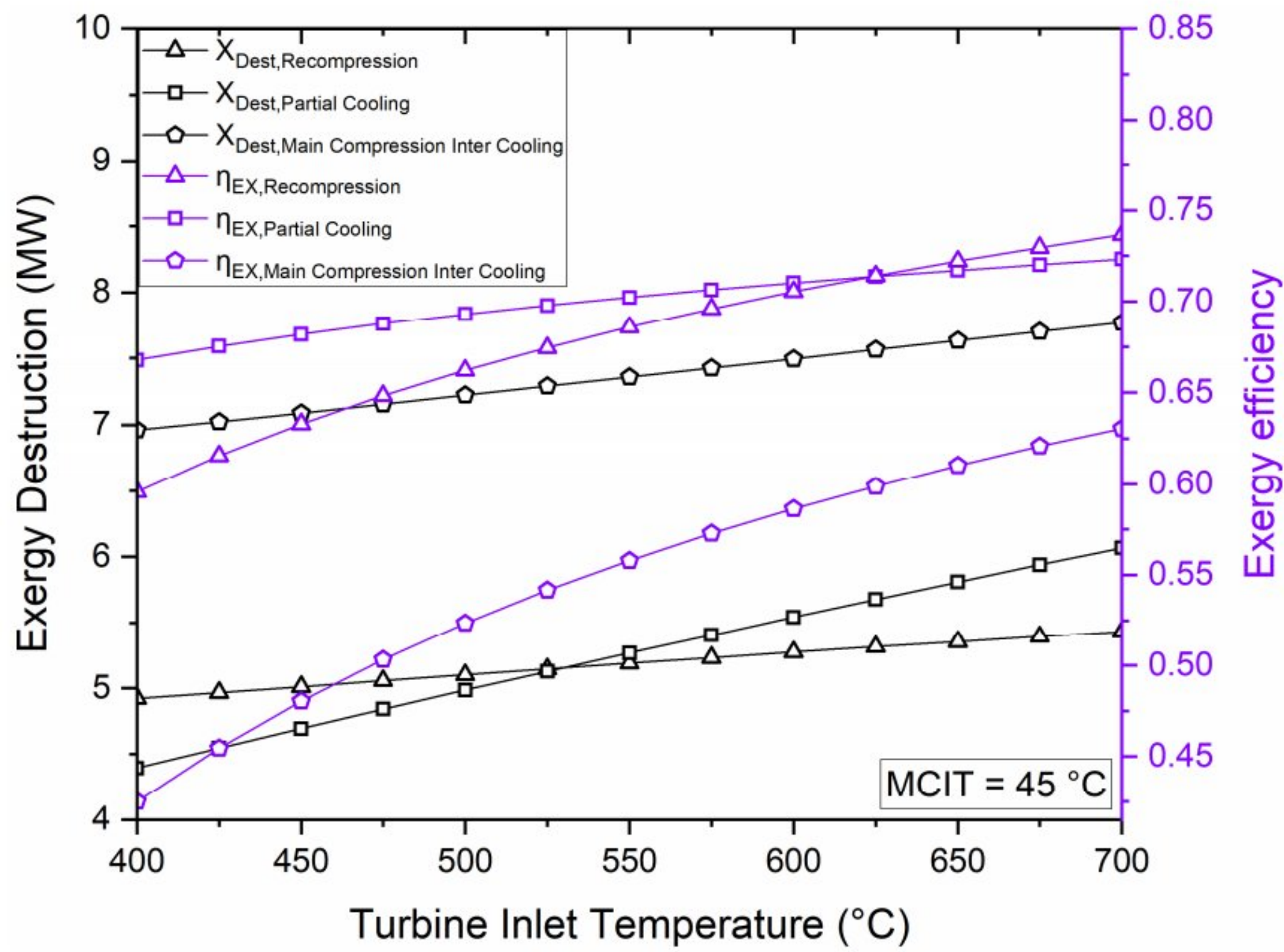
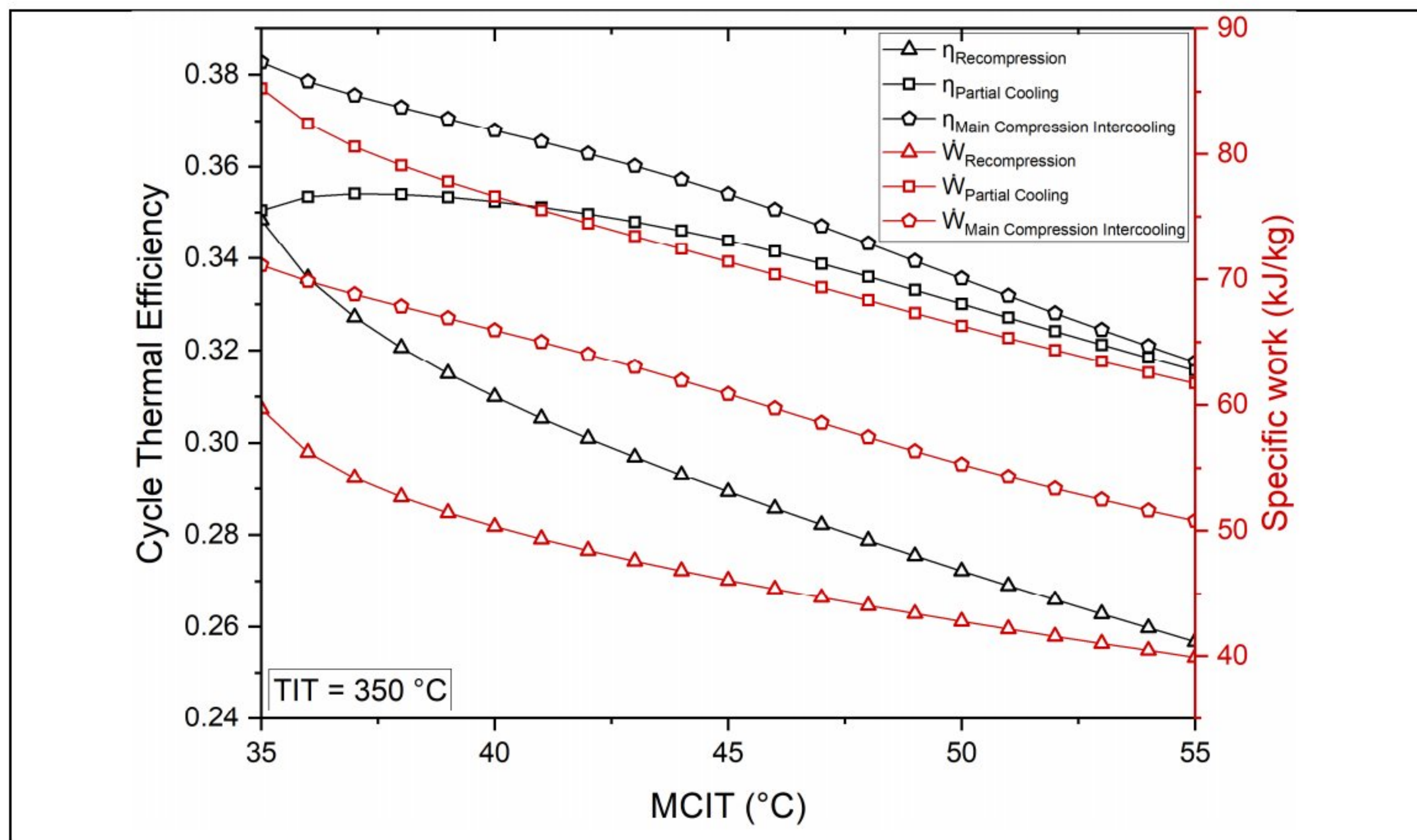


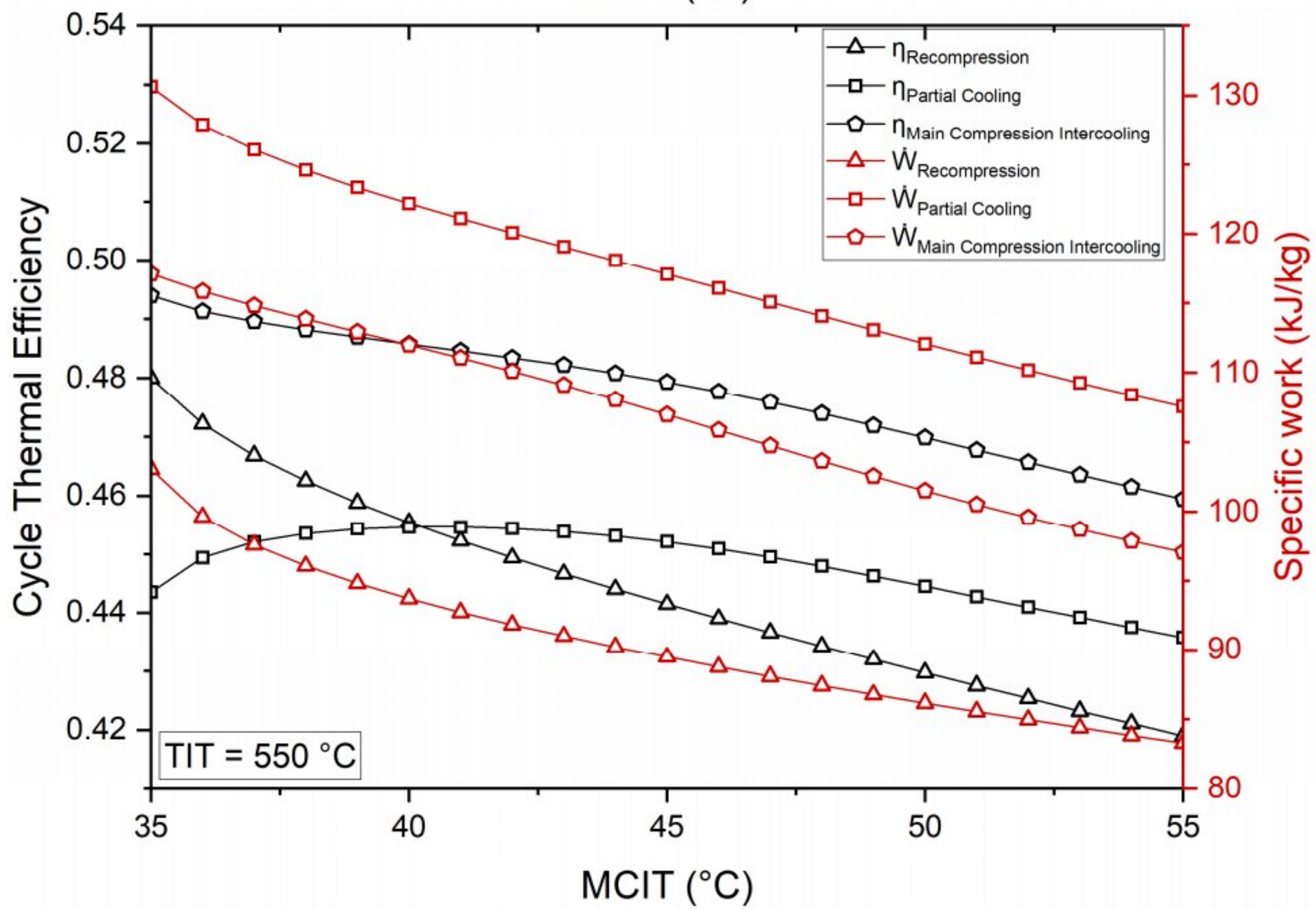
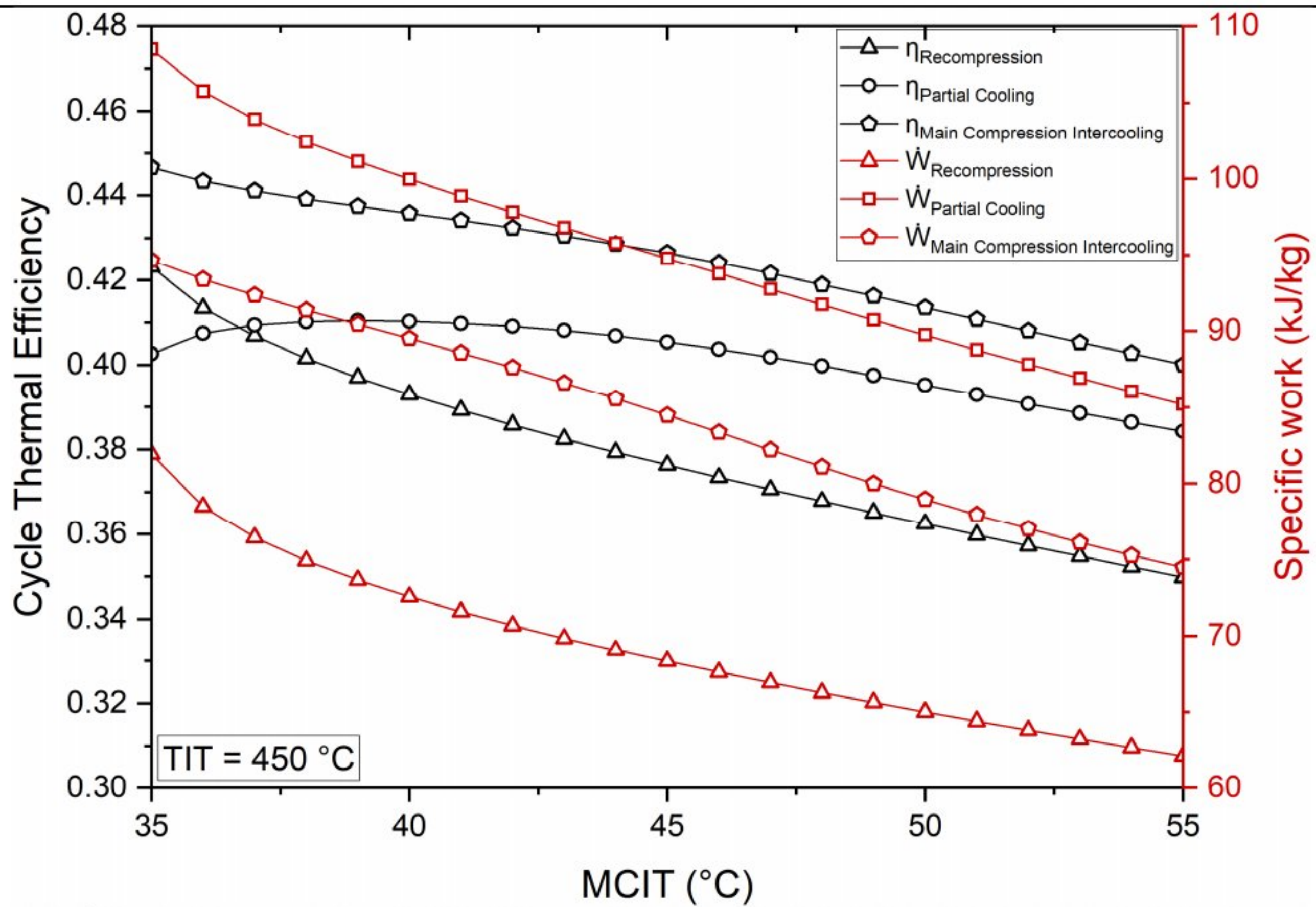
Figure 17: Exergy destruction & exergy efficiency comparison for recompression, partial cooling & intercooling cycle with the variation of the TIT at different compressor inlet temperature of 45°C and 50°C.

Fig16 & Fig.17 illustrates that turbine input temperature affects REC, PAR & INT SCO2BC exergy efficiency and exergy destruction. There is an optimal cycle pressure ratio because exergy efficiency grows rapidly, then gently, and even drops for each turbine inlet temperature. First, turbine power production increases faster than compressor power consumption, but when the pressure ratio increases, the opposite happens. Compressor performance and cycle efficiency are extremely important in a supercritical CO2 (sCO2) power cycle. Because of its high efficiency and small design, the sCO2 power cycle is a potential technology for power generation. The sCO2 power cycle's total performance is directly impacted by the compressor's operation. The system's power output, thermal efficiency, and overall performance are affected by the compressor's efficiency, pressure ratio, and specific work input. To achieve the necessary cycle efficiency and power output, accurate parameter selection and design optimization are required.

5.1.2 Effect of TIT

The turbine extracts energy from the expanding working fluid as it expands. The sCO2 power cycle's total performance, including the operation of additional components like heat exchangers, is influenced by the turbine inlet temperature. To achieve the desired heat transfer rates and maintain the temperature differences required for efficient cycle operation at higher turbine inlet temperatures, more effective and complex heat exchangers may be required.





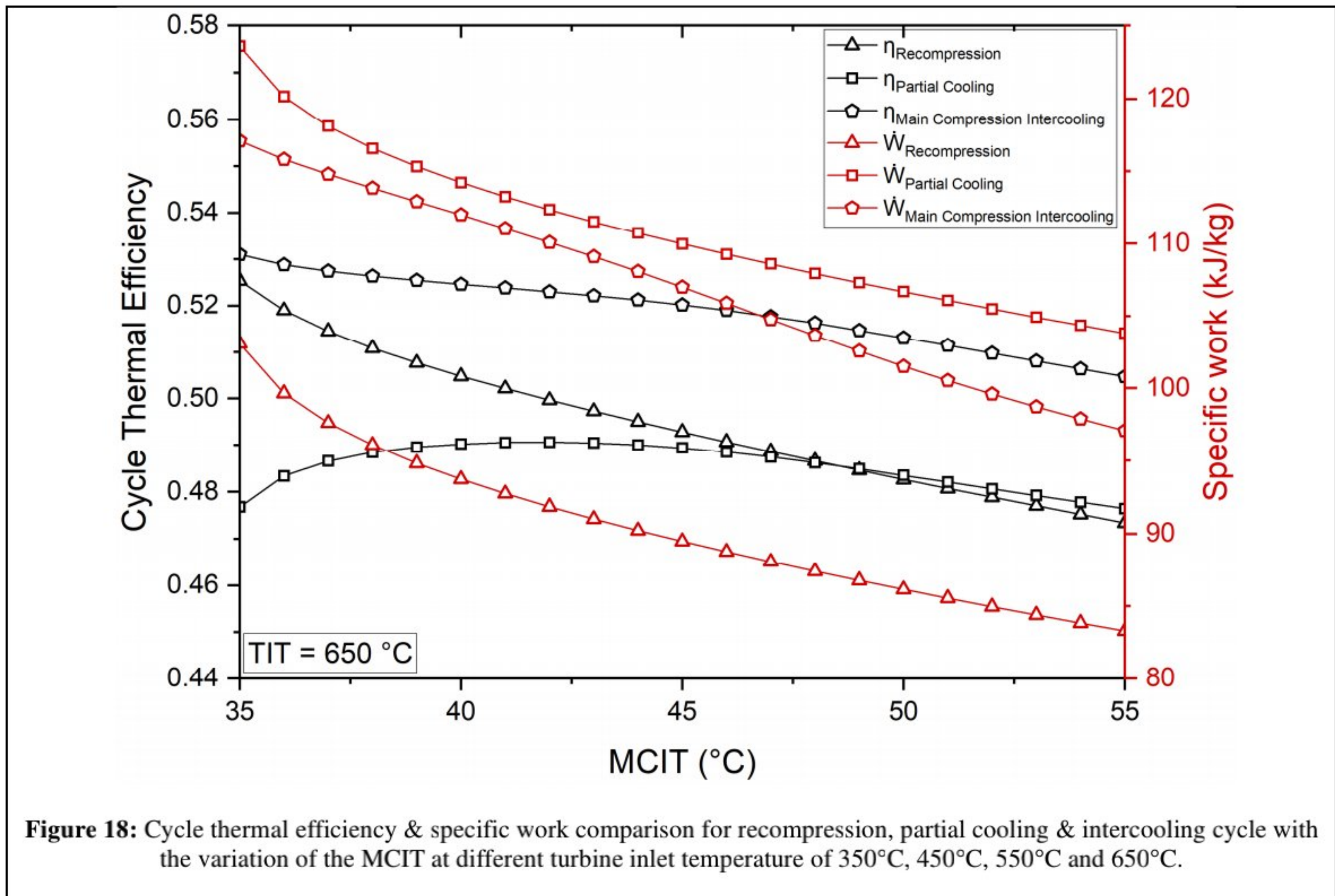
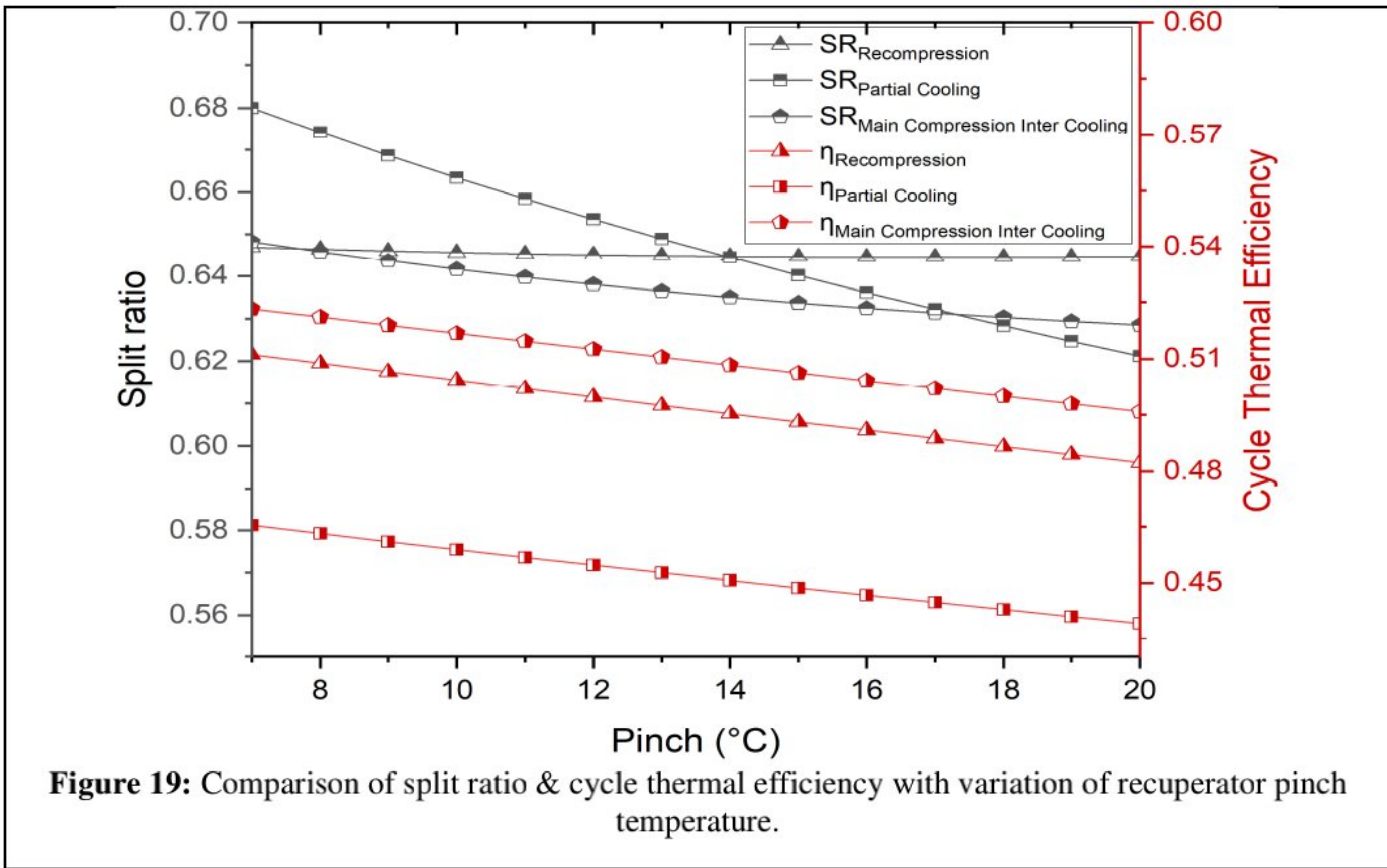


Figure 18: Cycle thermal efficiency & specific work comparison for recompression, partial cooling & intercooling cycle with the variation of the MCIT at different turbine inlet temperature of 350°C, 450°C, 550°C and 650°C.

As shown in Fig. 19, as the pinch temperature difference decreases, REC, PAR & INT SCO₂BC exergy efficiency increases because the condenser transfers more energy and LTR and HTR destroy more exergy. To avoid heat transmission degradation, the pinch temperature difference is normally greater than 7 K. The performance curves are essentially parallel throughout pinch temperature changes, indicating that pinch temperature difference affects REC, PAR & INT SCO₂BC similarly.

INT has higher cycle thermal efficiency than REC & PAR at every pinch temperature variation and is easier to attain the split ratio. The power output of the sCO₂ power cycle is directly impacted by the turbine inlet temperature. As the temperature of the CO₂ entering the turbine rises, more energy is transferred to the turbine, increasing power output. It is done so that more energy can be extracted from the expanding working fluid by the turbine, which increases power production.

5.1.3 Effect of Pinch Temperature



5.1.4 Effect of Compressor Efficiency

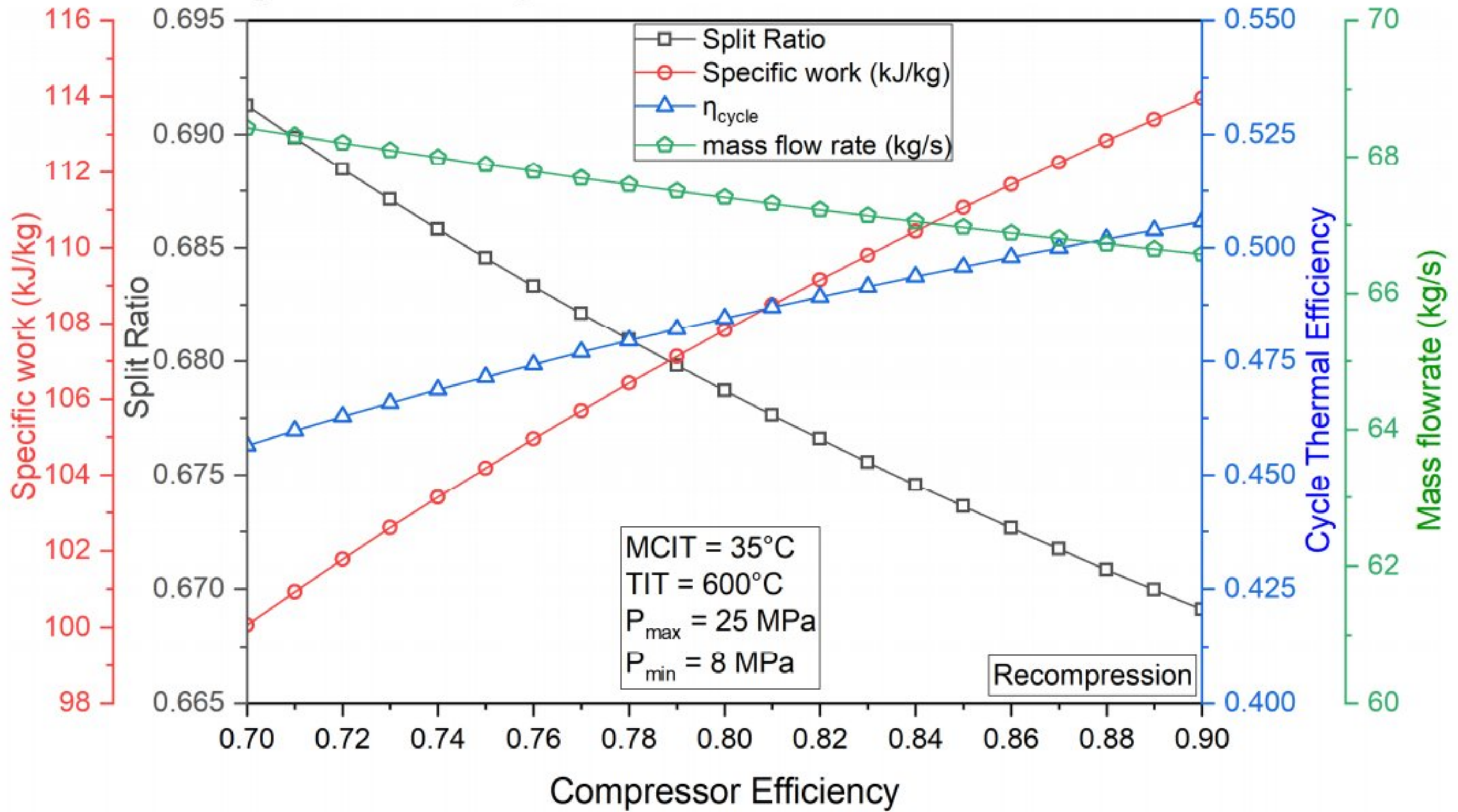


Figure 20: Recompression SCO2 cycle specific work, split ratio, cycle efficiency & mass flowrate with the variation of compressor efficiency.

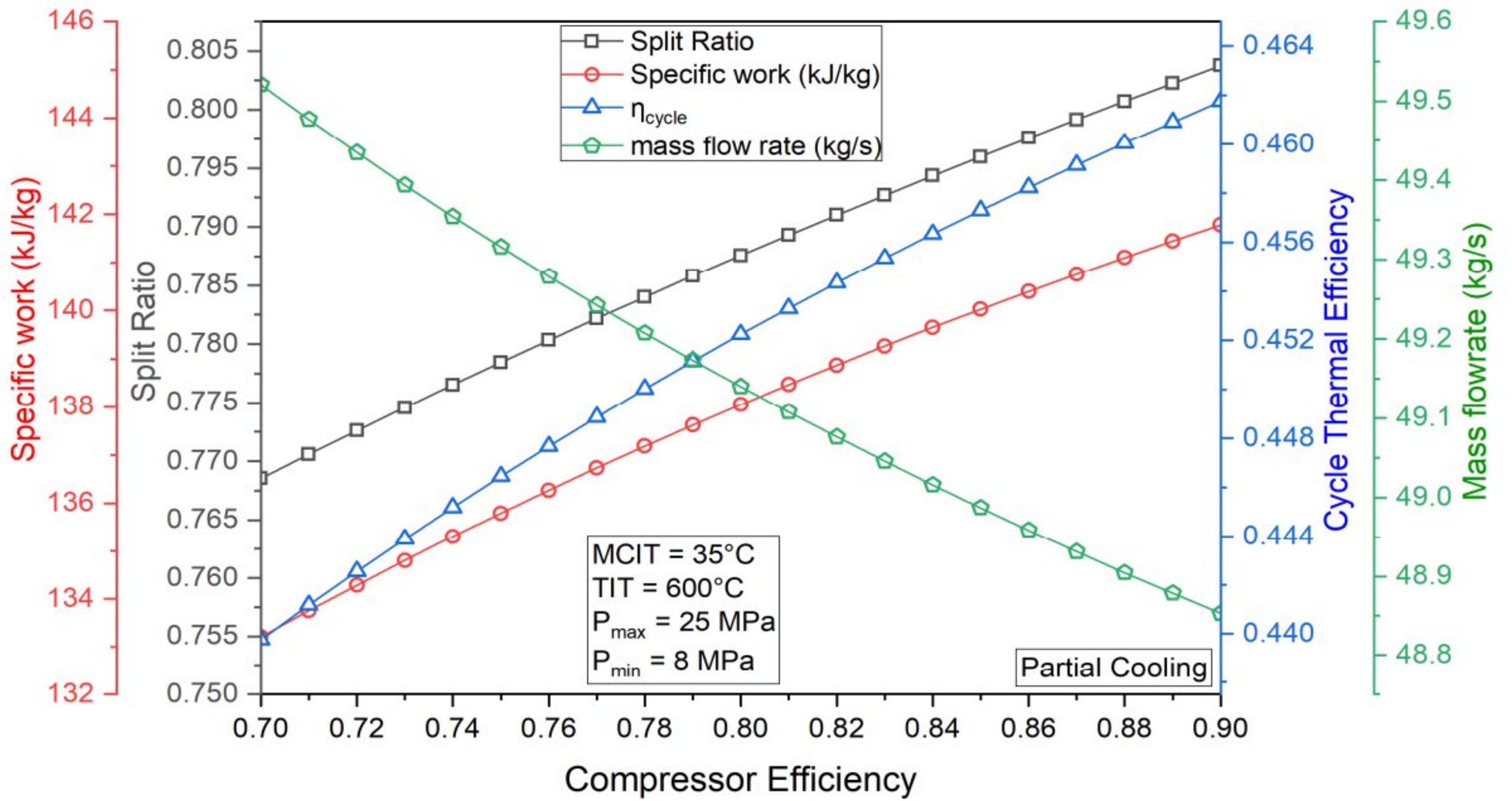


Figure 21: Partial cooling SCO2 cycle specific work, split ratio, cycle efficiency & mass flowrate with the variation of compressor efficiency.

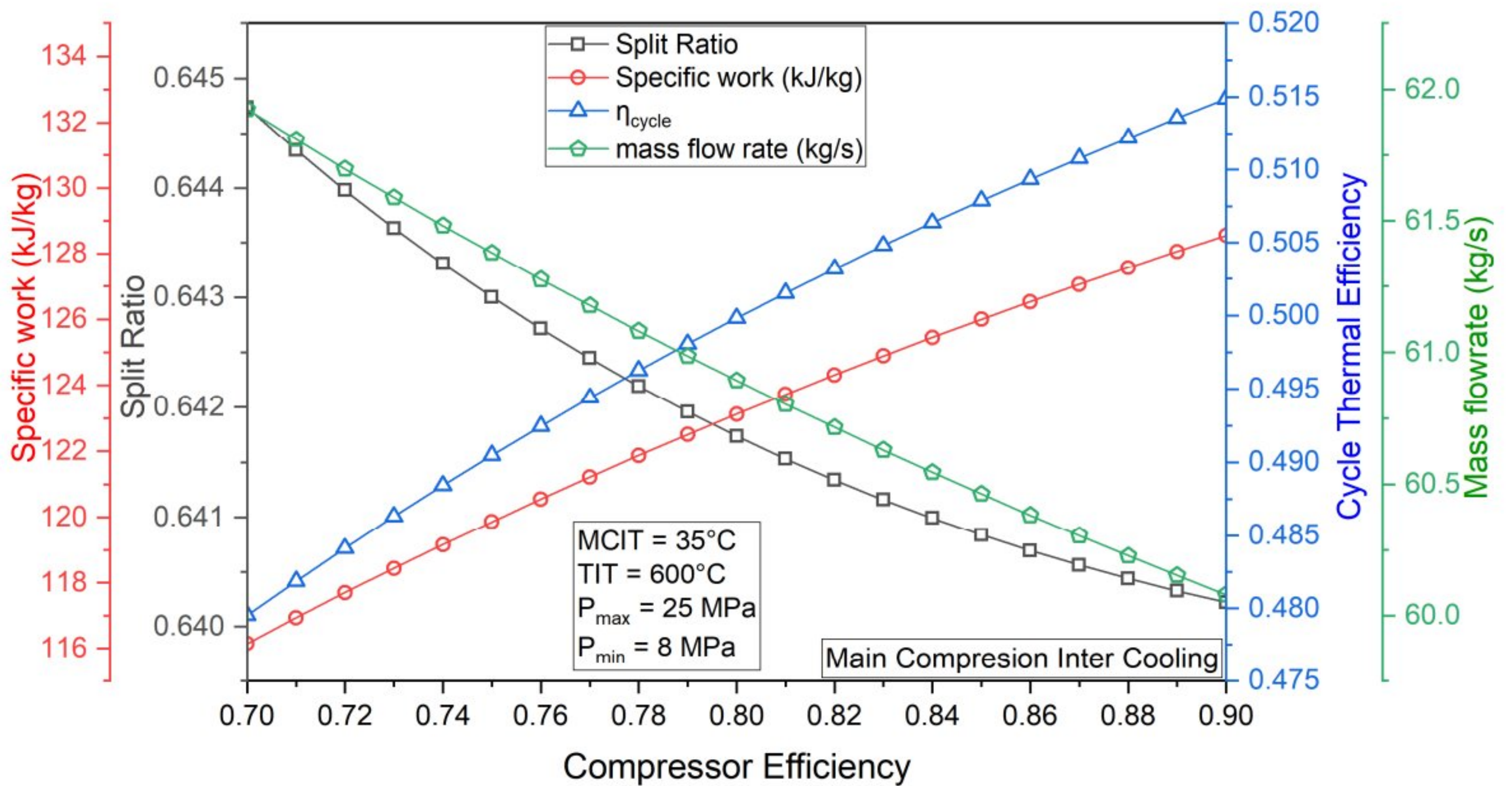


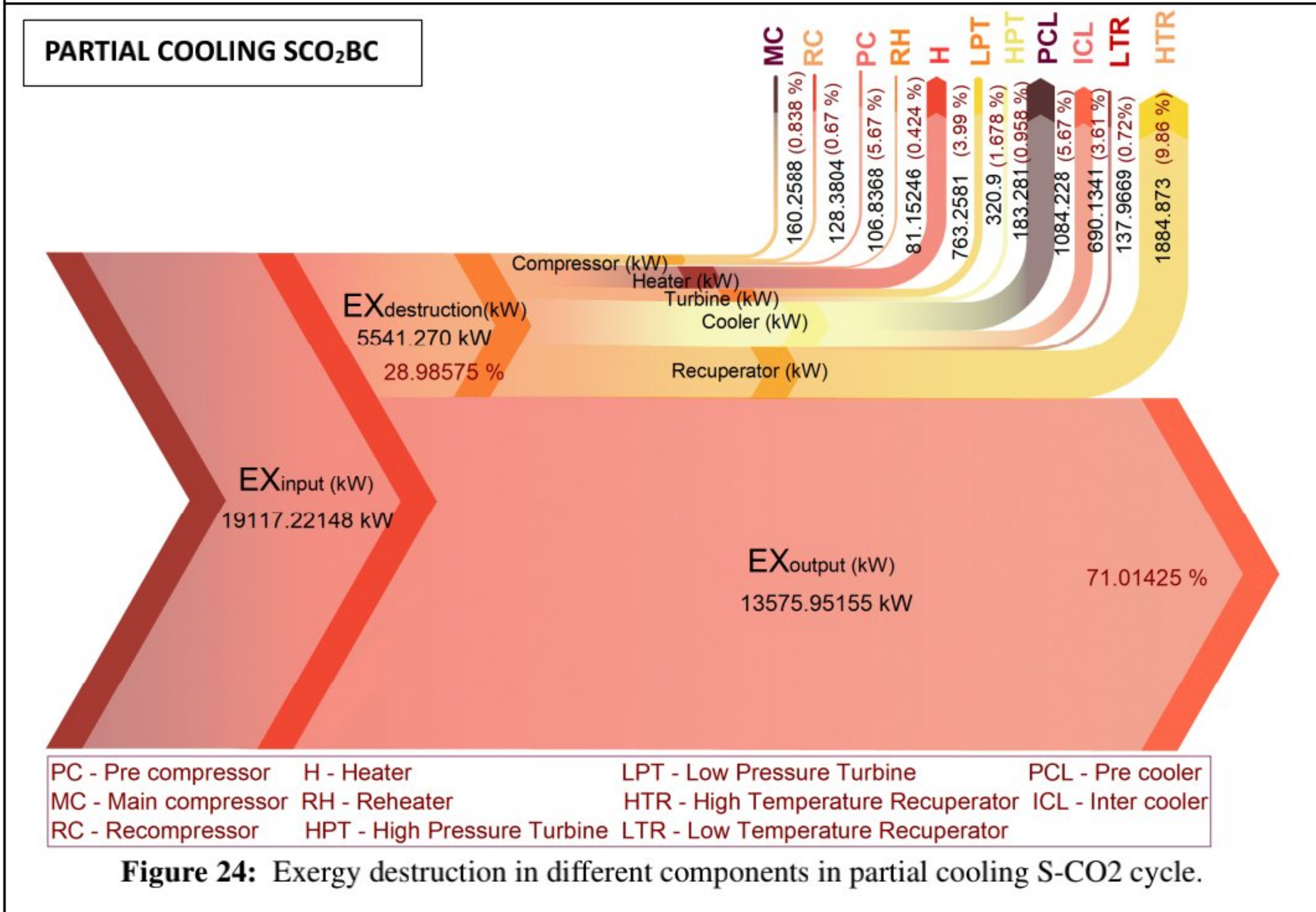
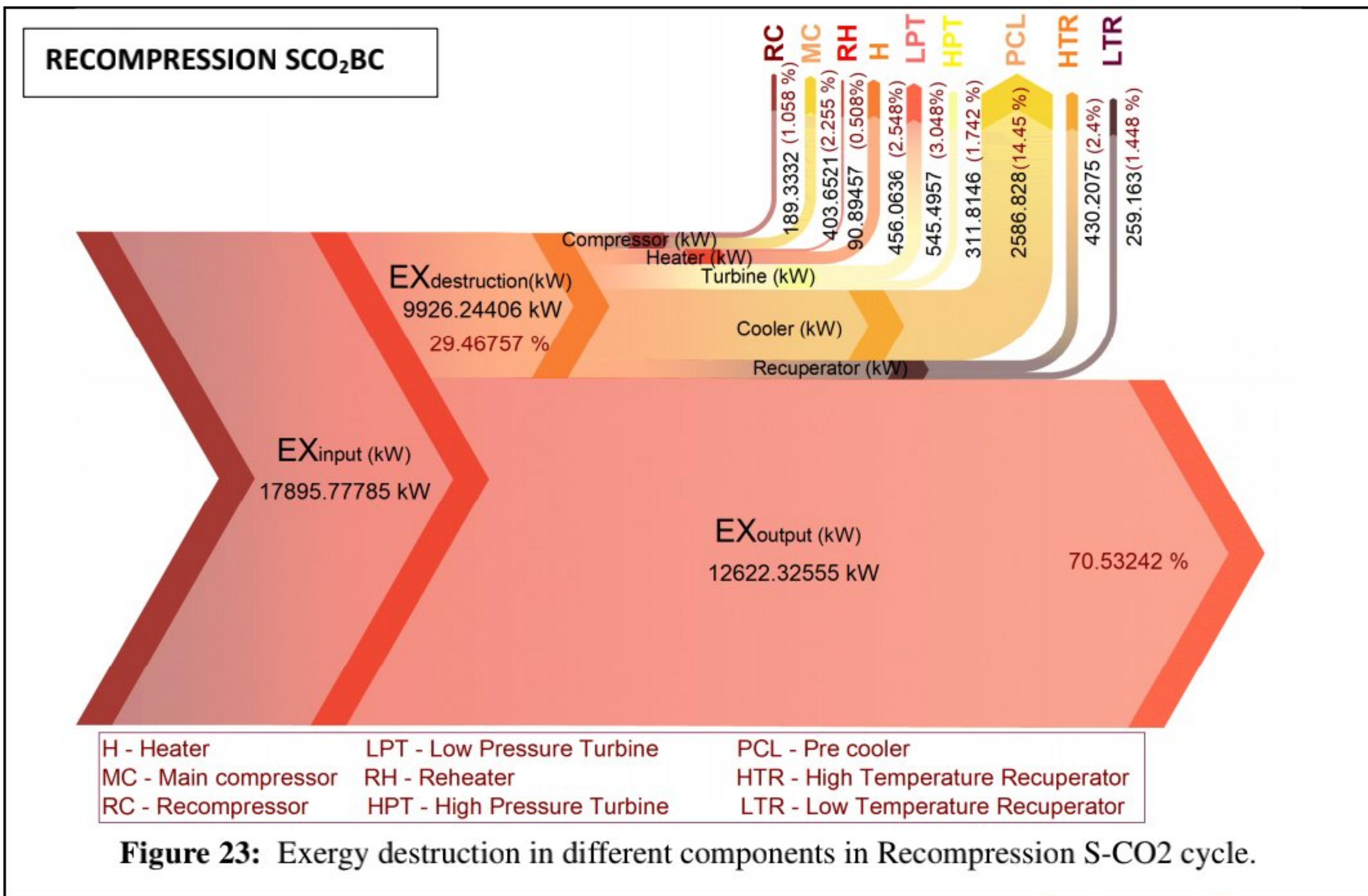
Figure 22: Main compression inter cooling SCO2 cycle specific work, split ratio, cycle efficiency & mass flowrate with the variation of compressor efficiency.

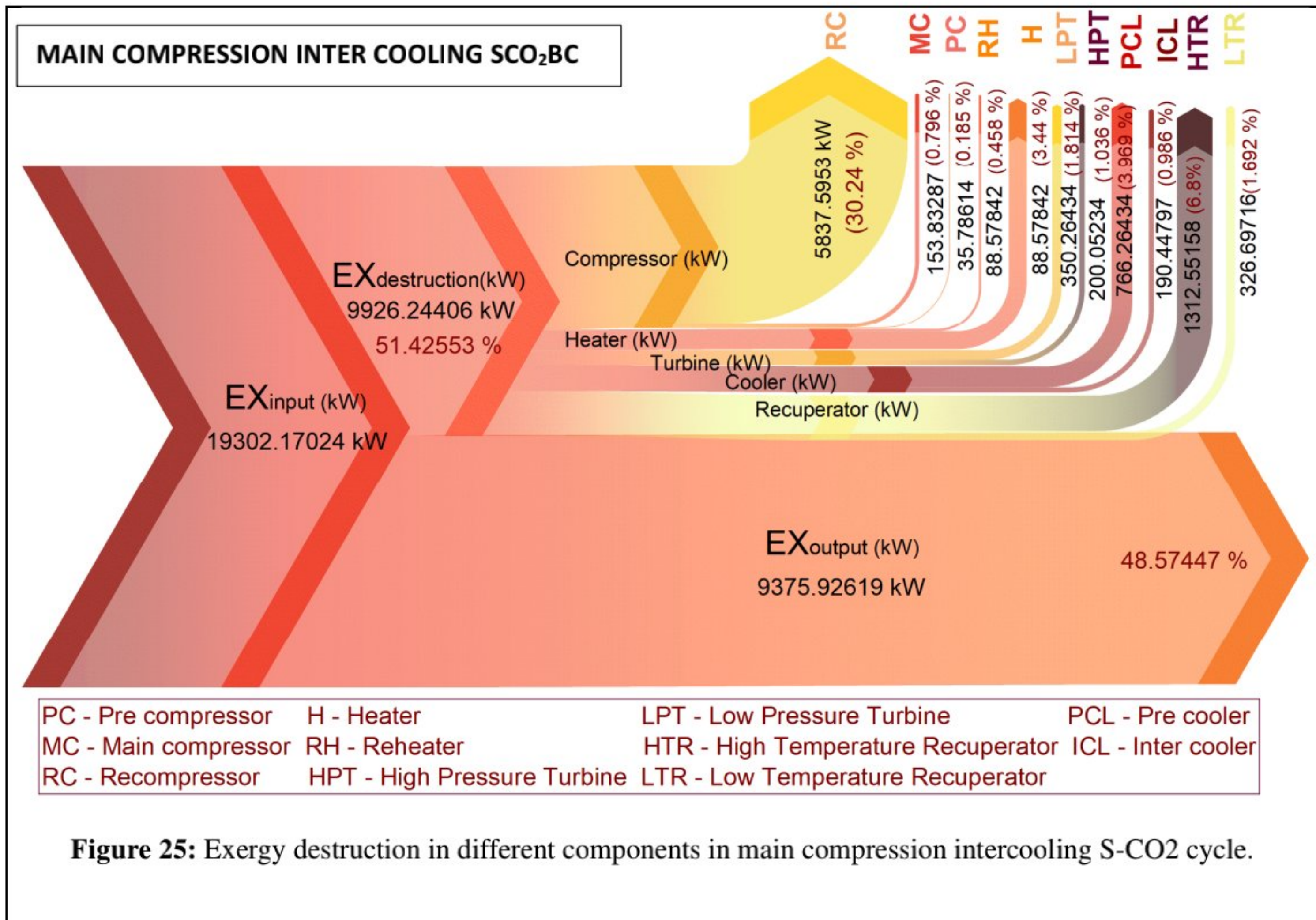
5.1.5 Exergy Analysis

Exergy analysis is employed in the study to evaluate cycle performance, identify areas of energy loss, and make recommendations for potential modifications. The main sources of inefficiency can be identified and improved by emphasizing efforts on those areas by quantifying the exergy destruction at various stages of the power cycle. Beyond what can be determined using only the first law of thermodynamics, the exergy analysis provides a more thorough understanding of the energy losses occurring within the system. Exergy analysis provides a useful tool for evaluating and improving $s\text{CO}_2$ cycle performances. It is to be used to develop strategies for enhancing performance, increasing energy efficiency, and lowering environmental impact by providing insights into the thermodynamic constraints and inefficiencies of the system.

Exergy efficiencies for each component of main compression intercooling cycle configuration is analyzed for $TIT = 600^\circ\text{C}$, $CIT = 34^\circ\text{C}$, $m=1 \text{ kg/s}$ and $RPR = 0.6$. As the cycle pressure ratio increases, the turbine, main compressor, cooler, and heater exergy destruction increases, but the recompression compressor and LTR do not. HTR exergy destruction is reducing. The turbine and primary compressor inlet-outlet entropy differential increases with cycle pressure ratio. The condenser releases more energy to the environment as its inlet temperature rises and its exit temperature remains constant. Total rate of exergy destruction is found out to be 9926.24 kW from the cycle model.

Rate of exergy input for main compression intercooling cycle is calculated to be 19302.17 kW. Percentage of exergy destruction along with their numerical values are represented graphically & it is evident that maximum amount of exergy is destruction occurs in RC (Re-compressor) with 30.24% followed by 6.8% in HTR (High temperature recuperator) for exergy efficiency of the main compression intercooling cycle 48.57% at TIT of 600°C .





5.2 Seasonal TIT, MCIT observation

All of three CSP plants' turbine inlet temperatures, TIT, vary due to DNI's intermittent nature. To maximize power generation when DNI exceeds 6.1 kW-hr/m², all three plants set TIT = 600 °C. Low DNI periods reduce central receiver molten salt mass flow. The central receiver maintains a constant mass flow of molten salt into the hot tank regardless of DNI conditions to fully charge the 12-hr TES.

Thus, during low DNI, MSHE-fed molten salt into the power block decreases. Figure shows that how climate affects tank temperature. Due to MSHE heat transfer, the TES cold tank temperature decreases with DNI. Lower DNI values impair MSHE heat transfer, raising cold tank temperature.

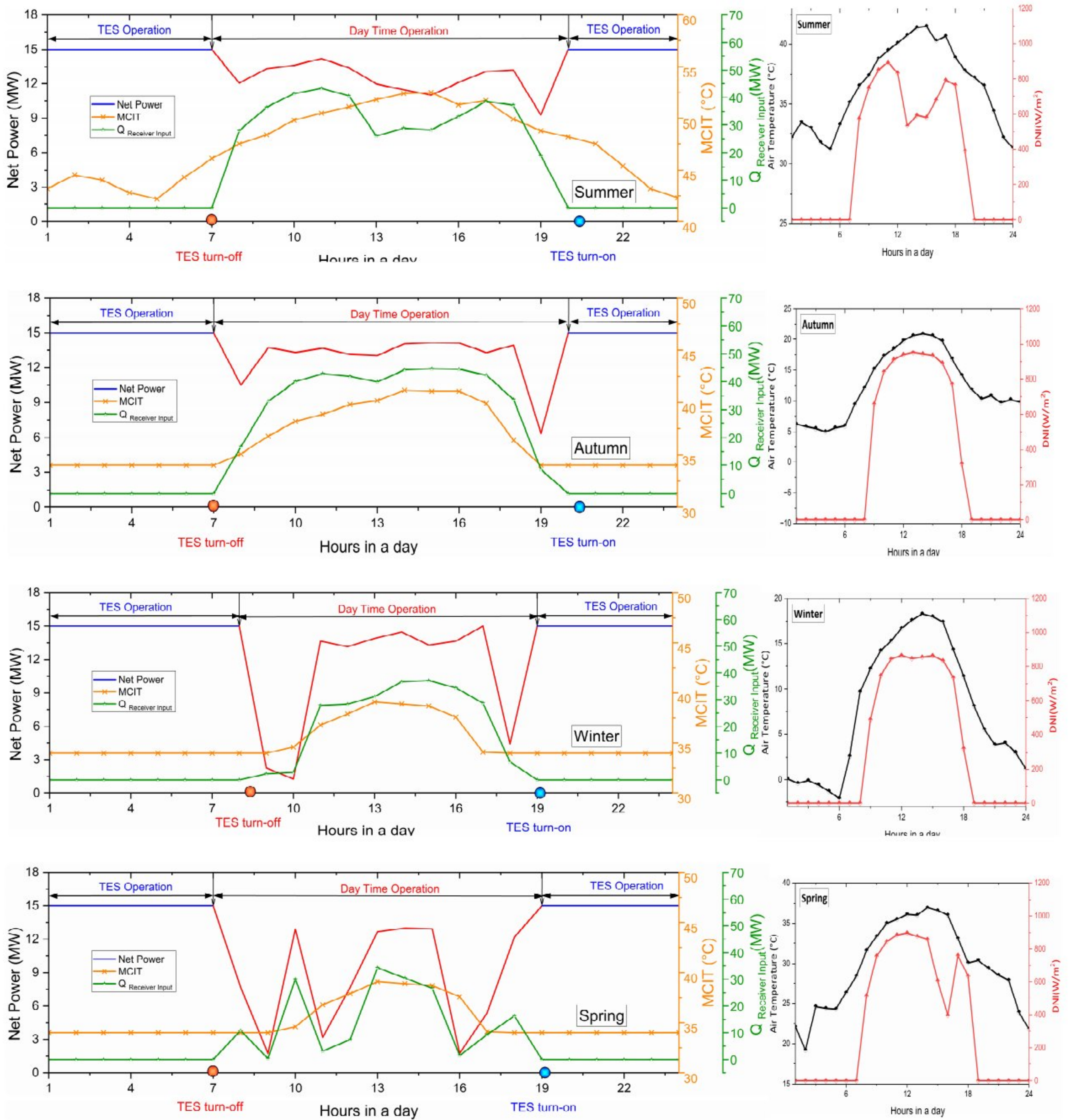


Figure 26: Recompression SCO₂ cycle hourly CSP plant performance for supplemented with TES at various seasonal climates.

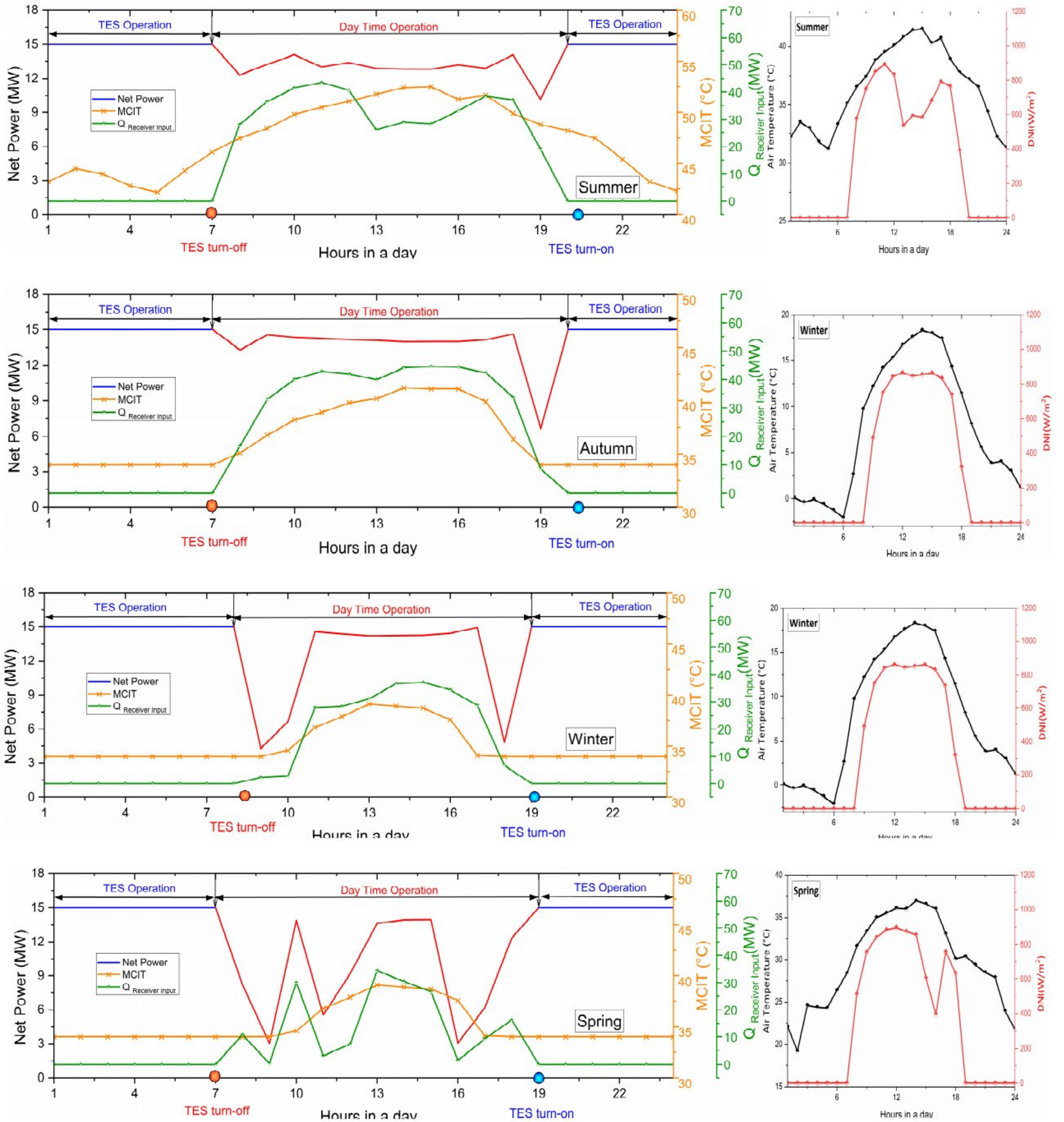


Figure 27: Partial cooling SCO_2 cycle hourly CSP plant performance for supplemented with TES at various seasonal climates.

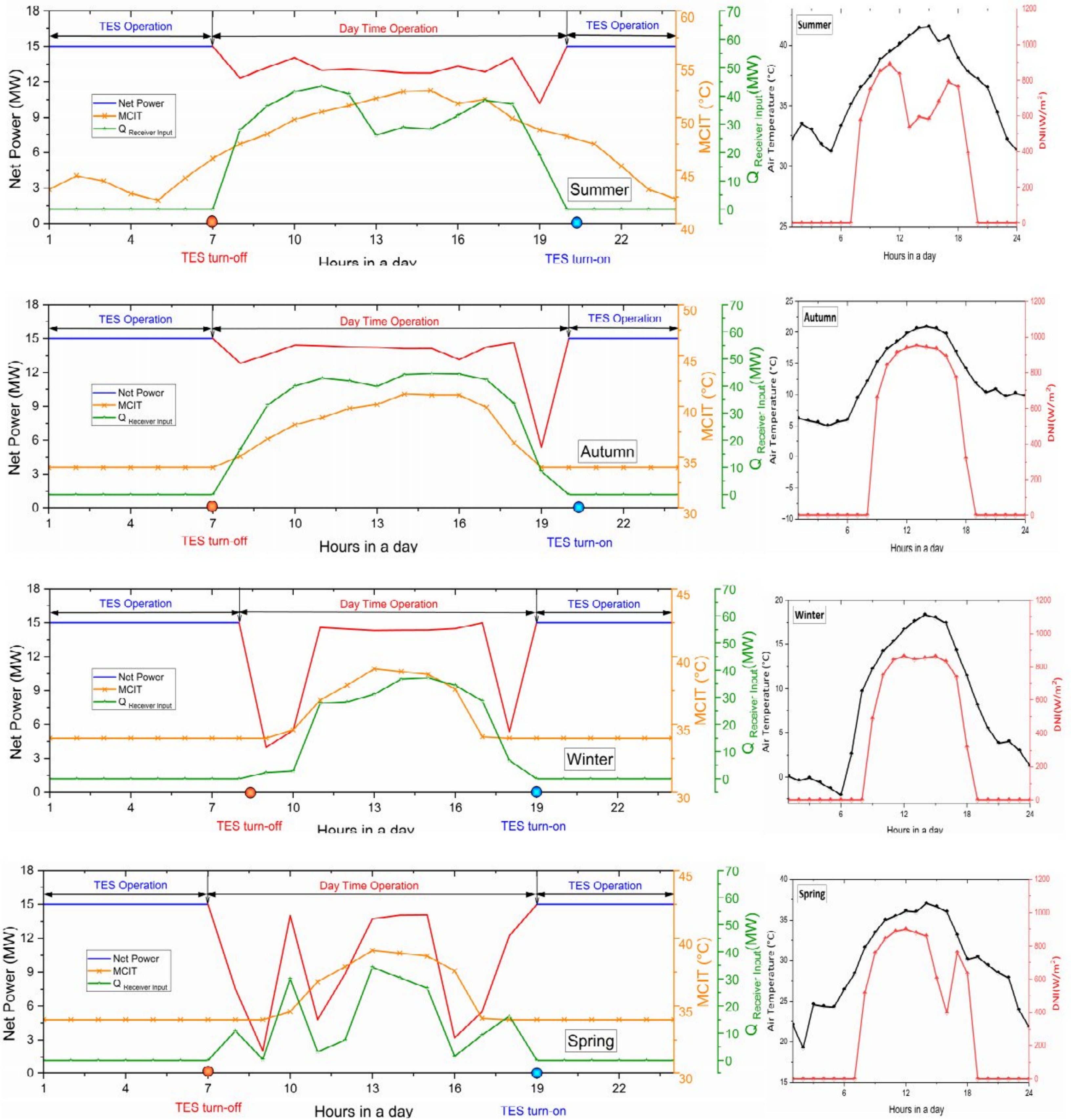


Figure 28: Main compression inter cooling SCO₂ cycle hourly CSP plant performance for supplemented with TES at various seasonal climates.

5.3 Machine Learning model error Evaluation

Following heat map is a graphic that employs color coding to show how a machine learning model performs or behaves given various combinations of different parameters (DNI, MCIT, TIT, pinch, RPR, SR, work output). It provides information about the behavior of the model and aids in the discovery of patterns and correlations between variables.

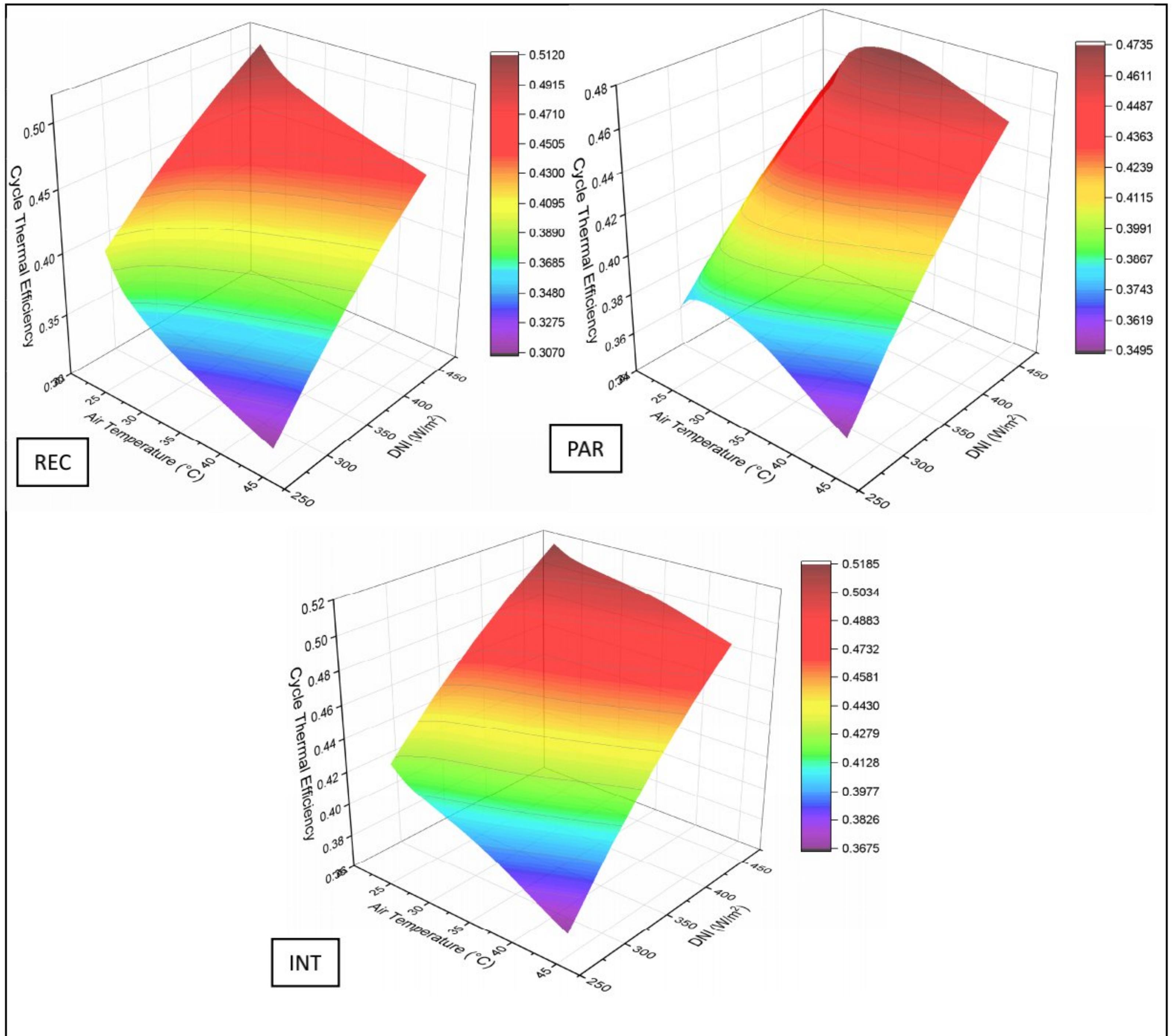


Figure 29: 3D plot for REC, PAR, INT SCO₂BC parameters.

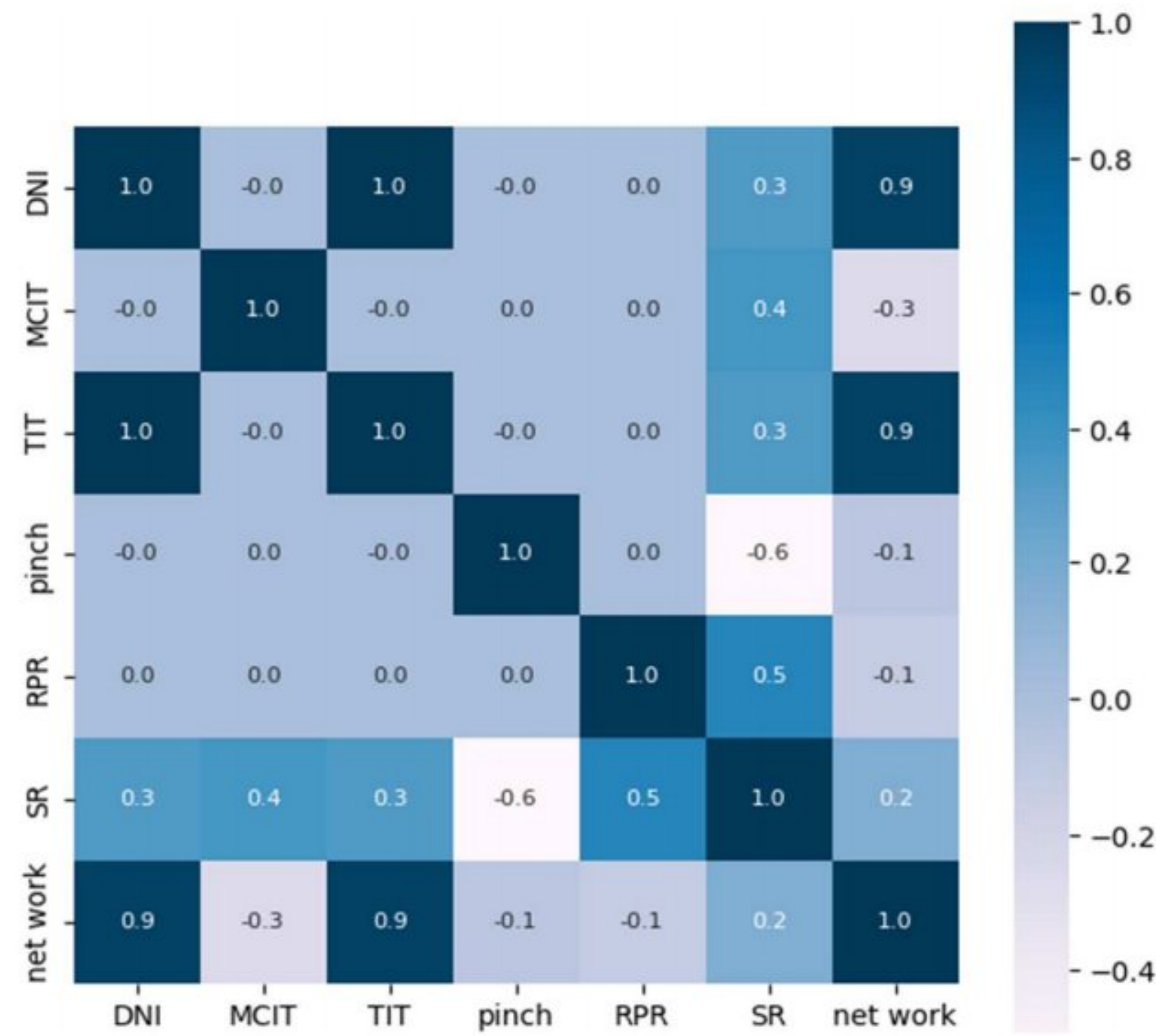


Figure 30: Heat map indicating correlation between cycle parameters.

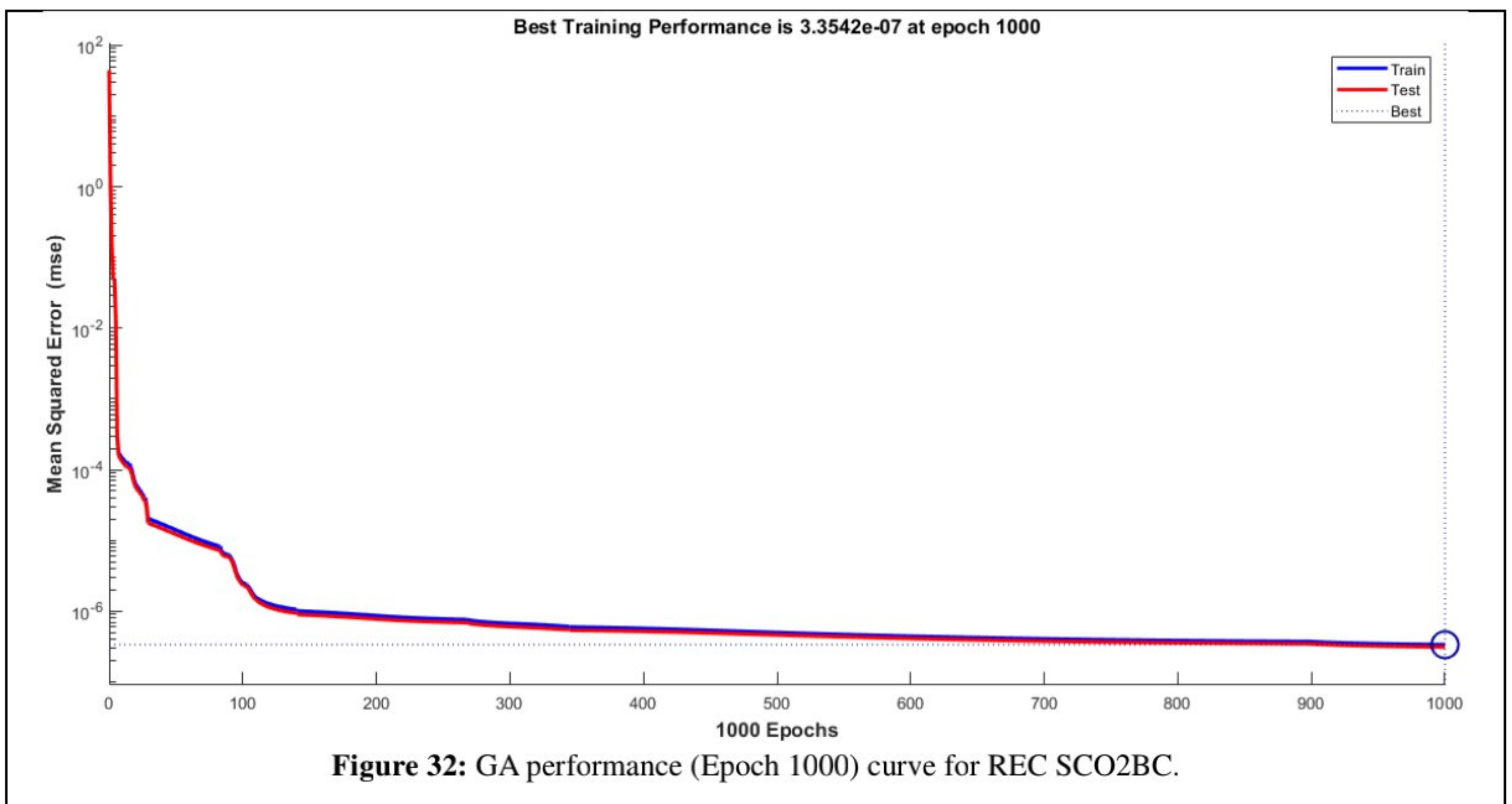
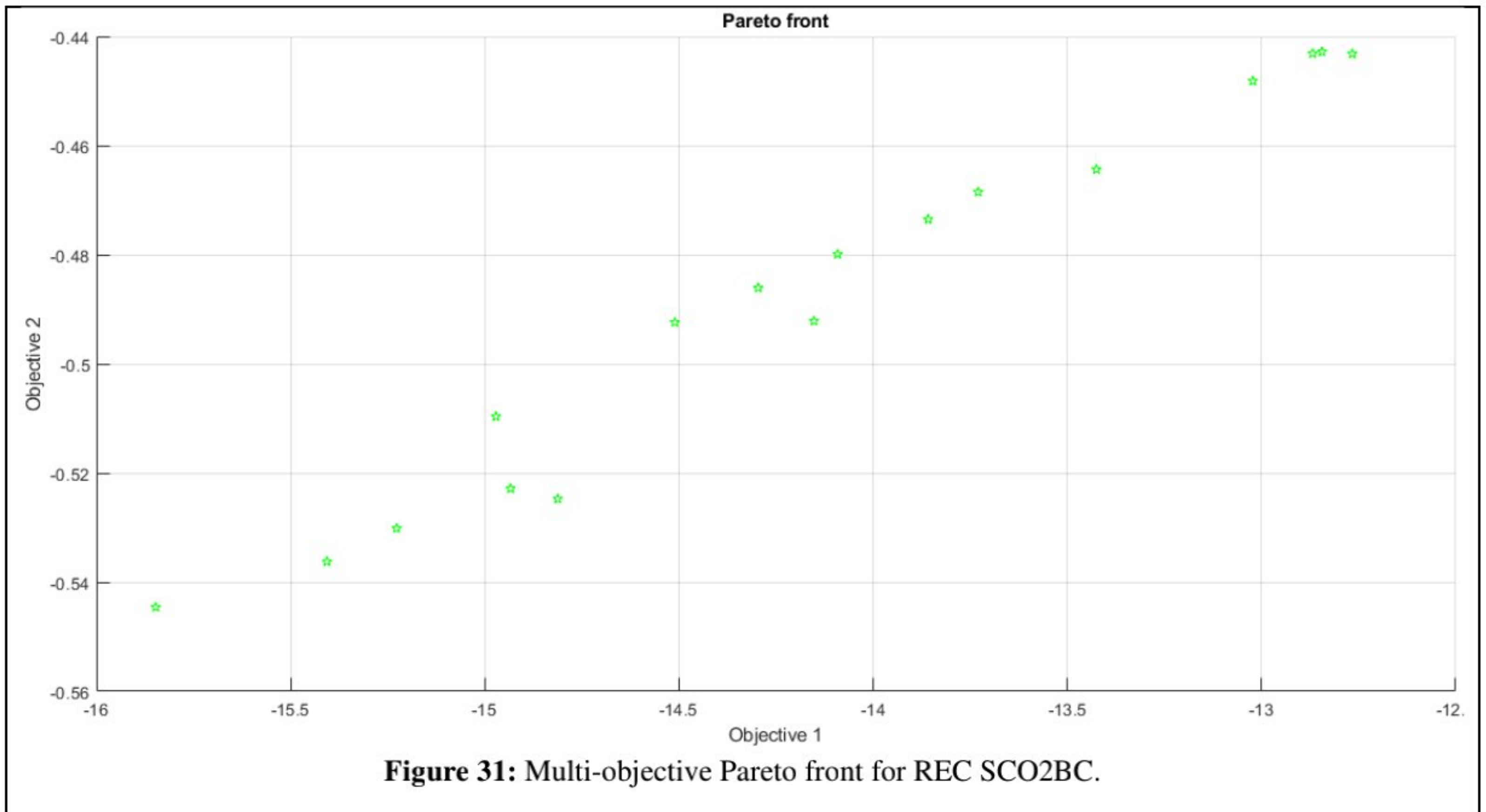
Table 12: Machine learning model prediction error comparison.

Model	Cycle	MSE	RMSE	R-squared
LightGBM	REC	0.0112265	1.0595512	99.9984903
	PAR	0.0927271	3.0451127	99.9863481
	INT	0.0920744	3.0343772	99.9871483
Random Forest	REC	1.39E-05	0.037307	99.9999982
	PAR	0.1539177	3.9232344	99.9793468
	INT	0.1528512	3.9096188	99.9794899
XGBoost	REC	5.54E-03	0.744417	99.9992786
	PAR	0.2062556	4.5415371	99.9723239
	INT	0.2062556	4.5415371	99.9723239

As shown in Table 8, for a similar amount of test-train data, the Random Forest model has the lowest MSE & RMSE for test data, while the XGBoost algorithm has higher percentage of errors. As lower error rates indicate better performance in predicting output values for a given set of input values, the Random Forest Regressor model was selected for further processing of the data.

5.3.1 Genetic Algorithm Optimization Results

GA multi-objective optimization for Recompression SCO₂ Cycle



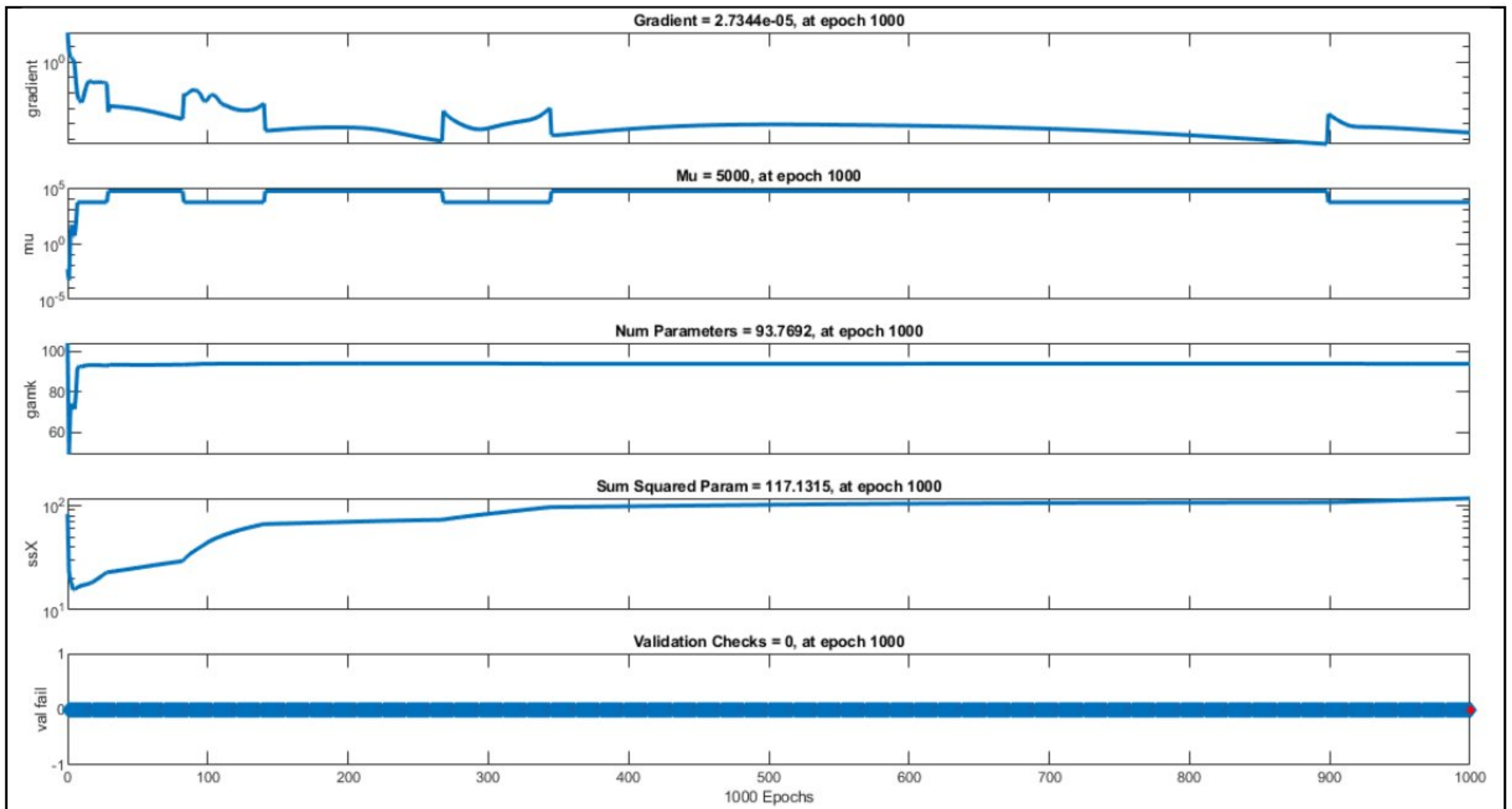


Figure 33: Training state for REC SCO2BC.

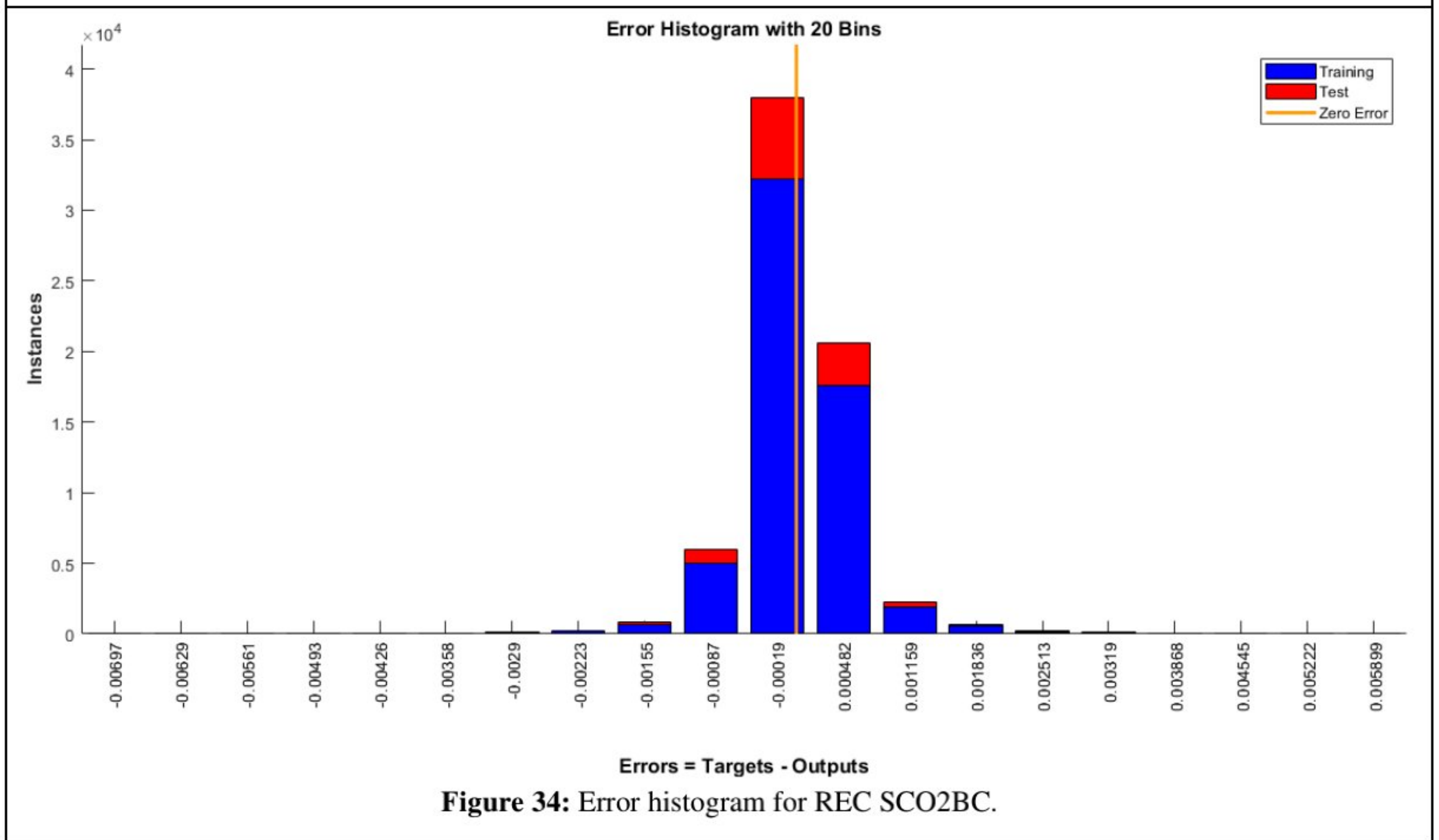


Figure 34: Error histogram for REC SCO2BC.

GA multi-objective optimization for Partial Cooling CO₂ Cycle

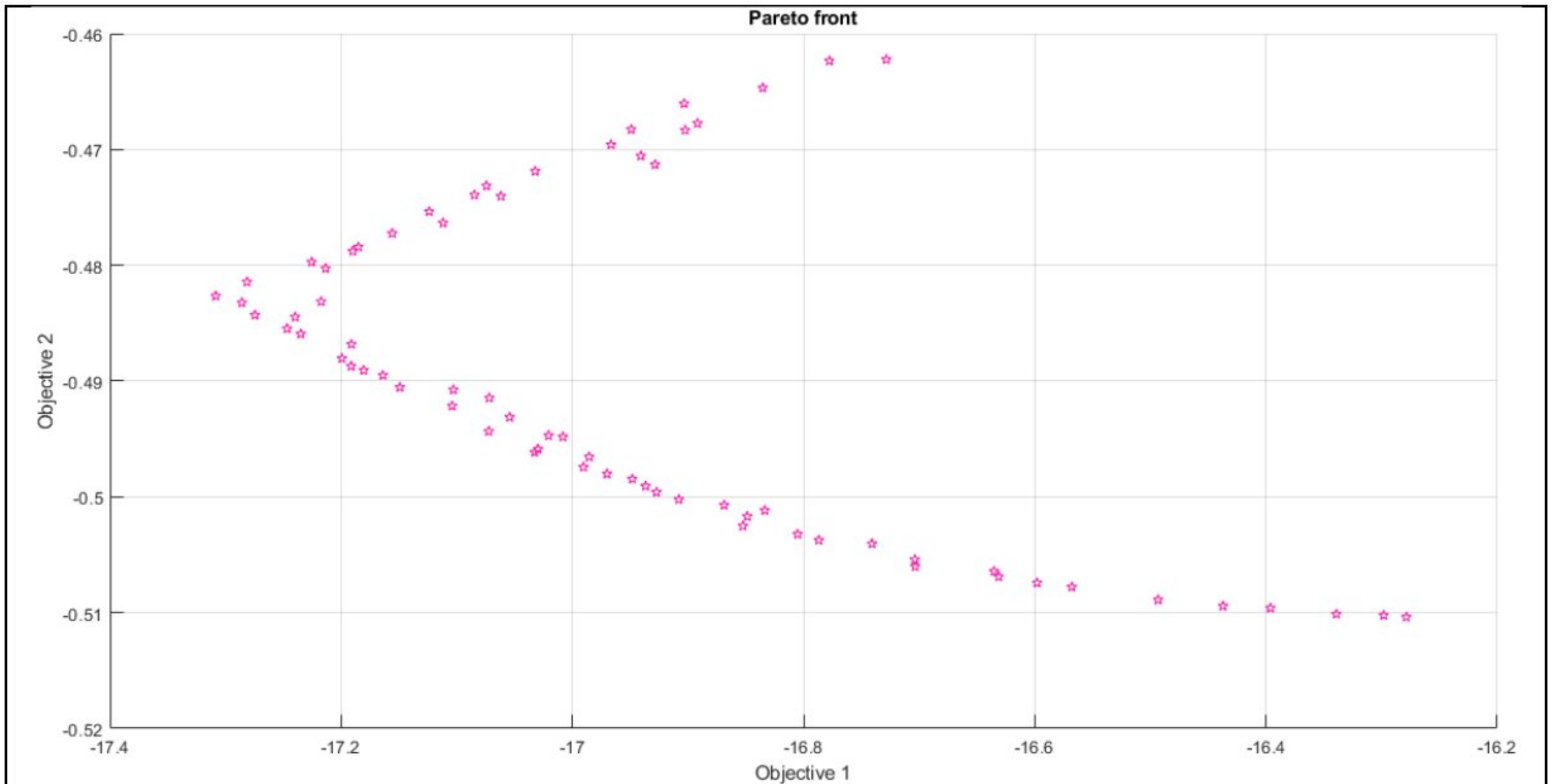


Figure 35: Multi-objective Pareto front for PAR SCO2BC.

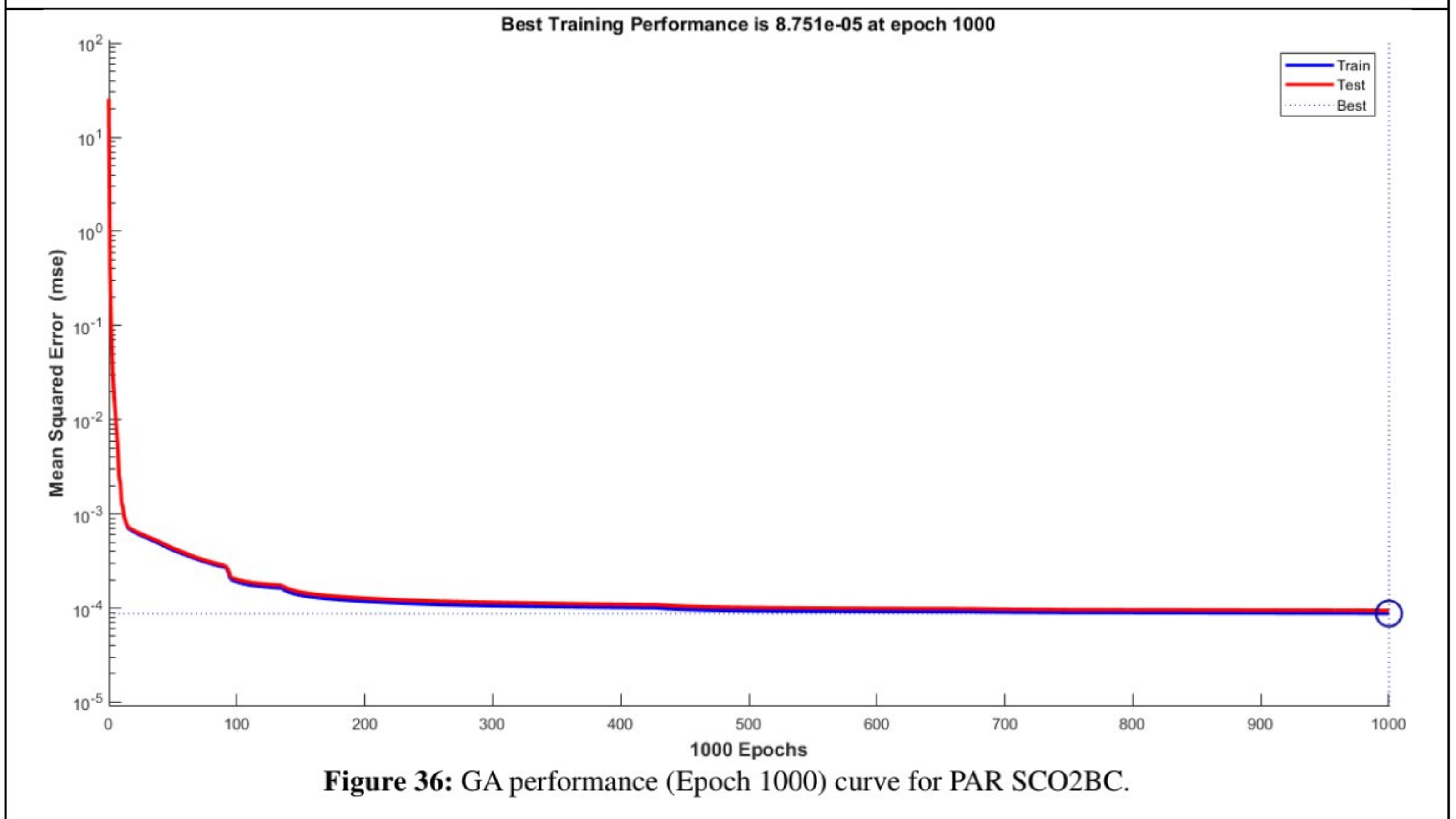


Figure 36: GA performance (Epoch 1000) curve for PAR SCO2BC.

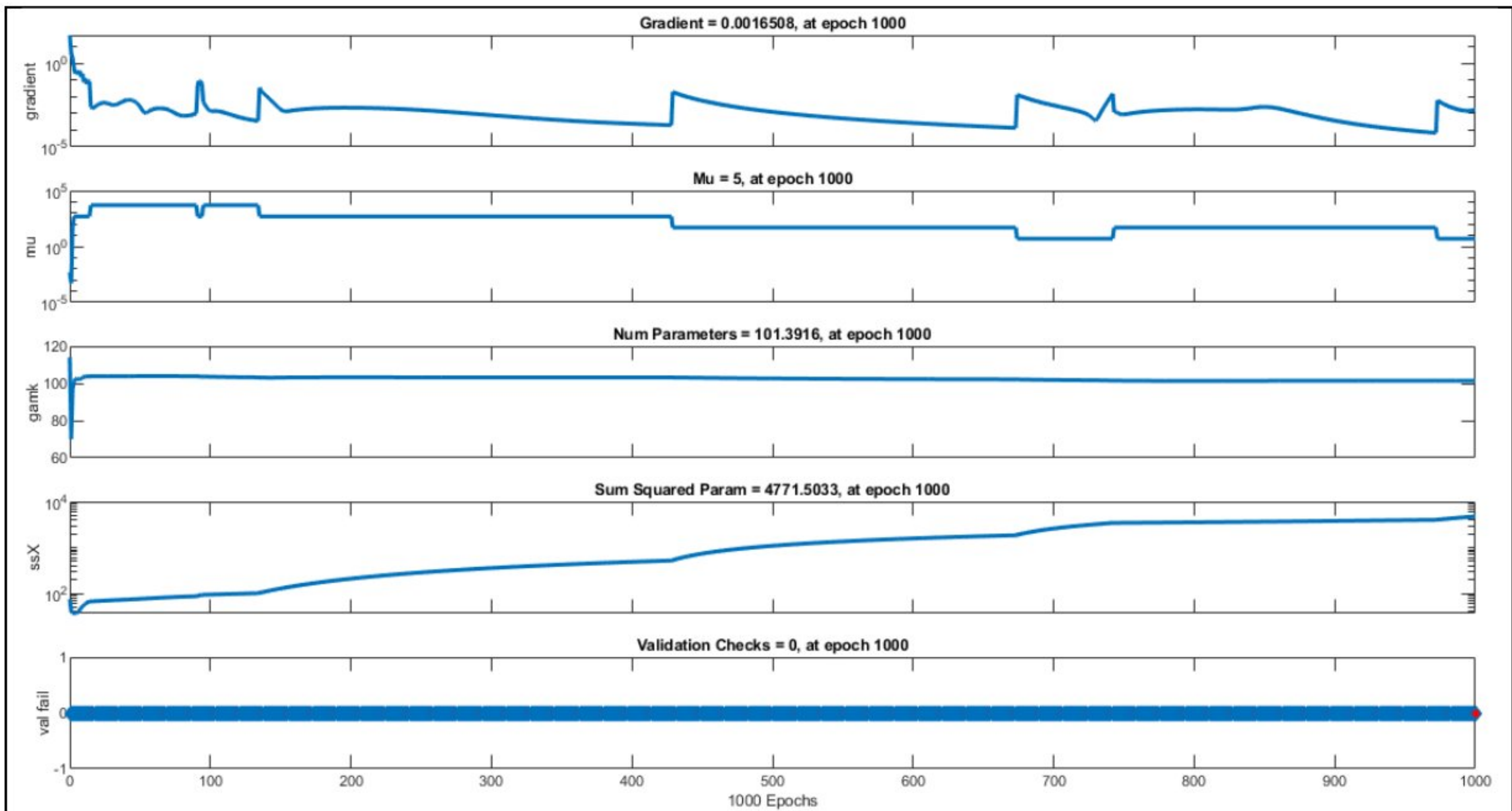


Figure 37: Training state for PAR SCO2BC.

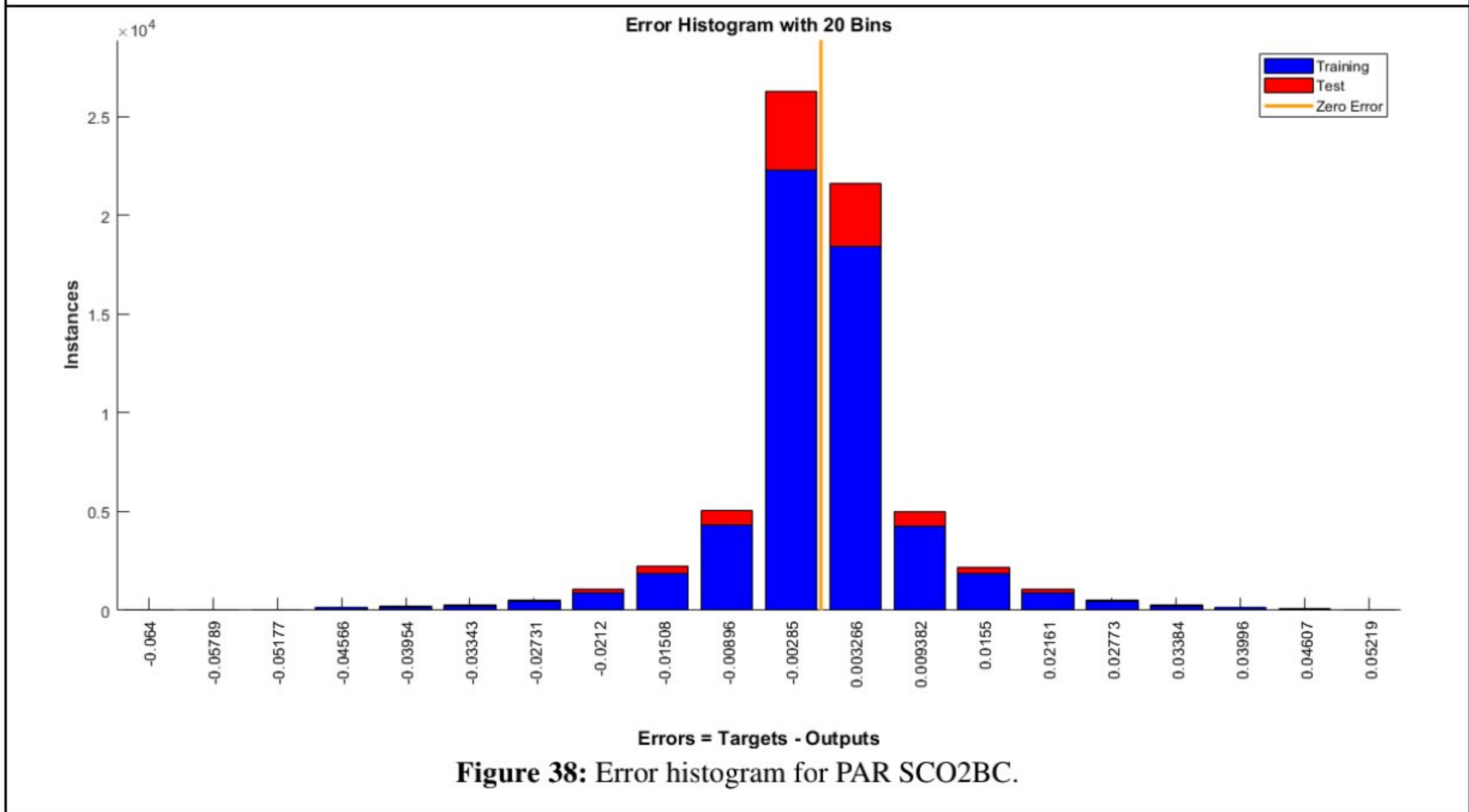


Figure 38: Error histogram for PAR SCO2BC.

GA multi-objective optimization for Main Compression Inter Cooling SCO₂ Cycle

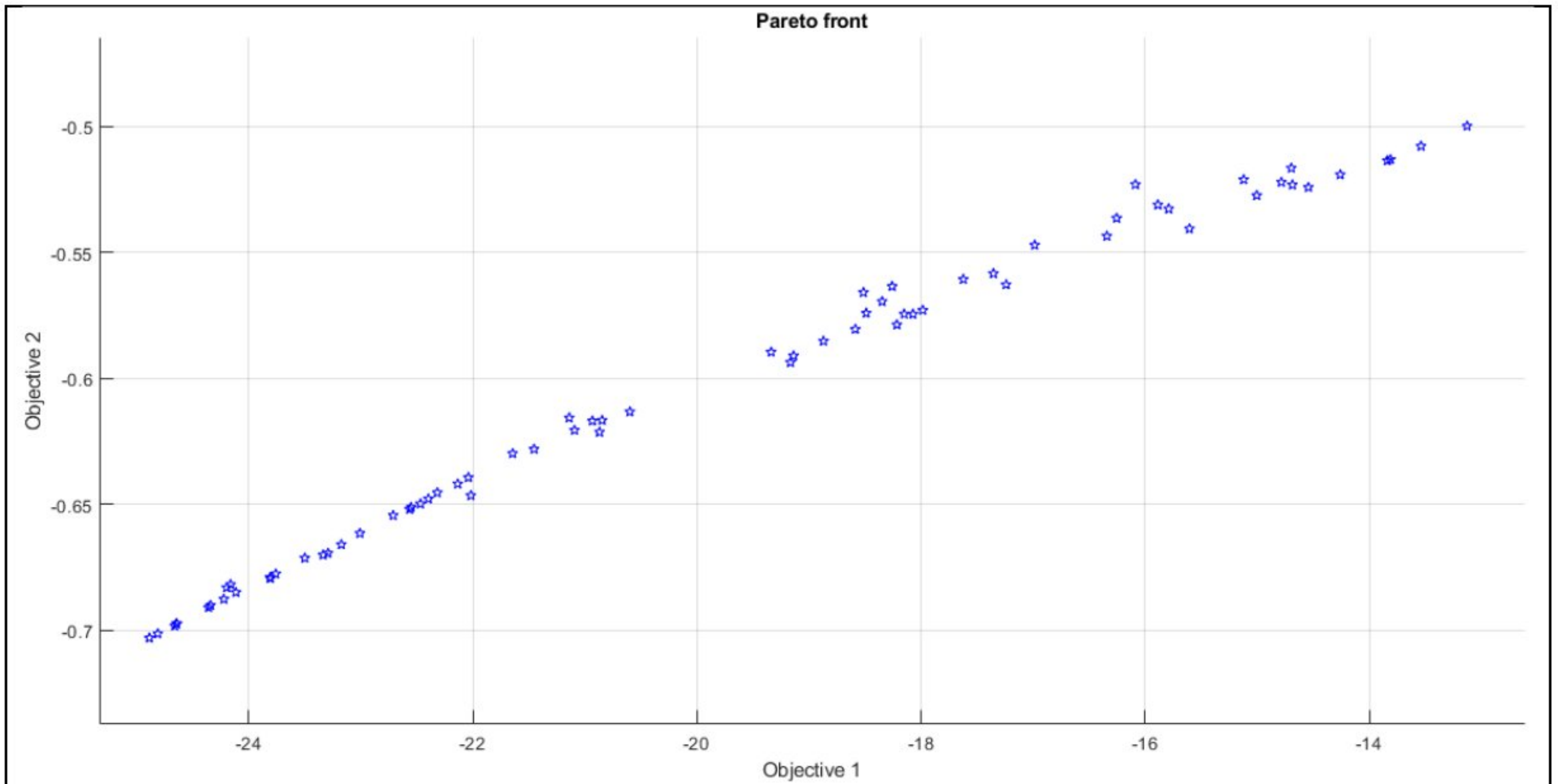


Figure 39: Multi-objective Pareto front for INT SCO₂BC.

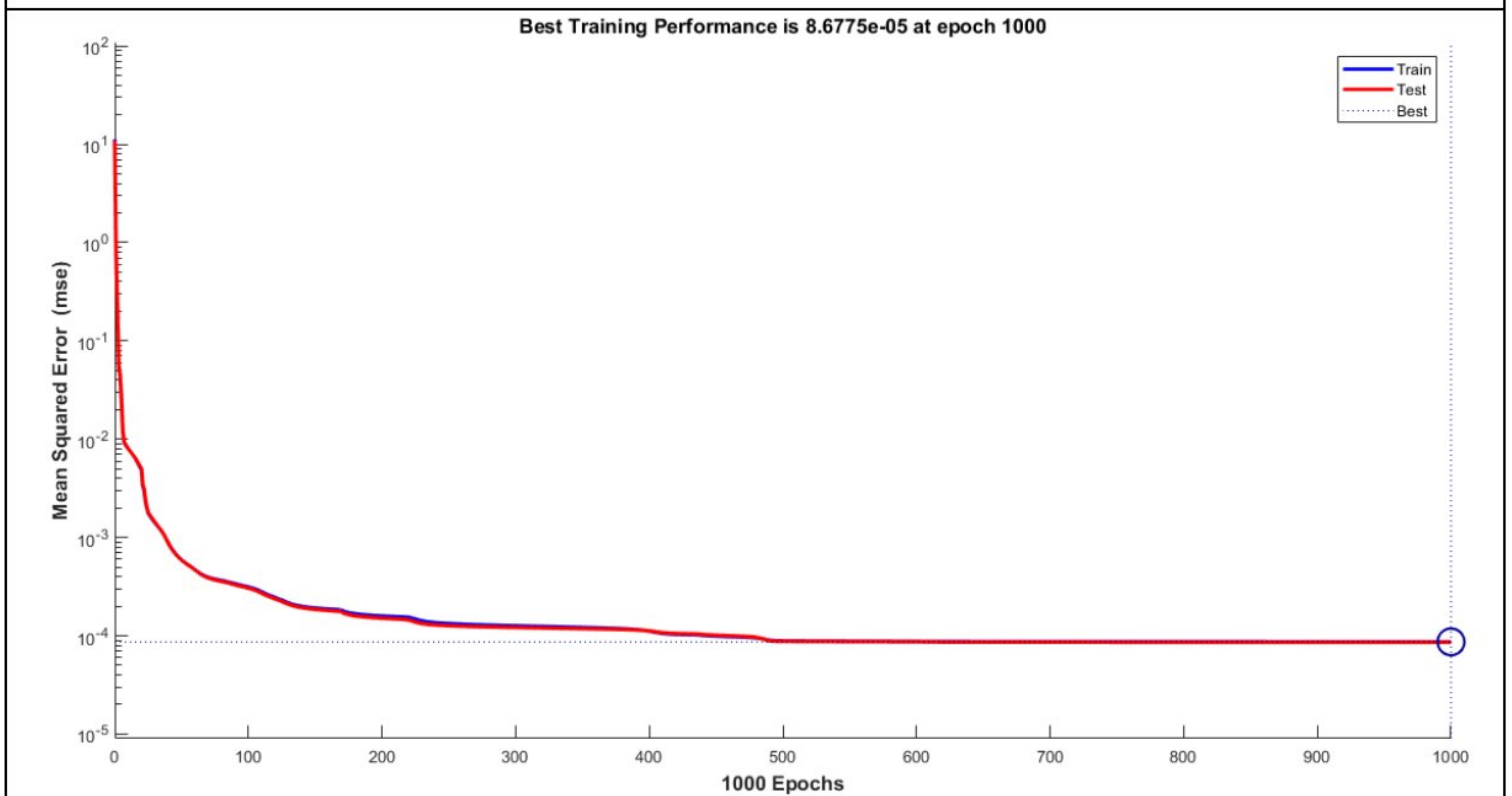
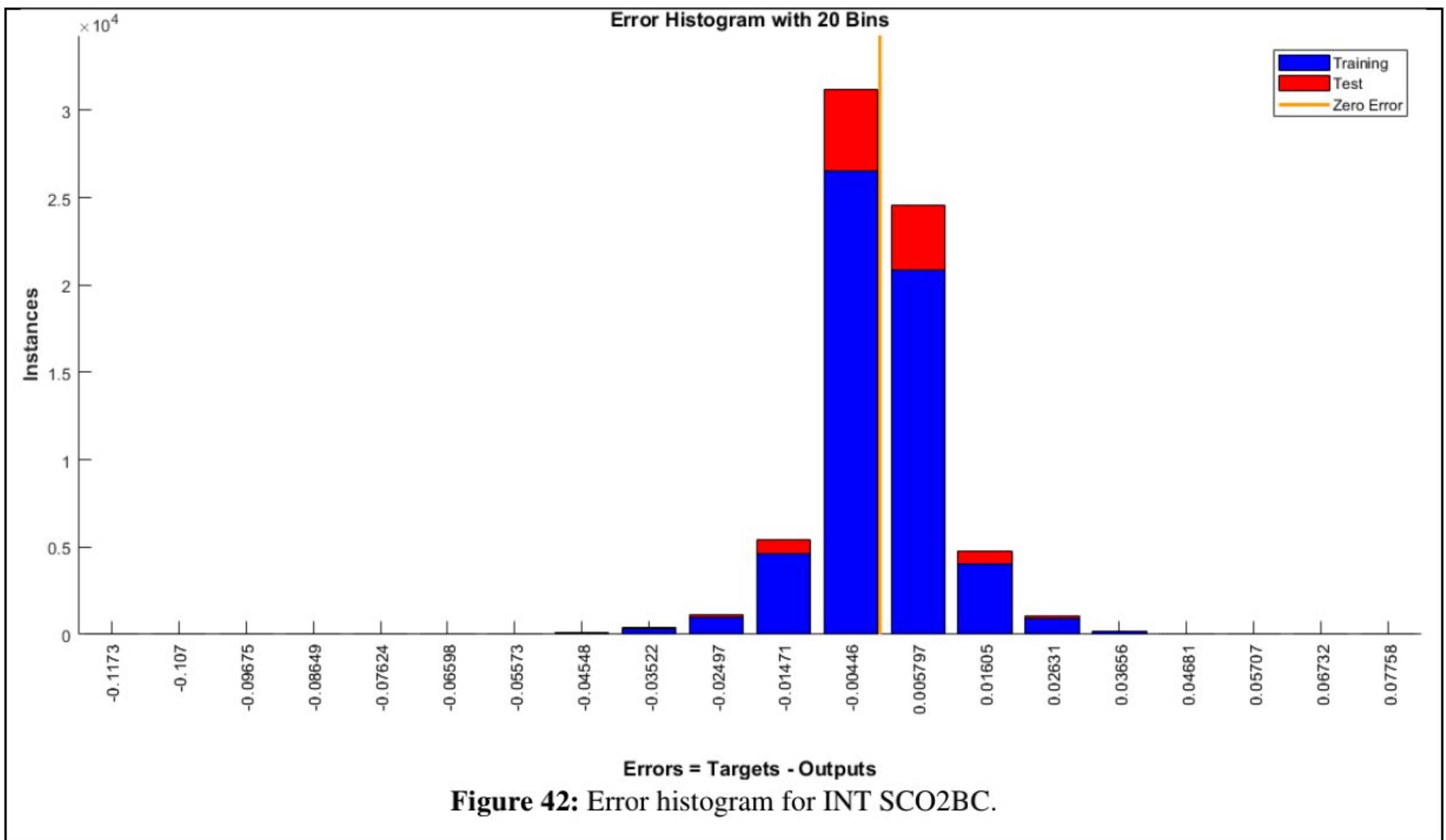
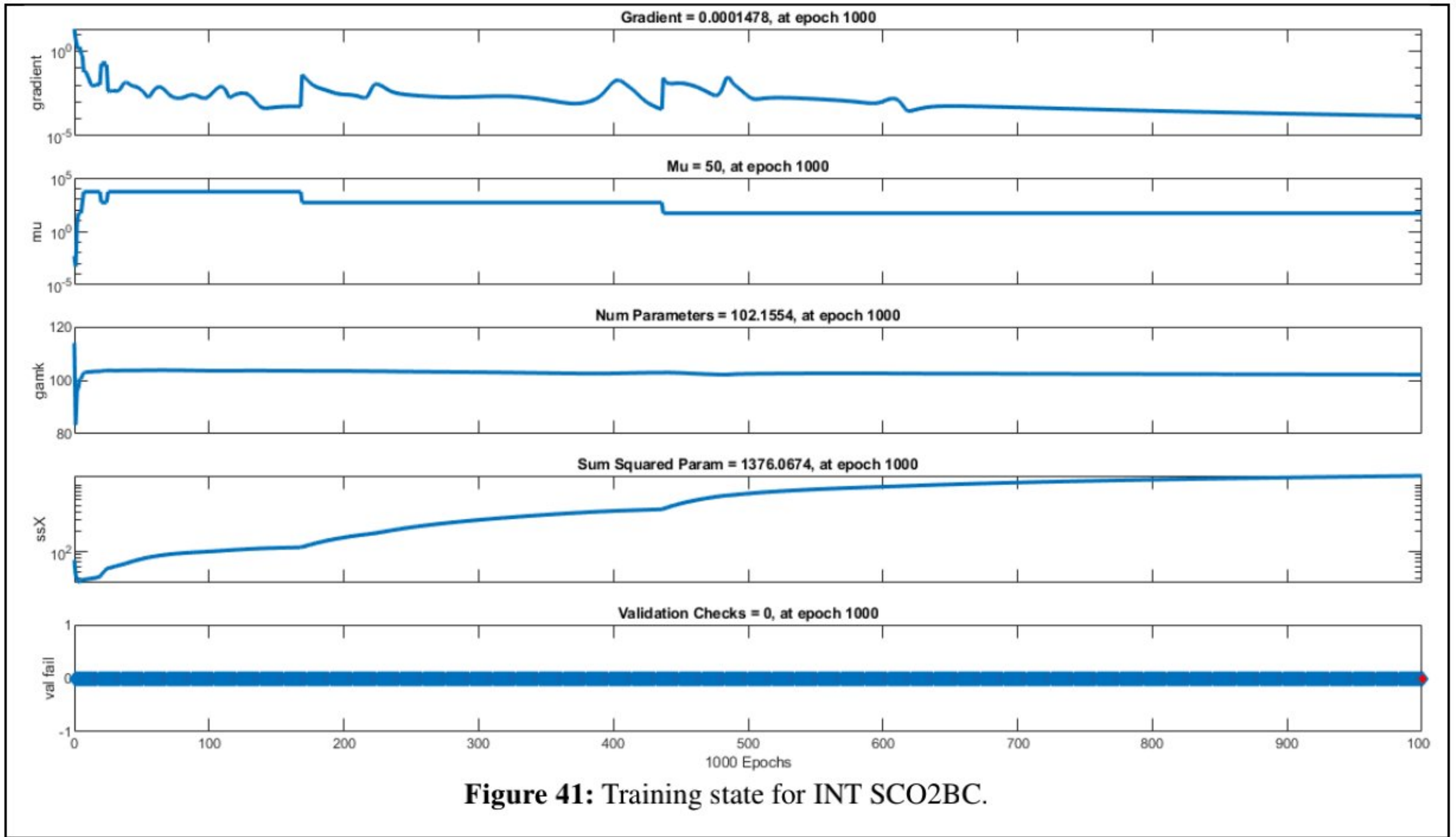


Figure 40: GA performance (Epoch 1000) curve for INT SCO₂BC.



5.3.2 TOPSIS Decision Analysis Results

The Pareto front diagram shows the optimized point for best output, as all points on the Pareto front have been optimized and give the best data. However, it is worth noting that a slight variation in input data may yield different optimized values.

Table 13: Optimized conditions obtained from TOPSIS for best performance.

Cycle	DNI (kW/m ²)	MCIT (°C)	TIT (°C)	T _{pinch}	RPR	SR	W _{net} (MW)	η _{cycle} (%)	X _{dest} (MW)	η _{exergy} (%)
REC	0.486247	54.7703	653.398	18.9855	-	0.79602	12.8408	44.3508509	6.83467	65.2561669
PAR	0.521002	34.0471	687.4	12.191	0.82564	0.71061	16.9024	46.8328048	7.96143	67.5327321
INT	0.472434	34.1036	656.477	9.90803	0.70858	0.56792	18.0712	57.4488273	7.7498	68.2970968

Table 13. shows the optimized parameters, such as DNI, MCIT, TIT, T_{pinch}, RPR, SR, obtained from this study using different tools for best performance possible (W_{net} , η_{cycle} , X_{dest} , η_{exergy}) for Recompression, Partial cooling & Main compression inter cooling sCO₂ cycle.

Chapter 6: Conclusion

6.1 Conclusion

In this study, Machine Learning methods are shown for evaluating sCO₂ Brayton cycle (e.g., Recompression Cycle, Partial Cooling Cycle & Main Compressor Intercooling Cycle). Random Forest Algorithm, XGBoost & LightGBM regression models are primarily implemented for cycle analysis & forecasting.

- The energy and exergy assessments of S-CO₂ power cycles investigated the contribution of the key functional factors to the thermal and second law efficiency. The effects of the cycles' low and high pressures are investigated at intake turbine temperatures of 450°C, 550°C, 650°C, and 750°C with a net output power of 15 MW. The study that is being done at this time has produced the results listed below.
- In order to regulate TIT and MCIT under various weather and seasonal conditions, the effect of variation in DNI and air temperature is implemented using weather data. For the CSP loop calculations, pre-designed TES is taken into account.
- The maximum thermal efficiency of 54.48% is achieved by the Main-Compression intercooling at RPR of 0.60, split ratio 0.85 TIT of 750°C, Cycle maximum pressure of 25 MPa, minimum pressure of 8 MPa and Compression inlet temperature of 34°C.
- The algorithms' hyperparameters have been adjusted to provide the lowest MSE value and highest R squared error. Through R Squared Error, the findings demonstrate the relationship between the variables and the target values; Random Forest and XGBoost both demonstrated 99.93% and 99.92% matching, correspondingly. In terms of 17250 values, Random Forest outperforms XGBoost Algorithm in terms of speed and accuracy. The results have demonstrated that Machine learning algorithms have been effectively adapted to the thermodynamic model.
- TOPSIS decision making tool was used to determine optimized points for each cycle to attain maximum cycle performance.

The results show that, in comparison to thermodynamic models, machine learning techniques may be used to predict & optimize SCO₂ cycles equipped with CSP loop with higher accuracy and efficiency.

6.2 Recommendation for future works

6.2.1 Design recommendation for future commercialization

In a dry area with high solar irradiation where there is a plentiful supply of water, the location of the future CSP plant with sCO₂ power block is extremely suitable. The unique characteristics of the sCO₂ power cycle, such as its compactness in heat exchangers and turbomachinery and ability to maintain superior performance at higher climate temperatures with dry cooling, can help reduce the CSP plant's capital cost even more.

For a particular CSP location, selecting the appropriate ambient temperature is essential when designing the cooling tower. To determine the ideal ambient temperature for a certain CSP location and enhance plant efficiency, an economic assessment is required. In order to achieve the greatest possible yearly CSP performance, this air temperature should fall between the mean temperature and the temperature with the highest frequency as determined by the climatic dataset. Our long-term research objective is the thorough economic evaluation and improvement of dry cooled sCO₂ power cycles created for use in CSP applications under varied climatic conditions.

6.2.2 Hyperparameter optimization & implementation of deep learning models

One of the most important steps in putting deep learning models into practice is hyperparameter optimization. Hyperparameters are variables that affect the model's behavior and performance but are set before training and are not learned from the data. Included in them are variables like learning rate, batch size, number of layers, activation functions, regularization methods, and more.

Determining the optimal values or combinations of hyperparameters that maximize the model's performance and generalization is the goal of hyperparameter optimization. The accuracy, speed of convergence, and robustness of the model can all be considerably enhanced by a carefully chosen set of hyperparameters.

Data Availability

Data will be made available on request.

References

- [1] W. Wang, S. Deng, D. Zhao, L. Zhao, S. Lin, and M. Chen, "Application of machine learning into organic Rankine cycle for prediction and optimization of thermal and exergy efficiency," *Energy Convers Manag*, vol. 210, Apr. 2020, doi: 10.1016/j.enconman.2020.112700.
- [2] J. Wang, P. Zhao, X. Niu, and Y. Dai, "Parametric analysis of a new combined cooling, heating and power system with transcritical CO₂ driven by solar energy," *Appl Energy*, vol. 94, pp. 58–64, 2012, doi: 10.1016/j.apenergy.2012.01.007.
- [3] K. J. Kimball and E. M. Clementoni, "GT2012-68204," 2016.
- [4] C. S. Turchi, Z. Ma, and J. Dyreby, "Supercritical carbon dioxide power cycle configurations for use in concentrating solar power systems," *Proceedings of the ASME Turbo Expo*, vol. 5, no. March, pp. 967–973, 2012, doi: 10.1115/GT2012-68932.
- [5] F. A. Al-Sulaiman and M. Atif, "Performance comparison of different supercritical carbon dioxide Brayton cycles integrated with a solar power tower," *Energy*, vol. 82, pp. 61–71, 2015, doi: 10.1016/j.energy.2014.12.070.
- [6] D. Vitale Di Maio, A. Boccitto, and G. Caruso, "Supercritical carbon dioxide applications for energy conversion systems," in *Energy Procedia*, Elsevier Ltd, 2015, pp. 819–824. doi: 10.1016/j.egypro.2015.11.818.
- [7] L. H. Zhi, P. Hu, L. X. Chen, and G. Zhao, "Multiple parametric analysis, optimization and efficiency prediction of transcritical organic Rankine cycle using trans-1,3,3,3-tetrafluoropropene (R1234ze(E)) for low grade waste heat recovery," *Energy Convers Manag*, vol. 180, pp. 44–59, Jan. 2019, doi: 10.1016/j.enconman.2018.10.086.
- [8] M. Saeed, M. I. Radaideh, A. S. Berrouk, and K. Alawadhi, "Machine learning-based efficient multi-layered precooler design approach for supercritical CO₂ cycle," *Energy Conversion and Management: X*, vol. 11, p. 100104, 2021, doi: 10.1016/j.ecmx.2021.100104.
- [9] Y. Ma, X. Zhang, M. Liu, J. Yan, and J. Liu, "Proposal and assessment of a novel supercritical CO₂ Brayton cycle integrated with LiBr absorption chiller for concentrated solar power applications," *Energy*, vol. 148, pp. 839–854, Apr. 2018, doi: 10.1016/j.energy.2018.01.155.

- [10] X. Li, Y. Huang, and Y. Shi, "Ultra-short term power load prediction based on gated cycle neural network and XGBoost models," *J Phys Conf Ser*, vol. 2026, no. 1, 2021, doi: 10.1088/1742-6596/2026/1/012022.
- [11] S. A. Wright, R. F. Radel, T. M. Conboy, and G. E. Rochau, "SANDIA REPORT Modeling and Experimental Results for Condensing Supercritical CO₂ Power Cycles." [Online]. Available: <http://www.ntis.gov/help/ordermethods.asp?loc=7-4-0#online>
- [12] M. V. J. J. Suresh, K. S. Reddy, and A. K. Kolar, "ANN-GA based optimization of a high ash coal-fired supercritical power plant," *Appl Energy*, vol. 88, no. 12, pp. 4867–4873, 2011, doi: 10.1016/j.apenergy.2011.06.029.
- [13] L. X. Chen, P. Hu, C. C. Sheng, and M. N. Xie, "A novel compressed air energy storage (CAES) system combined with pre-cooler and using low grade waste heat as heat source," *Energy*, vol. 131, pp. 259–266, 2017, doi: 10.1016/j.energy.2017.05.047.
- [14] P. Tüfekci, "Prediction of full load electrical power output of a base load operated combined cycle power plant using machine learning methods," *International Journal of Electrical Power and Energy Systems*, vol. 60, pp. 126–140, 2014, doi: 10.1016/j.ijepes.2014.02.027.
- [15] M. Persichilli, A. Kacludis, E. Zdankiewicz, and T. Held, "Supercritical CO₂ Power Cycle Developments and Commercialization: Why sCO₂ can Displace Steam Steam." [Online]. Available: www.echogen.com
- [16] S. M. Besarati and D. Yogi Goswami, "Analysis of Advanced Supercritical Carbon Dioxide Power Cycles With a Bottoming Cycle for Concentrating Solar Power Applications," *J Sol Energy Eng*, vol. 136, no. 1, Nov. 2013, doi: 10.1115/1.4025700.
- [17] J. Dyreby, S. Klein, G. Nellis, and D. Reindl, "Design Considerations for Supercritical Carbon Dioxide Brayton Cycles With Recompression," *J Eng Gas Turbine Power*, vol. 136, no. 10, Jul. 2014, doi: 10.1115/1.4027936.
- [18] S. A. Wright, R. F. Radel, T. M. Conboy, and G. E. Rochau, "SANDIA REPORT Modeling and Experimental Results for Condensing Supercritical CO₂ Power Cycles." [Online]. Available: <http://www.ntis.gov/help/ordermethods.asp?loc=7-4-0#online>

- [19] C. S. Turchi, Z. Ma, T. W. Neises, and M. J. Wagner, "Thermodynamic study of advanced supercritical carbon dioxide power cycles for concentrating solar power systems," *Journal of Solar Energy Engineering, Transactions of the ASME*, vol. 135, no. 4, 2013, doi: 10.1115/1.4024030.
- [20] D. A. Wood, "Combined cycle gas turbine power output prediction and data mining with optimized data matching algorithm," *SN Appl Sci*, vol. 2, no. 3, Mar. 2020, doi: 10.1007/s42452-020-2249-7.
- [21] D. Vitale Di Maio, A. Boccitto, and G. Caruso, "Supercritical carbon dioxide applications for energy conversion systems," in *Energy Procedia*, Elsevier Ltd, 2015, pp. 819–824. doi: 10.1016/j.egypro.2015.11.818.
- [22] M. Khademi, A. Ahmadi, R. Dashti, and R. Shirmohammadi, "Thermoeconomic optimization of a solar-assisted supercritical CO₂ Brayton cycle, organic Rankine cycle and multi-effect distillation system," *Energy Reports*, vol. 8, pp. 13494–13503, Nov. 2022, doi: 10.1016/j.egy.2022.10.010.
- [23] Y. Cao, P. Li, Z. Qiao, S. Ren, and F. Si, "A concept of a supercritical CO₂ Brayton and organic Rankine combined cycle for solar energy utilization with typical geothermal as auxiliary heat source: Thermodynamic analysis and optimization," *Energy Reports*, vol. 8, pp. 322–333, Nov. 2022, doi: 10.1016/j.egy.2021.11.258.
- [24] M. M. Ehsan, X. Wang, Z. Guan, and A. Y. Klimenko, "Design and performance study of dry cooling system for 25 M² solar power plant operated with supercritical CO₂ cycle," *International Journal of Thermal Sciences*, vol. 132, pp. 398–410, Oct. 2018, doi: 10.1016/j.ijthermalsci.2018.06.024.
- [25] M. V. J. J. Suresh, K. S. Reddy, and A. K. Kolar, "ANN-GA based optimization of a high ash coal-fired supercritical power plant," *Appl Energy*, vol. 88, no. 12, pp. 4867–4873, 2011, doi: 10.1016/j.apenergy.2011.06.029.
- [26] R. V. Padilla, Y. C. Soo Too, R. Benito, and W. Stein, "Exergetic analysis of supercritical CO₂ Brayton cycles integrated with solar central receivers," *Appl Energy*, vol. 148, pp. 348–365, Jun. 2015, doi: 10.1016/j.apenergy.2015.03.090.
- [27] Z. Ma and C. S. Turchi, "Advanced Supercritical Carbon Dioxide Power Cycle Configurations for Use in Concentrating Solar Power Systems Preprint." [Online]. Available: <http://www.osti.gov/bridge>

- [28] M. M. Ehsan, S. Duniam, Z. Guan, H. Gurgenci, and A. Klimenko, "Seasonal variation on the performance of the dry cooled supercritical CO₂ recompression cycle," *Energy Convers Manag*, vol. 197, Oct. 2019, doi: 10.1016/j.enconman.2019.111865.
- [29] S. Kim, Y. Cho, M. S. Kim, and M. Kim, "Characteristics and optimization of supercritical CO₂ recompression power cycle and the influence of pinch point temperature difference of recuperators," *Energy*, vol. 147, pp. 1216–1226, Mar. 2018, doi: 10.1016/j.energy.2017.12.161.
- [30] T. Conboy, J. Pasch, and D. Fleming, "Control of a supercritical corecompression brayton cycle demonstration loop," *J Eng Gas Turbine Power*, vol. 135, no. 11, 2013, doi: 10.1115/1.4025127.
- [31] E. Ruiz-Casanova, C. Rubio-Maya, J. J. Pacheco-Ibarra, V. M. Ambriz-Díaz, C. E. Romero, and X. Wang, "Thermodynamic analysis and optimization of supercritical carbon dioxide Brayton cycles for use with low-grade geothermal heat sources," *Energy Convers Manag*, vol. 216, Jul. 2020, doi: 10.1016/j.enconman.2020.112978.
- [32] R. Chen, M. Romero, J. González-Aguilar, F. Rovense, Z. Rao, and S. Liao, "Design and off-design performance comparison of supercritical carbon dioxide Brayton cycles for particle-based high temperature concentrating solar power plants," *Energy Convers Manag*, vol. 232, Mar. 2021, doi: 10.1016/j.enconman.2021.113870.
- [33] T. Y. Liu, J. Z. Yang, Z. Yang, and Y. Y. Duan, "Multiparameter optimization and configuration comparison of supercritical CO₂ Brayton cycles based on efficiency and cost tradeoff," *Sci China Technol Sci*, vol. 64, no. 10, pp. 2084–2098, Oct. 2021, doi: 10.1007/s11431-021-1885-2.
- [34] R. Chen, M. Romero, J. González-Aguilar, F. Rovense, Z. Rao, and S. Liao, "Optical and thermal integration analysis of supercritical CO₂ Brayton cycles with a particle-based solar thermal plant based on annual performance," *Renew Energy*, vol. 189, pp. 164–179, Apr. 2022, doi: 10.1016/j.renene.2022.02.059.
- [35] A. Khadse, L. Blanchette, J. Kapat, S. Vasu, J. Hossain, and A. Donazzolo, "Optimization of Supercritical CO₂ Brayton Cycle for Simple Cycle Gas Turbines Exhaust Heat Recovery Using Genetic Algorithm," *Journal of Solar Energy Engineering, Transactions of the ASME*, vol. 140, no. 7, Jul. 2018, doi: 10.1115/1.4039446.

- [36] X. Wang, Q. Liu, Z. Bai, J. Lei, and H. Jin, "Thermodynamic Analysis of the Cascaded Supercritical CO₂ Cycle Integrated with Solar and Biomass Energy," in *Energy Procedia*, Elsevier Ltd, 2017, pp. 445–452. doi: 10.1016/j.egypro.2017.03.339.
- [37] C. S. Turchi, "Supercritical CO₂ for Application in Concentrating Solar Power Systems," 2009.
- [38] W. Wang, S. Deng, D. Zhao, L. Zhao, S. Lin, and M. Chen, "Application of machine learning into organic Rankine cycle for prediction and optimization of thermal and exergy efficiency," *Energy Convers Manag*, vol. 210, Apr. 2020, doi: 10.1016/j.enconman.2020.112700.
- [39] R. Siddiqui *et al.*, "Power Prediction of Combined Cycle Power Plant (CCPP) Using Machine Learning Algorithm-Based Paradigm," *Wirel Commun Mob Comput*, vol. 2021, 2021, doi: 10.1155/2021/9966395.
- [40] R. Siddiqui *et al.*, "Power Prediction of Combined Cycle Power Plant (CCPP) Using Machine Learning Algorithm-Based Paradigm," *Wirel Commun Mob Comput*, vol. 2021, 2021, doi: 10.1155/2021/9966395.
- [41] P. Tüfekci, "Prediction of full load electrical power output of a base load operated combined cycle power plant using machine learning methods," *International Journal of Electrical Power and Energy Systems*, vol. 60, pp. 126–140, 2014, doi: 10.1016/j.ijepes.2014.02.027.
- [42] H. Zhang, R. Chen, F. Wang, H. Wang, and Y. Wang, "Multi-objective Optimization for Operational Parameters of A Micro-turbine CCHP System Based on Genetic Algorithm," *Procedia Eng*, vol. 205, pp. 1807–1814, 2017, doi: <https://doi.org/10.1016/j.proeng.2017.10.236>.
- [43] J. A. Dowell, A. Hussain, J. Devane, and D. Young, "Artificial Neural Networks Applied to the In Vitro-In Vivo Correlation of an Extended-Release Formulation: Initial Trials and Experience," *J Pharm Sci*, vol. 88, no. 1, pp. 154–160, 1999, doi: <https://doi.org/10.1021/js970148p>.
- [44] J. Du, J. Guo, Z. Zhang, M. Li, F. Ren, and Y. Liu, "A triple cascade gas turbine waste heat recovery system based on supercritical CO₂ Brayton cycle: Thermal analysis and optimization," *Energy Conversion and Management: X*, vol. 16, Dec. 2022, doi: 10.1016/j.ecmx.2022.100297.
- [45] C. Yilmaz and I. Koyuncu, "Thermoeconomic modeling and artificial neural network optimization of Afyon geothermal power plant," *Renew Energy*, vol. 163, pp. 1166–1181, Jan. 2021, doi: 10.1016/j.renene.2020.09.024.

- [46] Q. Jin, S. Xia, P. Li, and T. Xie, "Multi-objective performance optimization of regenerative S-CO₂ Brayton cycle based on neural network prediction," *Energy Conversion and Management: X*, vol. 14, May 2022, doi: 10.1016/j.ecmx.2022.100203.
- [47] W. Seidel, "Model Development and Annual Simulation of the Supercritical Carbon Dioxide Brayton Cycle for Concentrating Solar Power Applications," 2010.
- [48] R. Vasquez Padilla, Y. C. Soo Too, R. Benito, R. McNaughton, and W. Stein, "Multi-objective thermodynamic optimisation of supercritical CO₂ Brayton cycles integrated with solar central receivers," *International Journal of Sustainable Energy*, vol. 37, no. 1, pp. 1–20, Jan. 2018, doi: 10.1080/14786451.2016.1166109.
- [49] M. Monjurul Ehsan, Z. Guan, A. Y. Klimenko, and X. Wang, "Design and comparison of direct and indirect cooling system for 25 M² solar power plant operated with supercritical CO₂ cycle," *Energy Convers Manag*, vol. 168, pp. 611–628, Jul. 2018, doi: 10.1016/j.enconman.2018.04.072.
- [50] Z. Ma and C. S. Turchi, "Advanced Supercritical Carbon Dioxide Power Cycle Configurations for Use in Concentrating Solar Power Systems Preprint." [Online]. Available: <http://www.osti.gov/bridge>
- [51] V. Dostal, M. J. Driscoll, P. Hejzlar, and N. E. Todreas, "ICONE10-22192 A SUPERCRITICAL CO₂ GAS TURBINE POWER CYCLE FOR NEXT-GENERATION NUCLEAR REACTORS." [Online]. Available: <http://www.asme.org/about-asme/terms-of-use>
- [52] M. Monjurul Ehsan, S. Duniam, J. Li, Z. Guan, H. Gurgenci, and A. Klimenko, "A comprehensive thermal assessment of dry cooled supercritical CO₂ power cycles," *Appl Therm Eng*, vol. 166, Feb. 2020, doi: 10.1016/j.applthermaleng.2019.114645.
- [53] X. Wang, Q. Liu, Z. Bai, J. Lei, and H. Jin, "Thermodynamic Analysis of the Cascaded Supercritical CO₂ Cycle Integrated with Solar and Biomass Energy," in *Energy Procedia*, Elsevier Ltd, 2017, pp. 445–452. doi: 10.1016/j.egypro.2017.03.339.
- [54] S. A. Wright, R. F. Radel, T. M. Conboy, and G. E. Rochau, "SANDIA REPORT Modeling and Experimental Results for Condensing Supercritical CO₂ Power Cycles." [Online]. Available: <http://www.ntis.gov/help/ordermethods.asp?loc=7-4-0#online>

- [55] M. M. Ehsan, S. Duniam, J. Li, Z. Guan, H. Gurgenci, and A. Klimenko, "Effect of cooling system design on the performance of the recompression CO₂ cycle for concentrated solar power application," *Energy*, vol. 180, pp. 480–494, Aug. 2019, doi: 10.1016/j.energy.2019.05.108.
- [56] Y. Ma, X. Zhang, M. Liu, J. Yan, and J. Liu, "Proposal and assessment of a novel supercritical CO₂ Brayton cycle integrated with LiBr absorption chiller for concentrated solar power applications," *Energy*, vol. 148, pp. 839–854, Apr. 2018, doi: 10.1016/j.energy.2018.01.155.
- [57] M. S. Shahin, M. F. Orhan, and F. Uygul, "Thermodynamic analysis of parabolic trough and heliostat field solar collectors integrated with a Rankine cycle for cogeneration of electricity and heat," *Solar Energy*, vol. 136, pp. 183–196, Oct. 2016, doi: 10.1016/j.solener.2016.06.057.
- [58] V. Zare and M. Hasanzadeh, "Energy and exergy analysis of a closed Brayton cycle-based combined cycle for solar power tower plants," *Energy Convers Manag*, vol. 128, pp. 227–237, Nov. 2016, doi: 10.1016/j.enconman.2016.09.080.
- [59] S. M. Besarati and D. Yogi Goswami, "A computationally efficient method for the design of the heliostat field for solar power tower plant," *Renew Energy*, vol. 69, pp. 226–232, 2014, doi: 10.1016/j.renene.2014.03.043.
- [60] R. Chen, Z. Rao, and S. Liao, "Determination of key parameters for sizing the heliostat field and thermal energy storage in solar tower power plants," *Energy Convers Manag*, vol. 177, pp. 385–394, Dec. 2018, doi: 10.1016/j.enconman.2018.09.065.
- [61] W. Ding *et al.*, "Hot corrosion behavior of commercial alloys in thermal energy storage material of molten MgCl₂/KCl/NaCl under inert atmosphere," *Solar Energy Materials and Solar Cells*, vol. 184, pp. 22–30, Sep. 2018, doi: 10.1016/j.solmat.2018.04.025.
- [62] J. Stekli, L. Irwin, and R. Pitchumani, "Technical challenges and opportunities for concentrating solar power with thermal energy storage," *J Therm Sci Eng Appl*, vol. 5, no. 2, May 2013, doi: 10.1115/1.4024143.
- [63] A. Palacios, C. Barreneche, M. E. Navarro, and Y. Ding, "Thermal energy storage technologies for concentrated solar power – A review from a materials perspective," *Renewable Energy*, vol. 156. Elsevier Ltd, pp. 1244–1265, Aug. 01, 2020. doi: 10.1016/j.renene.2019.10.127.

- [64] S. Kuravi, J. Trahan, D. Y. Goswami, M. M. Rahman, and E. K. Stefanakos, "Thermal energy storage technologies and systems for concentrating solar power plants," *Progress in Energy and Combustion Science*, vol. 39, no. 4, pp. 285–319, Aug. 2013. doi: 10.1016/j.pecs.2013.02.001.
- [65] Y. Zhu, R. Zhai, H. Peng, and Y. Yang, "Exergy destruction analysis of solar tower aided coal-fired power generation system using exergy and advanced exergetic methods," *Appl Therm Eng*, vol. 108, pp. 339–346, Sep. 2016, doi: 10.1016/j.applthermaleng.2016.07.116.
- [66] Q. Jin, S. Xia, P. Li, and T. Xie, "Multi-objective performance optimization of regenerative S-CO₂ Brayton cycle based on neural network prediction," *Energy Conversion and Management: X*, vol. 14, May 2022, doi: 10.1016/j.ecmx.2022.100203.
- [67] K. Alawadhi, A. Alfalah, B. Bader, Y. Alhouli, and A. Murad, "An optimization study to evaluate the impact of the supercritical CO₂ brayton cycle's components on its overall performance," *Applied Sciences (Switzerland)*, vol. 11, no. 5, Mar. 2021, doi: 10.3390/app11052389.
- [68] A. Ghasemi, A. A. Shayesteh, A. Doustgani, and M. Pazoki, "THERMODYNAMIC ASSESSMENT AND OPTIMIZATION OF A NOVEL TRIGENERATION ENERGY SYSTEM BASED ON SOLAR ENERGY AND MSW GASIFICATION USING ENERGY AND EXERGY CONCEPT," Yildiz Technical University Press, 2021.
- [69] K. M. Hamdia, X. Zhuang, and T. Rabczuk, "An efficient optimization approach for designing machine learning models based on genetic algorithm," *Neural Comput Appl*, vol. 33, no. 6, pp. 1923–1933, Mar. 2021, doi: 10.1007/s00521-020-05035-x.
- [70] A. H. Khan, S. Hossain, M. Hasan, M. S. Islam, M. M. Rahman, and J. H. Kim, "Development of an optimized thermodynamic model for VVER-1200 reactor-based nuclear power plants using genetic algorithm," *Alexandria Engineering Journal*, vol. 61, no. 11, pp. 9129–9148, Nov. 2022, doi: 10.1016/j.aej.2022.02.052.
- [71] S. Katoch, S. S. Chauhan, and V. Kumar, "A review on genetic algorithm: past, present, and future," *Multimed Tools Appl*, vol. 80, no. 5, pp. 8091–8126, Feb. 2021, doi: 10.1007/s11042-020-10139-6.
- [72] I. S. Ike *et al.*, "ANN-GA, ANFIS-GA and Thermodynamics base modeling of crude oil removal from surface water using organic acid grafted banana pseudo stem fiber," *Applied Surface Science Advances*, vol. 9, Jun. 2022, doi: 10.1016/j.apsadv.2022.100259.

- [73] C. Kim, R. Batra, L. Chen, H. Tran, and R. Ramprasad, "Polymer Design using Genetic Algorithm and Machine Learning," 2020. [Online]. Available: <https://www.sciencedirect.com/science/article/pii/S0927025620305589>
- [74] K. Zhang *et al.*, "Thermodynamic analysis and optimization of variable effect absorption refrigeration system using multi-island genetic algorithm," *Energy Reports*, vol. 8, pp. 5443–5454, Nov. 2022, doi: 10.1016/j.egy.2022.04.004.
- [75] S. M. Besarati, K. Atashkari, A. Jamali, A. Hajiloo, and N. Nariman-zadeh, "Multi-objective thermodynamic optimization of combined Brayton and inverse Brayton cycles using genetic algorithms," *Energy Convers Manag*, vol. 51, no. 1, pp. 212–217, Jan. 2010, doi: 10.1016/j.enconman.2009.09.015.
- [76] M. Saeed and M. H. Kim, "Analysis of a recompression supercritical carbon dioxide power cycle with an integrated turbine design/optimization algorithm," *Energy*, vol. 165, pp. 93–111, Dec. 2018, doi: 10.1016/j.energy.2018.09.058.
- [77] S. M. Alirahmi, M. Rostami, and A. H. Farajollahi, "Multi-criteria design optimization and thermodynamic analysis of a novel multi-generation energy system for hydrogen, cooling, heating, power, and freshwater," *Int J Hydrogen Energy*, vol. 45, no. 30, pp. 15047–15062, May 2020, doi: 10.1016/j.ijhydene.2020.03.235.
- [78] M. Verma and J. Rajasankar, "A thermodynamical approach towards multi-criteria decision making (MCDM)," Dec. 2015, doi: 10.1016/j.asoc.2016.10.033.
- [79] C. H. Chen, "A novel multi-criteria decision-making model for building material supplier selection based on entropy-AHP weighted TOPSIS," *Entropy*, vol. 22, no. 2, Feb. 2020, doi: 10.3390/e22020259.
- [80] P. Mojaver, S. Jafarmadar, S. Khalilarya, and A. Chitsaz, "Study of synthesis gas composition, exergy assessment, and multi-criteria decision-making analysis of fluidized bed gasifier," *Int J Hydrogen Energy*, vol. 44, no. 51, pp. 27726–27740, Oct. 2019, doi: 10.1016/j.ijhydene.2019.08.240.